10-31-2011

MRI: ID-Development of a Hybrid Scanning Fluorescence and Sum Frequency Spectroscopy Imaging Microscope

Michael D. Mason
Principal Investigator; University of Maine, Orono, mmason@umche.maine.edu

David J. Neivandt
Co-Principal Investigator; University of Maine, Orono, dneivandt@umche.maine.edu

Michael Grunze
Co-Principal Investigator; University of Maine, Orono

Samuel T. Hess
Co-Principal Investigator; University of Maine, Orono, Sam.T.Hess@umit.maine.edu

Final Report for Period: 08/2010 - 07/2011 **Submitted on:** 10/31/2011

Principal Investigator: Mason, Michael D. **Award ID:** 0722759

Organization: University of Maine

Submitted By:

Mason, Michael - Principal Investigator

Title:

MRI: ID-Development of a Hybrid Scanning Fluorescence and Sum Frequency Spectroscopy Imaging Microscope

Project Participants

Senior Personnel

Name: Mason, Michael

Worked for more than 160 Hours: Yes

Contribution to Project:

Name: Grunze, Michael

Worked for more than 160 Hours: No

Contribution to Project:

Dr. Grunze has been an active participant in the grant project over the past nine months, however, his total involvement in years 1 and 2 will be closer to 100 hours. In year three, where the solution cell is to be completed and implemented, his involvment is expected to increase significantly.

Name: Neivandt, David

Worked for more than 160 Hours: Yes

Contribution to Project:

Name: Hess, Samuel

Worked for more than 160 Hours: Yes

Contribution to Project:

Name: Gunewardene, Mudalige

Worked for more than 160 Hours: Yes

Contribution to Project:

Siyath (Mudalige) was hired this past year as a secondary graduate student to assist in this project and has worked on incorporating the new fluorescence components into the existing sum frequency microscope. He has significant experience with advanced fluorescence techniques.

She is currently supported at a level of 50% on the MRI grant.

Post-doc

Graduate Student

Name: Allgeyer, Edward

Worked for more than 160 Hours: Yes

Contribution to Project:

Ed was hired this past year as the primary graduate student to be involved on the project. He has been outstanding in all regards. He has become proficient in his understanding physics involved in this project and has worked tirelessly on acquisition and set up of the instrument.

He is currently supported at a level of 100% on the MRI grant.

Name: Sterling, Sarah

Worked for more than 160 Hours: Yes

Contribution to Project:

Sarah was hired this past year as a secondary graduate student to assist in this project and has worked on incorporating the new instrumental components into the existing sum frequency microscope, of which whe has significant expertise.

She is currently supported at a level of 50% on the MRI grant.

Name: Dasilva, Erik

Worked for more than 160 Hours: Yes

Contribution to Project:

Erik is primarily responsible with establishing, monitoring, and assessing the effectiveness of our UMAINE supported MRI outreach program associated with this project.

Undergraduate Student

Technician, Programmer

Other Participant

Research Experience for Undergraduates

Organizational Partners

Other Collaborators or Contacts

Activities and Findings

Research and Education Activities: (See PDF version submitted by PI at the end of the report)

See Attached.

Findings: (See PDF version submitted by PI at the end of the report)

See Attached

Training and Development:

To date 16 undergraduate students and 4 graduate students have been involved in this project. The graduate students involved have now completed advanced science degrees in Physics and Chemical Engineering. The 16 undergraduate students are pursuing bachelors degrees in Physics, Chemical Engineering, and Biological Engineering.

Outreach Activities:

In conjunction with this cutting edge project educational and outreach programs were developed demonstrating to an audience of high school students and educators the capabilities of the proposed instrument as well as the importance of new instrument development to the broader research community. Through this program nearly 150 high school students have participated in a one day directed research experience, and 4 high school students and 2 science teachers participated in a two month NSF supported research program, and an additional 6 high school students have participate in related research based on an internal matching grant.

Over two summers (2008, 2009) a Master of Science and Teaching (MST) Student (Erik DeSilva) was hired in conjunction with this MRI development project to specifically develop 1) course curricula/teaching modules for a new Biological Engineering Instrumentation and Advanced Methods Course, 2) development of high school outreach activities and curricula including on-campus research experiences (BEAR Program http://www.umche.maine.edu/bear/). Funding for this position was provided by UMaine Sponsored Programs in response to the proposed MRI funded outreach and educational activities. In addition, this student has completed a high school classroom teaching module

which he has implemented on a trial basis. Also completed are the two halves of the online description of the technology development, including the underlying photophysics, associated with this project. This can be found online at: http://www.physics.umaine.edu/FPALM_SFS_NOV09/sfs.html.

Journal Publications

Gould, TJ; Gunewardene, MS; Gudheti, MV; Verkhusha, VV; Yin, SR; Gosse, JA; Hess, ST, "Nanoscale imaging of molecular positions and anisotropies", NATURE METHODS, p. 1027, vol. 5, (2008). Published, 10.1038/nmeth.127

Juette, MF; Gould, TJ; Lessard, MD; Mlodzianoski, MJ; Nagpure, BS; Bennett, BT; Hess, ST; Bewersdorf, J, "Three-dimensional sub-100 nm resolution fluorescence microscopy of thick samples", NATURE METHODS, p. 527, vol. 5, (2008). Published,

Gould TJ, Verkhusha VV, Hess ST, "Fluorescence Photoactivation Localization Microscopy", Nature Protocols, p. , vol. , (2009). Submitted,

Allgeyer, E; Pongan, A; King, M; Mason MD, "Signal comparison of single fluorescent molecules and Raman active gold nanoprisms????", Nano Letters, p. 3816, vol. 9 (11), (2009). Published,

Books or Other One-time Publications

Gould TJ, Hess ST, "Nanoscale Imaging of Intracellular Fluorescent Proteins: Breaking the Diffraction Barrier", (2008). Book, Accepted
Editor(s): Detrich HW
Collection: Methods in Cell Biology, Biophysical Tools for Biologists, Volume 2: Methods in Vivo
Bibliography: Elsevier Press, New York ISBN: 978-0-12-372521-9

Hess ST, Gould TJ, Gunewardene M, Bewersdorf J, Mason MD, "Ultra-High Resolution Imaging of biomolecules by Fluorescence Photoactivation Localization Microscopy", ( ). Book, Accepted
Editor(s): Lee JW
Collection: Methods in Molecular Biology
Bibliography: Springer Press, New York

Edward S. Allgeyer, "DEVELOPMENT OF INSTRUMENTATION FOR SUM FREQUENCY SPECTRAL IMAGING COMBINED WITH CONFOCAL FLUORESCENCE IMAGING AND ADDITIONAL TOPICS", (2011). Thesis, Accepted
Editor(s): UMaine
Collection: Thesis
Bibliography: Thesis

Web/Internet Site

URL(s):

http://www.physics.umaine.edu/FPALM_SFS/index.htm

Description:

This website will serve as an ongoing description of the instrument development effort including the design, construction, and application of this new technology. It is an ongoing development effort of our Masters of Science Teaching student focused on disseminating this work to a broader audience.

Other Specific Products

Contributions

Contributions within Discipline:

Do date, our publications have been focused on the single molecule fluorescence capabilities of the MRI instrument. Through the NSF support of this project, single molecule imaging techniques have been developed which are expected to dramatically affect the fields of biology and materials science.

These have been extended to include the originally proposed model membrane system specifically designed for use on the combined sum-frequency/fluorescence system.

Contributions to Other Disciplines:

This project has a significant outreach program. It has specifically involved graduate Physics Education students as will as high school educators. In this way it has contributed to the knowledge base around how high tech instrumentation, and the physical processes associated with these tools, can be desseminated and explained to a broader audience.

Contributions to Human Resource Development:

Fluorescence instruments based on the single molecule fluorescence methods developed in part by this MRI project have now resulted in the development of several related instruments. These instruments are now being implemented at a number of universities.

Contributions to Resources for Research and Education:

Both through direct involvement in this project and through the related MRI outreach activities a number of undergraduate and high school students have now been exposed to this instrument and the specific physical principles and engineering technologies involved in its development.

Contributions Beyond Science and Engineering:

Conference Proceedings

Categories for which nothing is reported:

Organizational Partners

Any Product

Contributions: To Any Beyond Science and Engineering

Any Conference

Final Report on NSF Award No. CHE-0722759: MRI: Development of a Hybrid Scanning Fluorescence and Sum Frequency Spectroscopy Imaging Microscope

Edward S. Allgeyer[2], Samuel T. Hess[2], Michael D. Mason[1], David J. Neivandt[1], Sarah M. Sterling[1], Mudalige Gunewardene[2]

[1]Department of Chemical and Biological Engineering, University of Maine, Orono, ME 04469
[2]Department of Physics and Astronomy, University of Maine, Orono, ME 04469

Abstract

This MRI project was focused on developing a hybrid scanning fluorescence (FL) and sum-frequency (SF) vibrational spectroscopic microscope. Now completed, the microscope will expand the capabilities of the nation's research infrastructure by combining the benefits of two powerful imaging and spectroscopic techniques. This combination enables the direct correlation between localized or distributed photophysical (FL) molecular properties and the structure of the environment (SF). In its current form the instrument has diffraction limited resolution in the fluorescence channel (~250 nm), and ~10 μm resolution in the sum-frequency channel. The instrument is capable of obtaining 2D (or 3D) image sets comprised of single pixel fluorescence information and complete (1024 pixel) high resolution (< 0.1 cm^{-1}) Sum-Frequency spectra. An additional point probe mode was included which allows for high temporal resolution (<1 ns) fluorescence detection with single molecule sensitivity and simultaneous high spectral resolution sum-frequency detection. The 'particle-in-a-bath' capabilities of the proposed instrument will have utility in biology, biochemistry, materials science, chemistry and physics. For example, it is anticipated that future research conducted with this new instrument will provide breakthroughs in our understanding of membrane and film organization at the molecular level. Sample data illustrating the power of our instrument is presented. Much of the final project description presented here has been excerpted from the outstanding PhD thesis of the primary graduate student working on this project (Edward S. Allgeyer).[1]

I. INTRODUCTION

To further advance the research and educational capabilities of the University of Maine and the Institute for Molecular Biophysics (IMB), we proposed to capitalize on our expertise in sum-frequency (SF) spectroscopy and fluorescence (FL) imaging to develop an instrument with unique capabilities crucial to the study of a broad range of systems from materials to bio-membranes. Ideally, this imaging spectrometer would measure molecular conformations, photophysical properties, and dynamics in a temporal regime which is inaccessible, yet entirely complementary, to existing instrumentation available for our current research efforts.

Sum Frequency (SF) is a vibrational technique based on non-linear optical mixing of photons of two different energies. SF provides detailed structural information on an ensemble of molecules at an interface within an optically-defined sample volume, including absolute orientation and conformational configuration. SF has been used to analyze thin film systems in a number of instrumental geometries including transmitting[i,ii] and reflective substrates.[iii] For example, in two recent publications by Cimatu and Baldelli, SF was used to observe the spatial distribution of CO on platinum surfaces[iv] and chemically distinct regions of self-assembled alkane-thiol monolayers.[v] Fluorescence (FL) spectroscopy

complements SF by providing access to single-molecule properties of individual species within an ensemble of molecules on 10^{-12} s to $>10^{2}$ s timescales. Ideally, both FL and SF methodologies would be employed simultaneously yielding localized dynamics of the single fluorophore (FL), or multiple fluorophores, and spatially correlated structural information about the local surroundings (SF). Additionally, the ability to select phase or structure specific fluorescent molecules allows one to correlate spatial and temporal fluorescence information with structural information regarding the surroundings. This *'particle-in-a-bath'* approach has found limited implementation due to differing optical requirements and inherent difficulties in distinguishing between the two signals; the MRI instrument developed by our group circumvents these issues by exploiting fundamental differences in the optical nature of SF and FL.

In the following sections we describe the individual Fluorescence and Sum-frequency components of the MRI instrument separately, and as a combined tool. It is important to note that our instrument has all of the capabilities of separate FL and SF equipment in addition to the expanded capabilities arising from this unique combination.

II. FLUORESCENCE COMPONENTS

A. Fluorescence Microscope Core

At the core of the combined Sum-frequency and Fluorescence instrument is a standard Olympus IX71 inverted microscope base as shown in Figure 1A. This base was chosen primarily due to its flexibility for multiple light source inputs and signal collection points. This base is widely used for either laser scanning or sample scanning confocal fluorescence microscopy (SCFM). The relatively open inverted design was chosen to allow for Sum-Frequency signal acquisition to occur from the top (epi-) and fluorescence signal acquisition to occur from either the bottom or the top (transmission or reflection modes).

Typical with all SCFM instruments, a laser is directed into the back aperture of a microscope objective which focuses the beam with a tight waist at the focal plane positioned inside the sample. Scattered or emitted light is collected by the same objective and focussed onto a pin hole placed confocally with the illumination spot in the image plane. The confocal pin hole discriminates against light originating from regions of the sample above or below the focal plane or laterally adjacent to the beam waist. This is geometrically apparent as the dotted rays in Figure 1B which are defocused when they reach the pin hole and are largely blocked, although some background light is admitted. Light which does pass the pin hole is detected with an avalanche photodiode (APD) whose signal is recorded by a computer. An image is collected point-wise by either raster scanning the sample and recording the detected light for each illuminated position. Collecting an image at varying axial sample positions generates a stack of 2-dimensional images that may be reconstructed to form a 3-dimensional image.

Although the confocal aperture provides a modest increase in lateral resolution its distinct advantage over wide field illumination and collection is the enormous increase in background suppression yielding greatly improved depth discrimination (Diaspro, 2007); the confocal pin hole restricts imaging to only a small sample slice. Certainly the modest improvement in lateral resolution, up to a factor of $\sqrt{2}$ (Sandison & Webb, 1994; Sandison *et al.*, 1995) is advantageous but alone is not enough to have propelled confocal microscopy into its present position as a virtual standard. Rather the 2-3 orders of magnitude increase in the signal to background ratio (Sandison & Webb, 1994; Sandison *et al.*, 1995), allowing for 3D sectioning and improved image quality, is responsible. Because of its greatly improved surface specificity, it is a clear choice for pairing with interface specific techniques such as sum frequency spectroscopy.

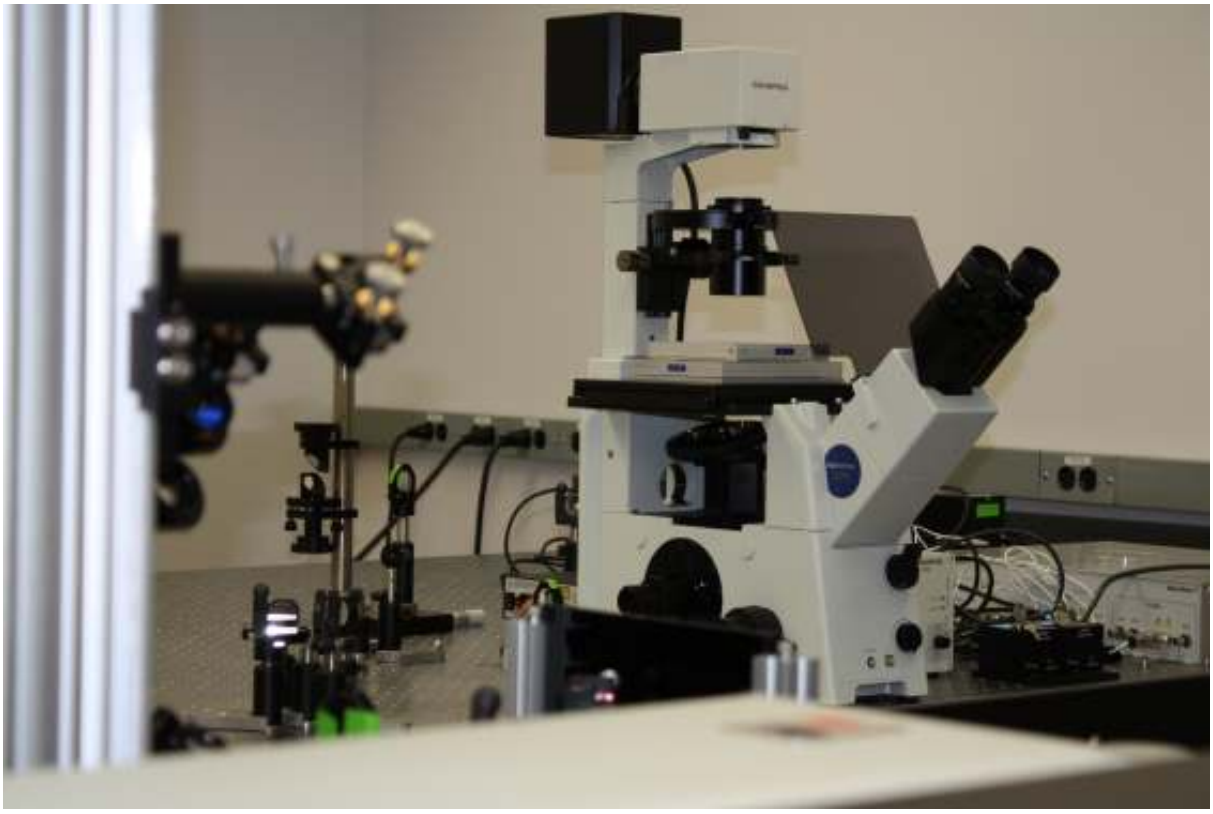

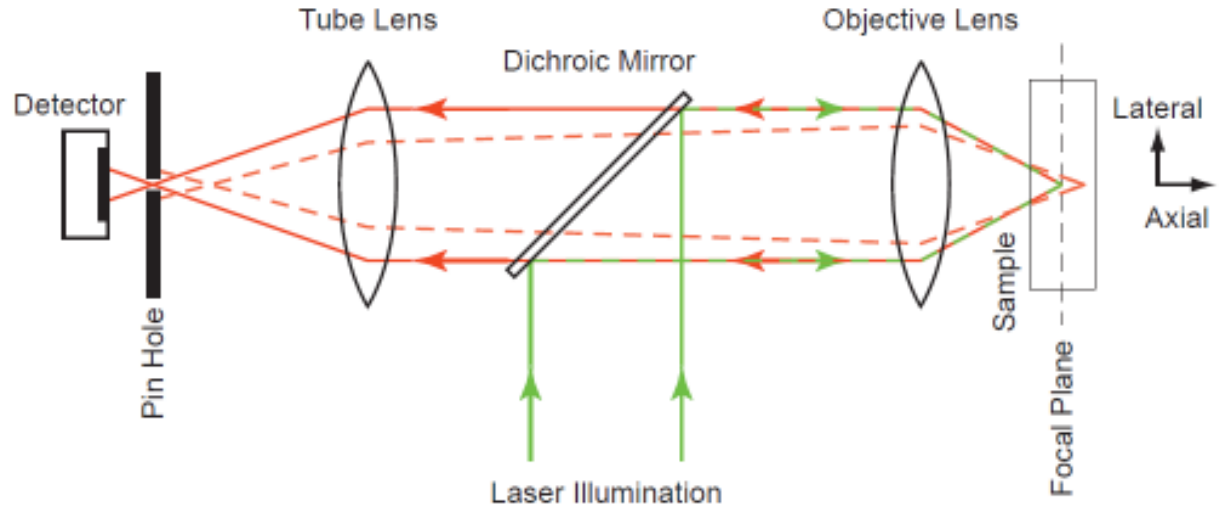

Figure 1. (Top) Basic illustration of a confocal microscope. Laser illumination is directed into the back aperture of a microscope objective with a dichroic mirror and focused inside the sample for excitation. Light is collected with the same objective lens, passed through the dichroic mirror, and is focused by the tube lens through a pin hole onto a photodetector (APD). Light originating outside the focal region (dotted rays) is defocused at the pin hole and largely blocked. (Bottom) Photo of the Olympus microscope body during the initial construction phase of the FL/SF combined instrument.

B. Low Drift Stage and Objective Holder

While the as-purchased XY-translation stage of the Olympus IX71 inverted microscope is considered to have excellent position stability, the rigorous demands of the combined SF and FL instrument required further refinements. Specifically, the z-position of the sample, relative to the excitation and collection optics, is critical to maintain stability in the SF signal and to ensure spatial correlation between the SF and FL information. As such, the factory shipped XY translation stage and objective turret were removed and replaced with a custom built isolation stage and objective mount (Figure 2A). All components of this custom stage were produced at UMaine.

In place of the original XY stage a 12.7mm thick 178 by 240mm block of aluminum was employed. A 32mm square was milled in the middle of the plate to accommodate our custom objective holder (detailed later) and four M6 clearance holes were drilled allowing the plate to be mounted on the IX71 base in place of the Olympus XY stage. Four holes were drilled and tapped for 1/4-20 screw size allowing for the attachment of a large aperture high performance two axis translation stage (Newport Corporation, 406) and our objective holder. Mounted on top of the aluminum plate is the afore mentioned large aperture Newport course XY stage. This stage has a 57.15mm diameter aperture to accommodate our objective holder and 13mm of travel in the X and Y directions allowing the sample to be manually positioned. A three axis piezo scan stage (Mad City Labs, Nano-T115) was mounted, via a connecting plate, on top of the Newport XY stage. This software controlled stage provides the XY motion required for sample scanning during FL and SF data acquisition. Finally, an acrylic sample cell holder that thermally insulates the scan stage from the sample cell sits atop the piezo scan stage.

The objective holder consists of an externally threaded 28.757mm outside diameter stainless steel rod, a brass mounting plate, and a brass lock ring. The brass mounting plate and lock ring have internal threads mated to the external threads of the rod. The stainless steel rod is 88.9mm long and has 76.2mm of external 44 threads per inch (tpi) threads (giving a 577μm axial advance per revolution). The inner diameter of the rod is 0.8 inch with internal RMS threads (20.32mm diameter and 36 tpi) at one end allowing attachment of a microscope objective. The brass mounting plate is attached to the top of the large aluminum plate while the stainless steel rod and lock ring thread in from beneath. Rotation of the threaded rod, accessed from under the aluminum plate, allows the microscope objective to be moved up and down. The lock ring allows the position of the objective to be fixed and the high tpi provides the necessary axial resolution for the objective. Fine tuning of the focus is easily accomplished with the Z-axis of the piezo scan stage. A schematic of the stage and objective holder is given in Figure 2A. With the setup described the sample cell is fixed to the top of the scan stage and the position of the objective relative to the sample is held constant once the lock ring is tightened. Thus, for a given piezo z-position, the critical feature of a fixed distance between the sample and objective is fulfilled while the Newport XY translation stage allows for the equally critical feature of course sample positioning. This level of position stability is often overlooked in fluorescence confocal imaging, and is critical for signal stability in SF techniques involving sample scanning.

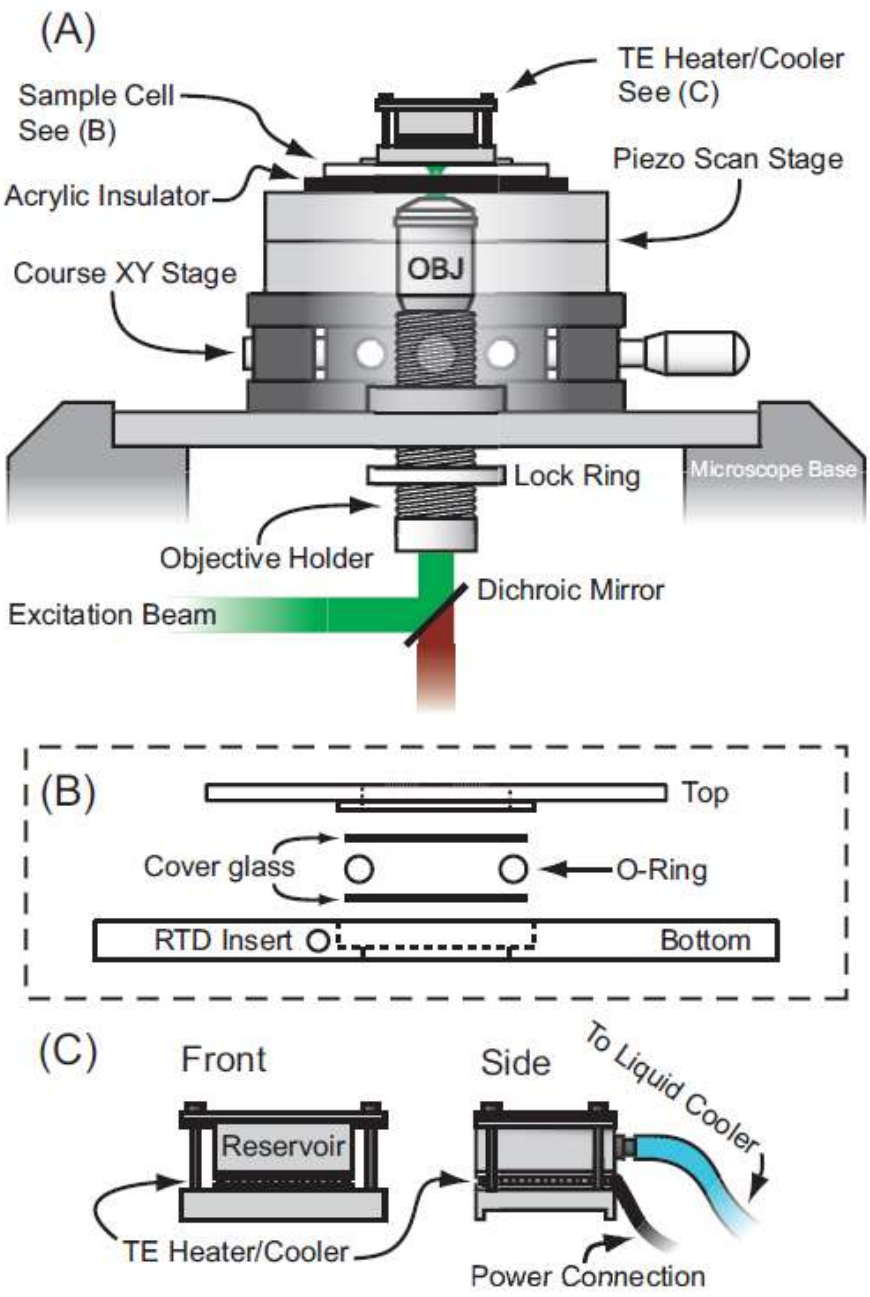

Figure 2. (A) Stage and objective holder as detailed in the text. (B) Liquid sample cell forming a cover glass o-ring sandwich for planar membrane systems. (C) TE heater/cooler sandwiched between circulating liquid reservoir and an aluminum plate that friction fits on top of the sample cell presented in (B).

C. Liquid cell and heater/cooler stage

As many of the samples of interest require a liquid environment as custom liquid sample cell was constructed. The custom built sample cell is composed of two 300 series stainless steel plates, one with a boss (top), and the other with a matching pocket (bottom) as show in Figure 2B. The lower portion of the sample cell is a 4.7625mm thick stainless steel bar comprised of a 22x22mm pocket milled in the center, two 4-40 clearance holes for direct mounting to the scan stage, and a 7.9375mm aperture to accommodate the microscope objective. The upper portion of the sample cell has a boss that fits inside the pocket of the lower portion. The depth of the pocket and height of the boss have been chosen so two No. 1.5 microscope cover slips may sandwich a PTFE coated o-ring inside the cavity and compress the o-ring by approximately 5%. The top portion of the sample cell attaches to the lower portion using four 4-40 stainless steel screws. Stainless steel is employed throughout to allow all parts to be rigorously cleaned. A 3.175mm hole machined into the side of the lower plate of the sample cell houses a friction-fit removable brass rod that penetrates to within 1.5mm of the liquid cavity. A 1.2mm hole machined longitudinally into the brass rod houses a thermistor (RTD) (TE Technology, MP-2444) mounted with thermal paste. This allows easy removal of the RTD rod unit for cleaning and sample mounting while providing accurate temperature data of the liquid cavity environment.

For measurements requiring temperature control a peltier-thermoelectric (TE) heater/cooler (TE Technology, TE-127-1.0-0.8) is sandwiched between an aluminum reservoir with liquid input and output ports and an aluminum block machined to fit on top of the sample cell as shown in Fig. 2C. The aluminum reservoir is connected to a circulating liquid cooler (Thermaltake, BigWater 780e ESA) to dissipate heat or cool one side of the TE heater/cooler. The fully assembled sample cell with the TE heater/cooler weighs 196g just under the maximum recommended vertical load of the scan stage of 200g.

Proportional-integral-derivative (PID) control (TE Technology, TC-36-25-RS232) was initially used to regulate the temperature of the TE heater/cooler and sample cell. After judicious determination of PID parameters, the PID controller was able to control the sample cell's temperature to within a tenth of a degree Celsius of the set point, however, doing so required the controller to modulate the TE heater/cooler's power. It was quickly noted, however, that the cycling of the power to the TE heater/cooler, although providing a relatively constant temperature, produced a change in the detected count rate from control samples (detailed later) as may be seen in Fig. 3 (the definite cause of this affect remains undetermined). This effect produced gross distortions in measured correlation curves and, subsequently, PID control was eliminated in favor of a constant power heating scheme. The controller was set to a constant power and the resulting steady state temperature was observed and recorded using a custom LabVIEW interface across a range of experimentally relevant temperatures. The results were fit using a second order polynomial allowing the power needed to achieve a desired temperature to be predicted. This scheme resulted in average steady state temperatures with standard deviations of only a few hundredths of a degree although the time necessary to reach the desired temperature was longer than that observed using PID control.

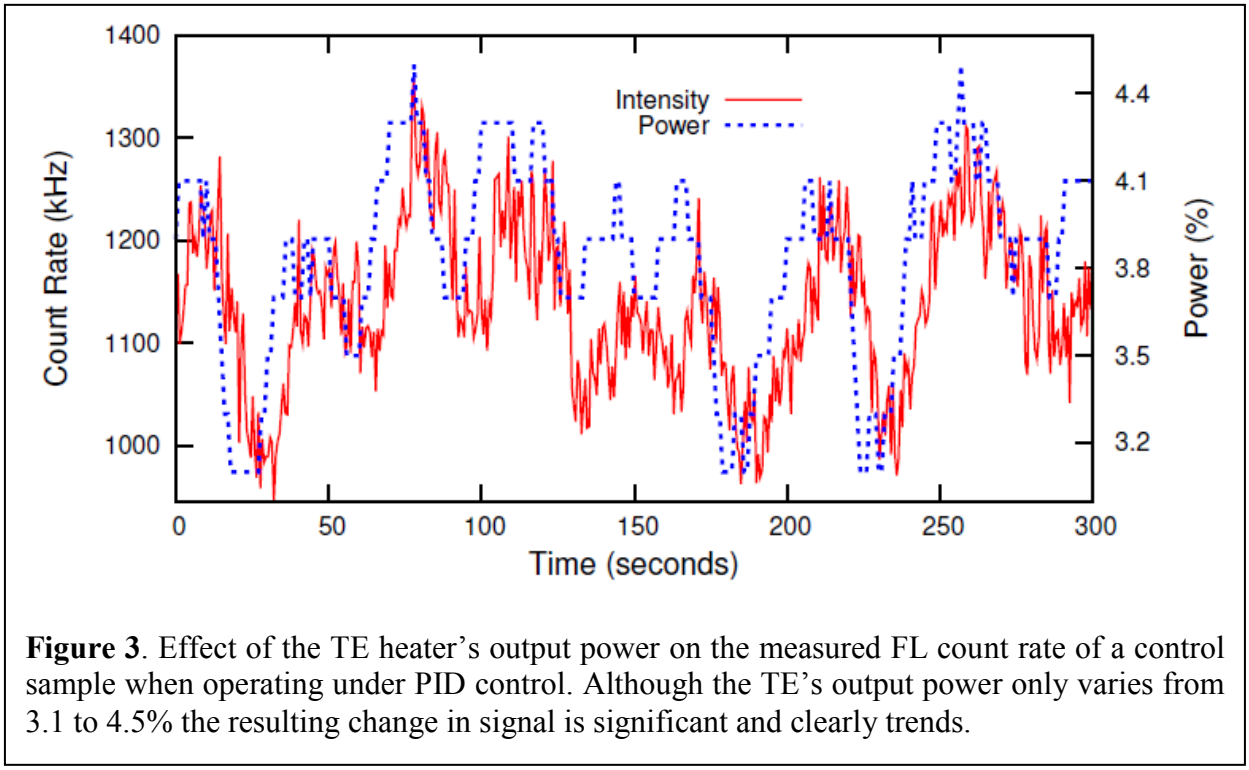

Figure 3. Effect of the TE heater's output power on the measured FL count rate of a control sample when operating under PID control. Although the TE's output power only varies from 3.1 to 4.5% the resulting change in signal is significant and clearly trends.

D. Stage and cell evaluation

Evaluation of the sample cell and stage's stability was carried out by loading the sample cell with two No. 1.5 coverslips and a PTFE coated o-ring but with liquid omitted from the cavity. The sample cell was mounted on the scan stage and the inner surface of the bottom coverslip was brought into focus using a 60X 1.2 N.A. UPlanApo/IR water immersion objective (Olympus) by monitoring the scattered laser light from the glass/air interface. Excitation and collection followed a standard confocal geometry using a 50μm diameter fiber in place of a pin hole and a fiber-coupled avalanche photo diode (APD) as the detector. Once the objective was brought into position, the brass lock ring was secured and a custom LabVIEW program was used to monitor the APD count rate and control the position of the piezo scan stage. The sample cell was scanned through the axial range of the scan stage, the APD count rate at each position was saved, fit to a Gaussian, and the center position of the fitted Gaussian recorded. The software was then set to scan the sample cell through the initial center position every 5 minutes. Scanning was performed from 3μm below to 3μm above the initial center position, in 500nm steps, and the APD count rate at each position was recorded along with the time at which each scan began. The fitted center position for each scan along with the time stamp allowed the position as a function of time to be tracked. Axial scanning of the sample cell using the custom stage setup yielded an average drift rate of 3.47±0.22 nm/min. A typical result is presented in Figure 4A. Similarly, the scan stage and sample cell were mounted on the factory shipped XY stage and the objective was mounted on the original objective turret, and the scan repeated. This yielded an average drift rate of (7.25±1.06)nm/min, as shown in Figure 4B, which is a factor of two larger than our custom setup. Furthermore, Figure 4A also presents occasional mechanical instabilities beyond the

reported average rate were observed suggesting that the stability of the stock stage and turret have the potential to heavily affect measurements on planar systems without operator awareness.

The same stability verification method was also employed to evaluate typical sample mounting methods relative to our custom sample cell. Here, cover glass was mounted to welled slide glass using wax and nail polish. The welled slide glass was inverted and held on the scan stage using clips typically found on microscope stages for said purpose. Typical results from investigating the stability of wax and nail polish sealed cover glass are shown in Fig. 4B along with the stability of our custom setup for comparison. Finally, a No. 1.5 bottom thickness 8-chambered well (Nunc, Lab-Tek II) was tested and the results are also presented in Fig. 4B. As can be seen in Fig. 4B the wax and nail polish sealed welled slide glass, as well as the 8-chamber well, are relatively unstable when compared with our custom setup.

As is clearly evidenced in Fig. 4 by comparing data presented in parts (A) and (B), although our custom stage setup does provide a factor of two decrease in axial drift, relative to the conventional system, it is clear that the custom sample cell employed herein plays an even more critical role. For typical z-scan step sizes (200-300nm) we find the sample′s maximum axial speed is 20.4μm/s (1.22mm/min) and likely not a cause of instability.

Both nail polish and wax seals have been observed to allow air bubbles into the sealed sample well if left for as little as 12 hours. This suggests that the wax and nail polish may form an unreliable seal and allow liquid to evaporate. In equivalent unsealed samples, we observe that as samples dry the loss of liquid due to evaporation causes a visually apparent concave deformation in the cover glass. If the cover glass, which supports the sample, is deforming as a function of time this will clearly affect the absolute position of the sample from scan to scan. This is in contrast to our custom sample cell which allows samples to be examined promptly prior to the potential formation of air bubbles and without having to wait for nail polish or wax to dry. Bubbles have been observed to form in our custom sample cell but only after a few days. More importantly, our sample holder is physically attached to the scan stage using two 4-40 machine screws. This ensures good rigidity between the sample cell and scan stage whereas in the case of conventional microscope stage clips the sample is held by pressure and direct attachment of the sample to the stage is not possible.

To test the imaging stability of our setup a dilute 3nM solution of 200nm fluorescent beads (Invitrogen, F8784) were dried on a No. 1.5 cover glass and mounted in the sample cell. The sample cell was mounted on the piezo scan stage and the beads were brought into focus. An EMCCD camera (Andor, Luca) was used to capture an image of the beads every five minutes for 75 minutes after the initial focus was achieved. Initial and final images are shown in Fig. 2.4. Features in each image were fit to a 2D Gaussian using a custom MatLab script and the resulting $1=e^2$ radius of each feature was stored (features with fitted $1/e^2$ radii larger than would be expected for this imaging system and features not well spatially separated were excluded). Over the 75 minute period the average fitted $1=e^2$ radius increased by (209.4±137)nm (or (2.6±1)nm/min.) indicating the viability of this system for long term imaging.

In all the custom built scan stage and sample cell were proven to have stability far superior to that observed for the as-delivered stage, and typical sample mounting methods, respectively. Due to the z-stability requirements of the combined SF and FL technique this was a necessary achievement of this MRI project.

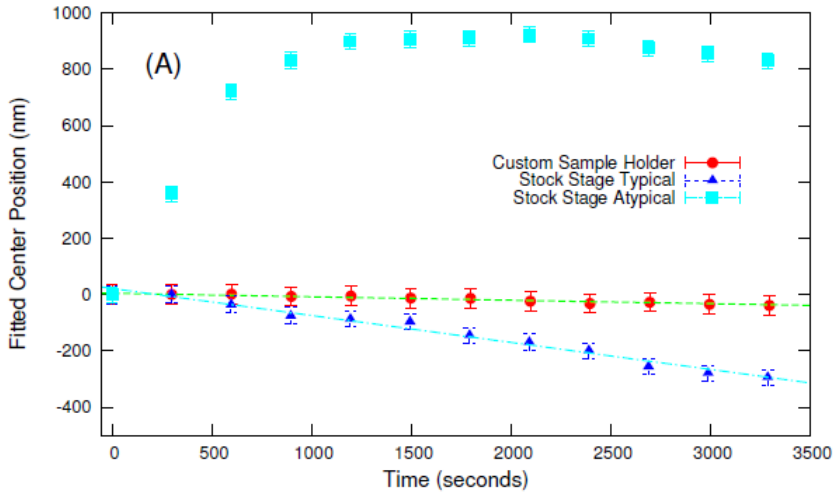

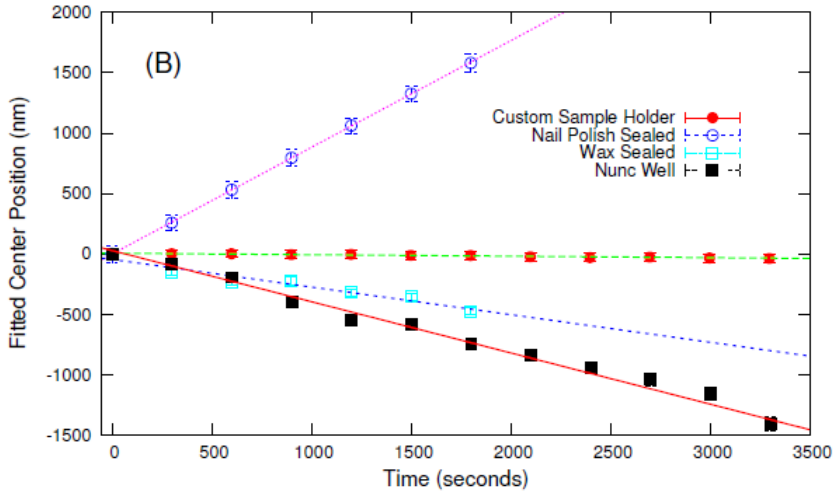

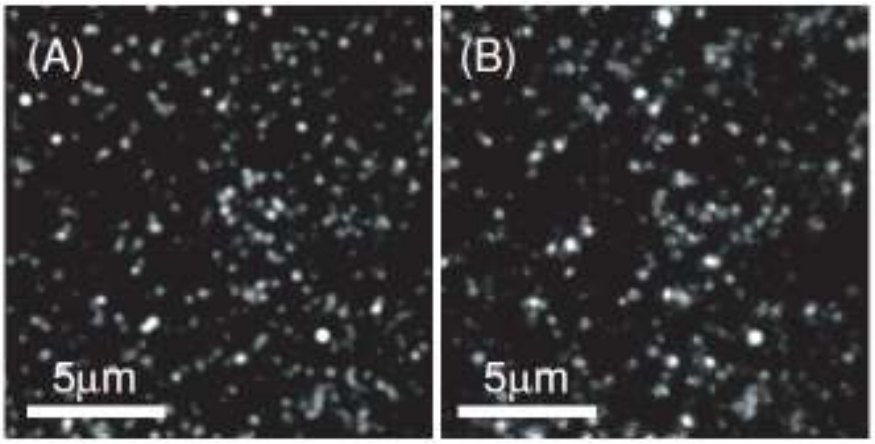

Figure 4. (Top) (A) Axial stability of the custom setup described here is compared with a typical and a typical result from a stock stage and turret. (B) Stability of our sample cell compared with nail polish and wax sealed coverglass and an 8 chamber well. (Bottom) Images of drop cast 200nm beads imaged (A) after initial focus and (B) 75 minutes later.

III. SUM-FREQUENCY COMPONENTS

A. Sum Frequency Basics

Sum frequency spectroscopy (SFS), an application of sum frequency generation (SFG), employs nonlinear optics for the elucidation of interfacial chemical, vibrational, orientation, and conformational information. SFG is produced by spatially and temporally overlapping two electric fields resulting in the creation of a third electric field with angular frequency equal to the sum the to exciting fields: $\omega_{SF} = \omega_1 + \omega_2$. Although the mixing of electric fields from any source, in principle, will produce SFG, in practice the power densities needed and phase matching requirements prohibit detectable SF from being generated by virtually anything other than pulsed lasers. Employing collimated laser excitation further aides in SF detection as the resulting light is emitted as a beam whose angle of emission may be calculated directly. For this reason SFS instruments are universally constructed with one goal: focusing pulsed, collimated, and coherent light onto an interface. A basic SF experimental setup is depicted in Figure 5 where both the SFS-VIS and SFS-IR beams are shown propagating in the positive *z* direction (co-propagating). Note also in Figure 5 indication of electric field polarization in the plane normal to the interface is referred to as *p*-polarized while electric field polarization parallel to the interface is *s*. Interfaces are of paramount importance as under the dipole approximation SFG is forbidden in bulk media with inversion symmetry. However, when inversion symmetry of isotropic centrosymmetric media is broken at an interface the interfacial molecules become sum frequency (SF) active giving SFS its inherent surface specificity.

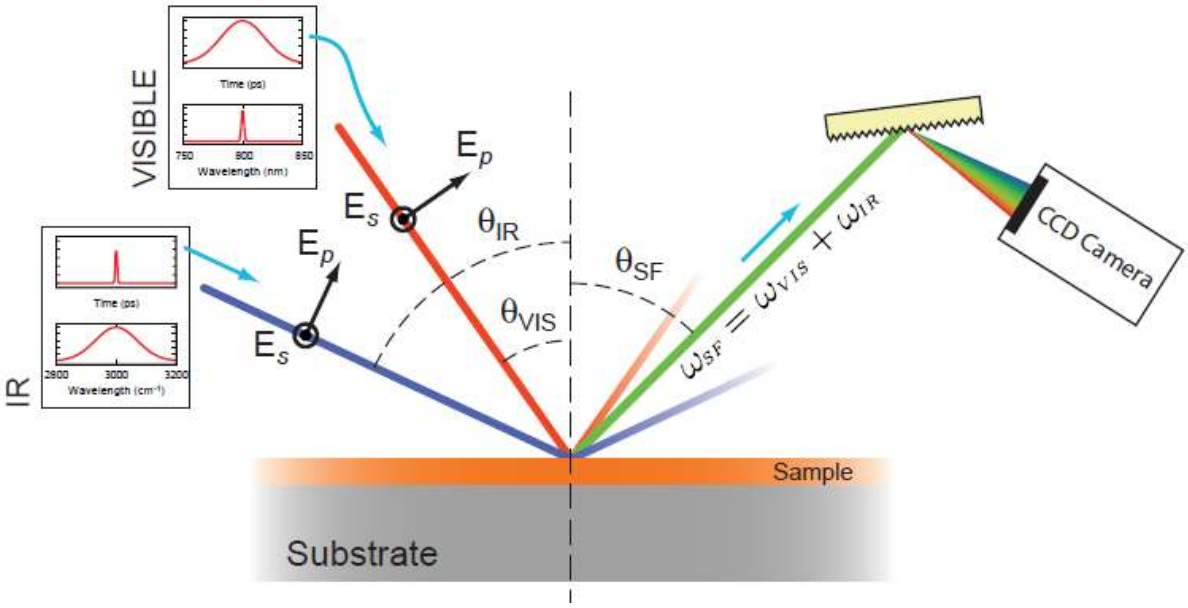

Figure 5. Basic SF experimental geometry. Two pulsed beams meet at an interface and generate SF. (B) Energy level diagram of SFG. Excitation of a vibrational mode is induced via an IR photon (broadband source). A second visible wavelength photon (monochromatic) excites to a virtual level and the photon emitted upon relaxation has an angular frequency equal to the sum of the incident angular frequencies. Complete SF spectra are dispersed from a grating onto a CCD detector in a single shot.

B. Stand alone sum frequency instrumentation

One of the primary goals of this MRI project was to construct the hybrid SF/FL microscope making use of an existing SF (non-imaging) instrument (Neivandt Lab), while maintaining its existing functionality as a user friendly non-spatially resolved spectrometer. However, the rigorous power and spectral demands of the hybrid instrument, as well as the stability required for SF light source switching between the two, required significant changes in configuration of the existing instrument. As such, contruction of the hybrid microscope began with the complete rebuild of the existing spectrometer and the installation of a new optical parametric amplifier (OPA). The basic layout of the updated SF instrument is shown in Figure 6 and a photo is shown in Figure 7.

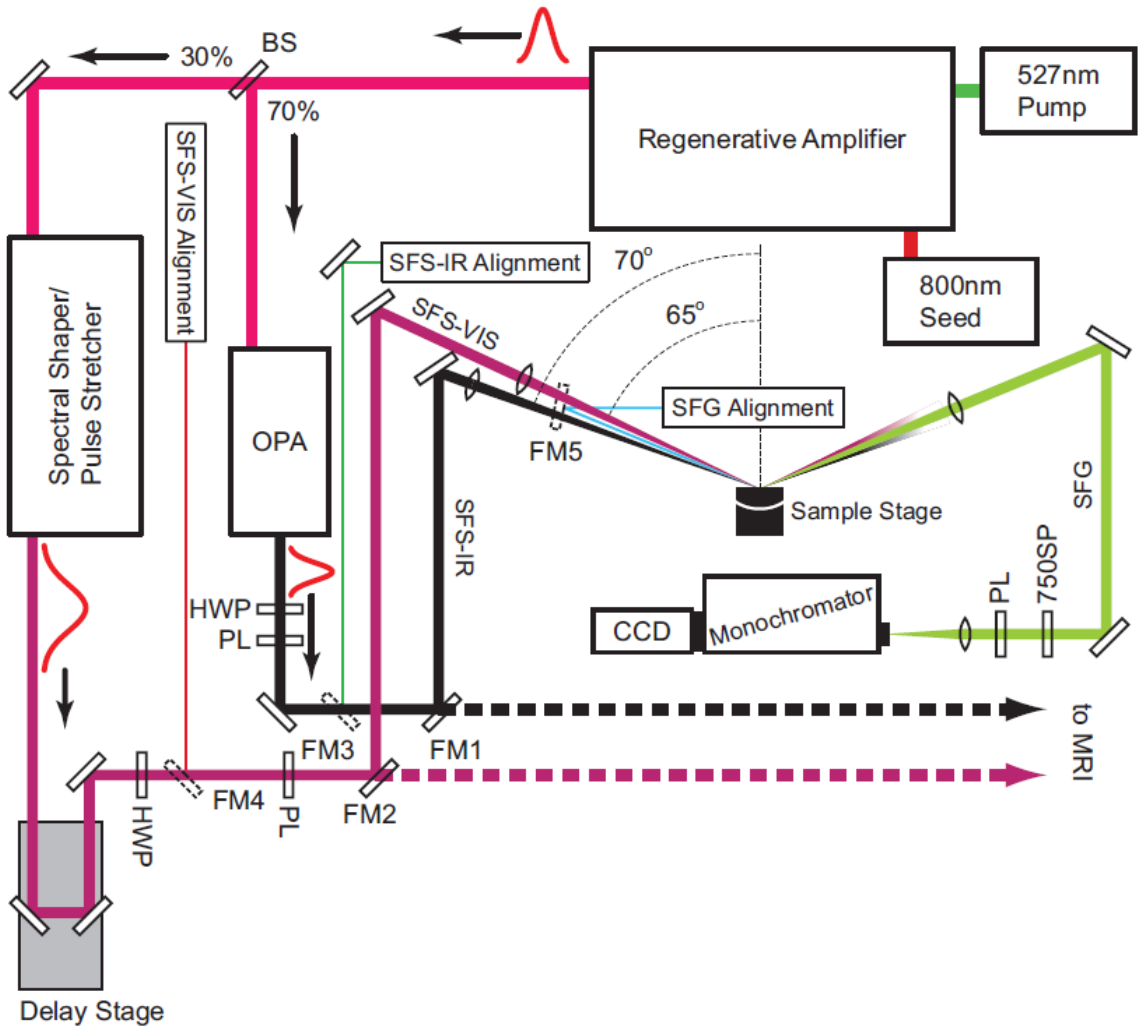

Figure 6. Layout of the rebuilt Neivandt spectrometer detail within the thesis text. FM1-5 are flip mirrors with FM1-2 used to direct the SFG excitation beams to either the Neivandt spectrometer (solid lines) or to the MRI instrument (dotted lines). FM3-4 allow the SFG excitation beams to be replaced with their respective alignment beams while FM5 serves the same function for the SFG signal beam. Abbreviations used are beam splitter (BS), half wave plate (HWP), polarizer (PL), 750nm short pass filter (750SP), and optical parametric amplifier (OPA).

Figure 7. Photo of rebuilt SF spectrometer (FL arm not shown).

In addition to a complete rebuild, optical elements were added to the beam paths to allow for redirection of the light sources to the hybrid instrument. As indicated in Figure 6 three flip mirrors (dotted outlines, FM3-5) may direct three alignment lasers to follow the optical path of the SFS excitation beams and the SFG beam. These are extremely necessary as directly viewing the SFS-VIS beam is hazardous, and the SFS-IR beam is not visible to humans. Two additional flip mirrors (FM1 and FM2) either reflect the excitation beams to the Neivandt sample stage or pass them to the hybrid MRI microscope.

Because the hybrid microscopy and SF excitation lasers reside on separate optical tables an investigation of beam stability on the MRI table, relative to the Neivandt table, was performed. If the SFS excitation beams were found to be excessively unstable, or wander significantly on short time scales, additional stabilization would be required. Beam stability across the two tables was assessed using the SFS-IR alignment laser. The SFS-IR alignment laser was allowed to trace the path of the SFS-IR beam onto the MRI table and the stability was assessed by imaging with a CCD camera at three locations along the beam path. At each of the three camera positions along the beam path, the CCD was set to image the SFS-IR alignment laser every two seconds for fifteen minutes. Image analysis was used to determine the mean and time-dependent angular displacement ((3.23±1.91)μrads, (2.72±1.60)μrads, and (3.38±1.85)μrads, respectively). Based on these results no further stabilization was implemented.

IV. COMBINED SF AND FL INSTRUMENT

A. Hardware

As mentioned above, an inverted microscope base (Olympus, IX71) serves as the hybrid microscope's main body with FL excitation and collection from below and SFS excitation and collection from above. The overall instrumental setup is presented in Figures 8 and 9. FL excitation beams pass through a computer controlled shutter and into the rear port of the IX71. From there a dichroic mirror directs the beam into the back aperture of the microscope objective focusing it to a diffraction limited spot at the sample while a flipper mounted lens at the rear port allows wide-field illumination for sample positioning. Due to the longer working distance requirements imposed by the sample holder an Olympus 40X 0.65NA PLAN N infinity corrected objective lens corrected for No. 1.5 thickness cover glass is employed. FL is collected through the same objective, passes through the dichroic mirror and a bandpass filter, and out the side port of the microscope. Collected FL is sent directly to a fiber coupled APD, via a flipper mirror, to an EMCCD camera for wide field imaging/sample positioning. Atop the microscope body and course XY scan stage resides a high resolution piezo scan stage (Nano T115; Mad City Labs; Madison, Wisconsin). The scan stage is operated in closed loop mode and is controlled by computer. The scan stage has 100μm of travel in X and Y (lateral) directions and a maximum 50μm range in Z (axial) with 0.2 and 0.4nm resolution respectively. The piezo scan stage scans the sample for both FL and SF imaging.

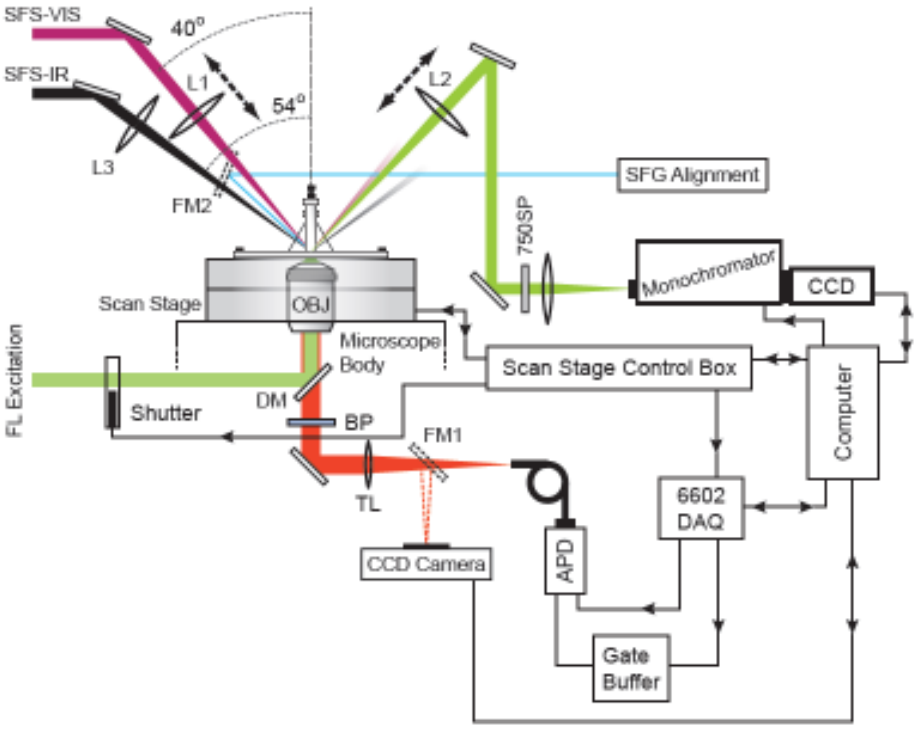

Figure 8. Hybrid SF/FL microscope hardware setup.

Figure 9. Photo of hybrid SF/FL microscope hardware setup.

Visible in Figure 9 are vertical breadboards coupled to the IX71 base which facilitates SFS excitation and collection. The beams are directed up while en route from the Neivandt to hybrid microscope table. Both beams are directed to the center of the sample stage, accounting for deviations due the equilateral prism (described below), and are focused by a 150mm focal length CaF2 lens and an uncoated 100mm focal length BK7 lens for SFS-IR and -VIS respectively. The SFS-VIS focus lens is additionally mounted on an axial translator for fine focus adjustments. (It was experimentally determined that SFS-IR focus is also critical for strong SFG, an additional axial translator for this lens would be a good future addition). For work at the air-solid interface SFS-TIR theory suggests incident beam angles at, or just below, the critical angle will maximize SFG. As such an SFS-VIS incident angle of 40° with respect to the table normal, resulting in an internal incident angle of 46° at the CaF_2 air interface (2° below the critical angle), was employed. Hardware mounting limitations resulted in the SFS-IR beam incident at approximately 53° with respect to the table normal resulting in an internal incident angle 10° beyond its critical angle in CaF_2.

SFG signal was collected by at 175mm focal length BK7 lens positioned at the detection angle predicted by the K-matching condition, one focal length away from the sample. Like the SFS-VIS lens the SFG collection lens is mounted for axial translation and collection optimization. The collected SF signal is directed through a 700 short pass filter (Part number;

Thorlabs; Newton, NJ) and focused with a 100mm focal length lens the entrance slit of a spectrograph consisting of a monochromator (2300, Princeton Instruments) and an EMCDD camera (1024 ProEM, Princeton Instruments). A flipper mirror in the excitation path allows an additional laser to reflect from a metalic substrate, in place of the prism, and into the detection path, simulating the SFG's path, for alignment.

B. TIR-SFS/FL Sample Holder

Like Raman, SFG is a relatively weak phenomena and direct detection without en- hancement is rarely employed. The two most common enhancement mechanisms for SFS are reflective metallic substrates, similar to SERS in Raman, and total internal reflection. These modes thus dictate sample cell design. We require something amenable to confocal fluorescence from below (due to the inverted microscope base) and SF excitation from above. Clearly enhancement from a thick metallic substrate would be a poor choice as it excludes FL imaging, leaving TIR as the viable choice. The ability to image using SFG further requires an experimental geometry amenable to sample scanning eliminating two obvious prism choices, hemi-cylinder and hemi-spherical. An equilateral prism, however, should meet the design criteria; it allows for TIR and sample scanning without grossly affecting the SFS excitation beam's incident positions on its inner surface. Thus an equilateral 1" CaF_2 prism (ISP Optics, Irvington, New York) is employed for SFS imaging. A custom sample cell for prism TIR, from above, and confocal imaging, from below, was fabricated as illustrated in Figure 10.

The use of TIR and the prism interface, is a departure from the original proposal were a much more complicated assembly of CaF_2 meniscus lenses was proposed as a means of improving resolution of the SF method. While this approach still remains possible, it was necessarily abandoned due to the general lack of availability of the necessary optical elements following closing of the few commercial vendors. While the TIR/prism method exhibits limited spatial resolution, the dramatic reduction in background and increase in signal allows for more rapid image acquisition, a significant downside of the originally proposed design.

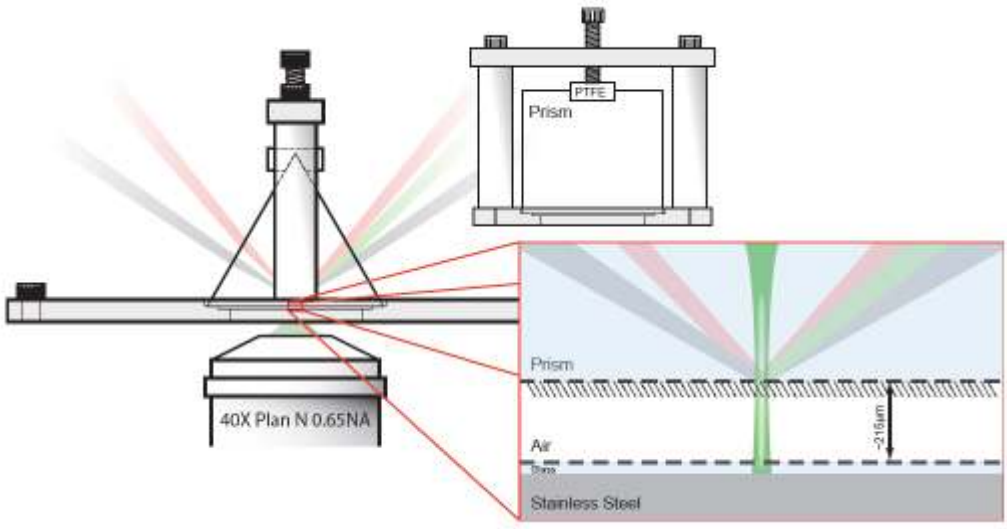

Figure 10. Side view of the custom TIR-SFS/FL sample holder (A) and 90° rotated from (A) side view.

B. Software

The basic data acquisition approach of the hybrid microscope is one of synchronous point-by-point data acquisition, as illustrated in Figure 11. Briefly, 2D images are obtained by raster scanning the sample through a series of software controlled positions, collecting SF and FL information at each location. Unlike traditional FL imaging, each pixel has multidimensional data which is post processed by the user. Control of the microscope is accomplished with a custom built LabVIEW control program. Much effort has been expended to make the MRI control program intuitive and simple. Whenever possible operations have been automated and all initialization/ shutdown routines are performed without the need for user input. The program is composed of one primary interface screen with two additional screens, one for CCD camera and monochromator setup/control (Figure 14) and the other for manual stage positioning, live count rate from the APD, and sample focusing (Figure 13). Unlike many LabVIEW programs that employ an infinite loop to keep the program running, which unnecessarily hogs processor time and slows the computer down, the hybrid microscope's control software uses event based architecture.

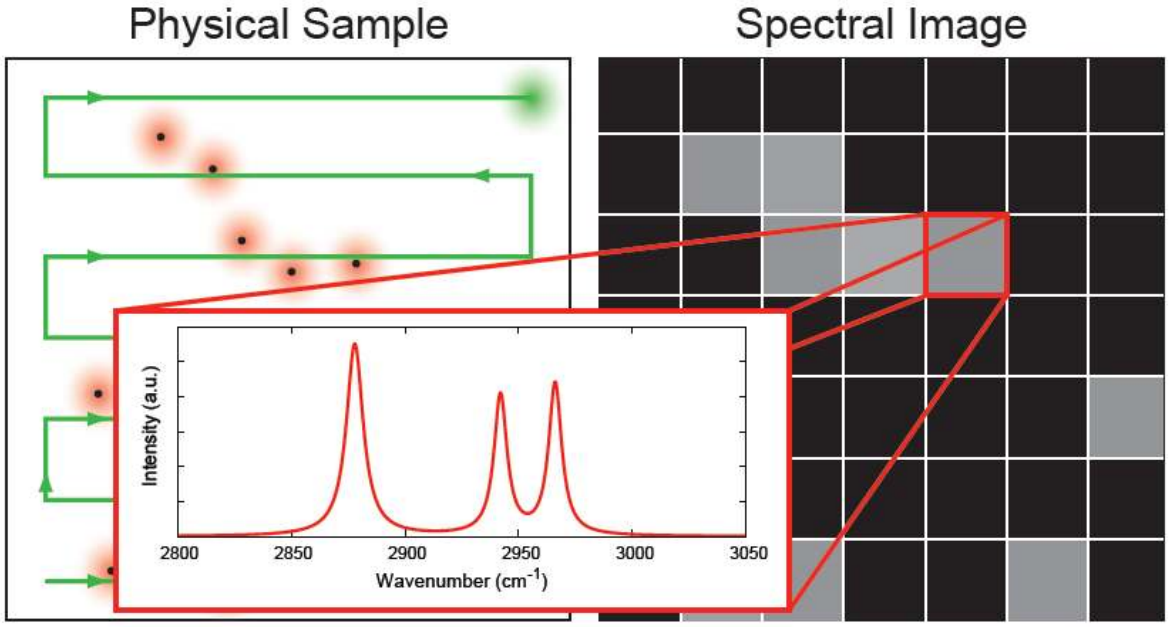

Figure 11. Depiction of sample raster scanning and data acquisition of the MRI hybrid instrument.

At the center of the primary screen is a large display showing acquired images and real-time acquisition progress (Figure 12). Above the primary image display is a plot that dynamically changes based on the acquisition being performed; it automatically shows the confocal line scans or SF spectra as they are being acquired, for example. To the left of the central display are indicators allowing easy checking of relevant setup parameters. These show if

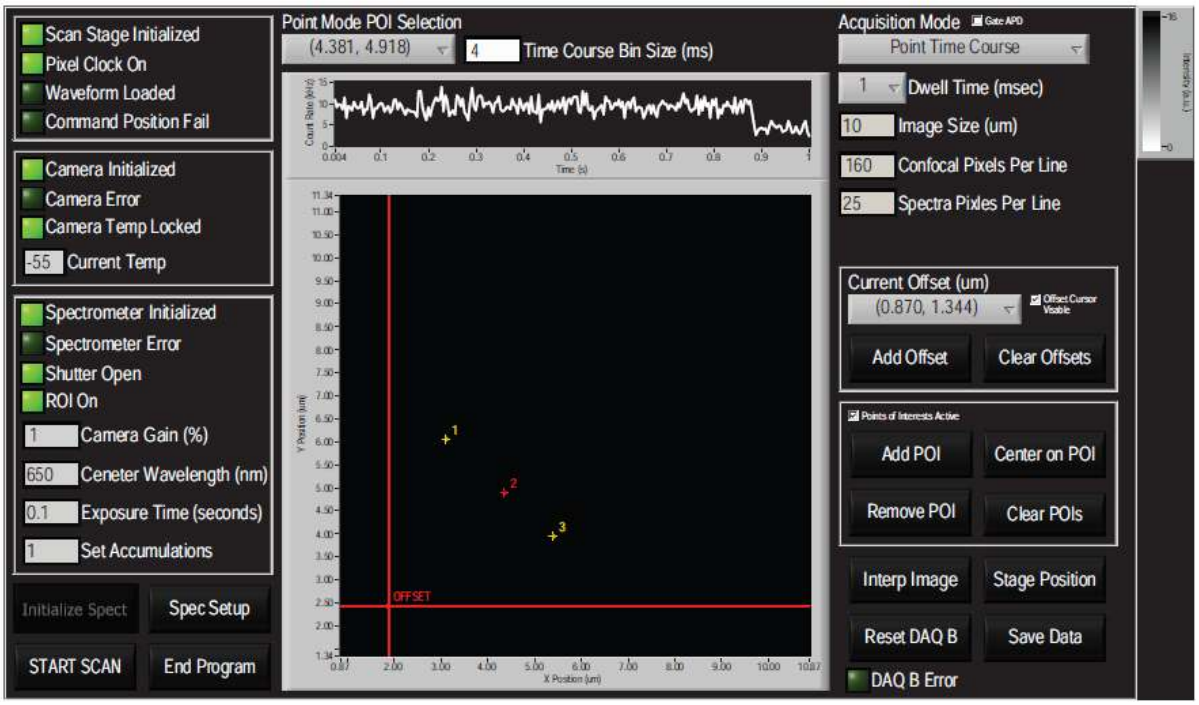

Figure 12. Primary acquisition display screen.

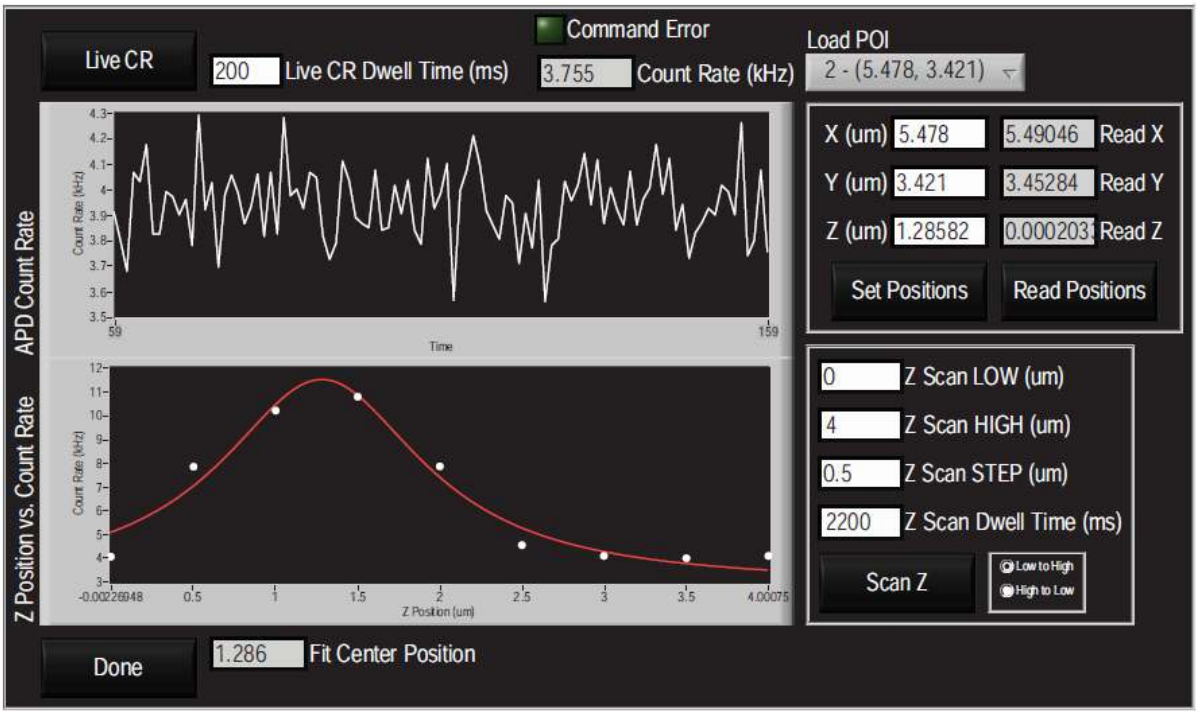

Figure 13. Manual stage positioning, live count rate from the APD, and sample focusing control panel.

the scan stage has been initialized, if the pixel clock is on, if the waveform is loaded, if the stage has failed to reach the commanded position, if the camera is initialized, if the camera temperature is stable, what the current camera temperature is, if the camera, spectrometer, or if the data acquisition (DAQ) board have reported errors, if the camera shutter is open, if a specific region-of-interest (ROI) has been set on the CCD, what the camera's reported EM gain is, the current CCD exposure time and accumulations, and the spectrometer's reported center wavelength. To the right of the primary display a drop down menu allows selection of the acquisition mode and numeric input fields allow specification of imaging parameters. Currently, the supported acquisition modes are confocal imaging, spectral imaging, confocal and spectral imaging, point time course and point spectum modes. These modes, along with the function of the primary and secondary screen's remaining elements will be detailed in the rest of this section (the only element not covered is the "Reset DAQ B" button which simply resets the DAQ board should an error arise).

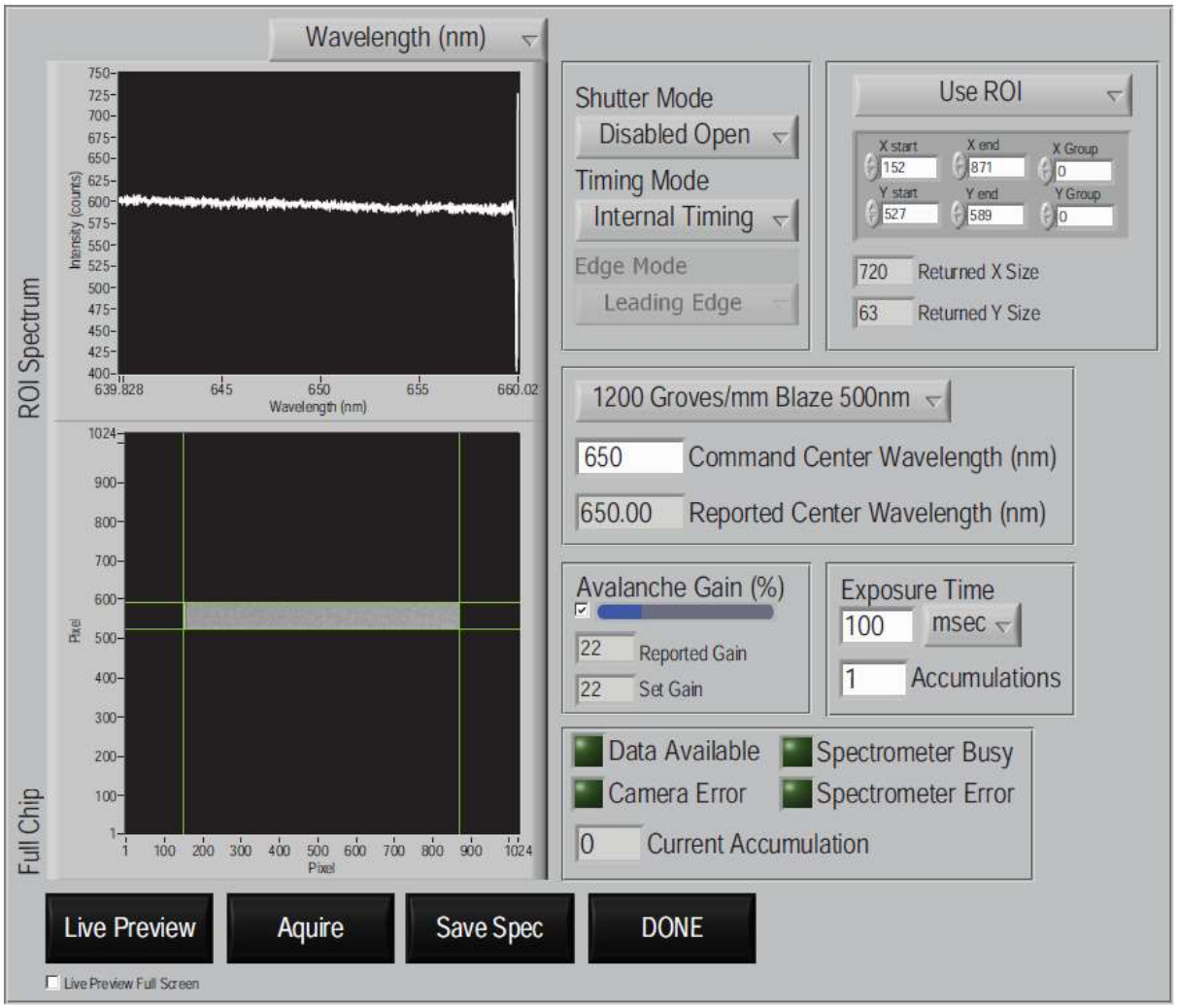

Figure 14. CCD camera and monochromator setup/control display.

C. Metrics / Standards

Calibration of the scan stage was verified by confocal reflectance imaging of a scanning electron microscope calibration standard (C1500-AB, SPI Supplies, West Chester, Pennsylvania) (Figure 15). This calibration sample is fabricated from pure silicon with a uniform lattice of orthogonal 1.9μm±5% wide grooves etched by electron beam lithography and spaced 10μm apart. Pure flat silicon is highly reflective and imaging was accomplished by collecting a small amount of reflected laser light from the sample. Interpolated images of the SPI standard are presented in Figure (3.11) and suggest the scan stage and all image acquisition components function correctly. As an additional test 20nm fluorescent beads (F8784, Invitrogen, Carlsbad, California) were imaged via wide-field excitation using a CCD camera and fluorescent confocal microscopy as presented in Figure 15. Good agreement between the confocal and wide-field images is clear from Figure (3.12) further demonstrating correct operation of the confocal imaging setup. Despite correct functioning confocal scanning hardware the potential affects of imaging with the highly sensitive APD while the SFS excitation beams are also incident on the sample must be considered.

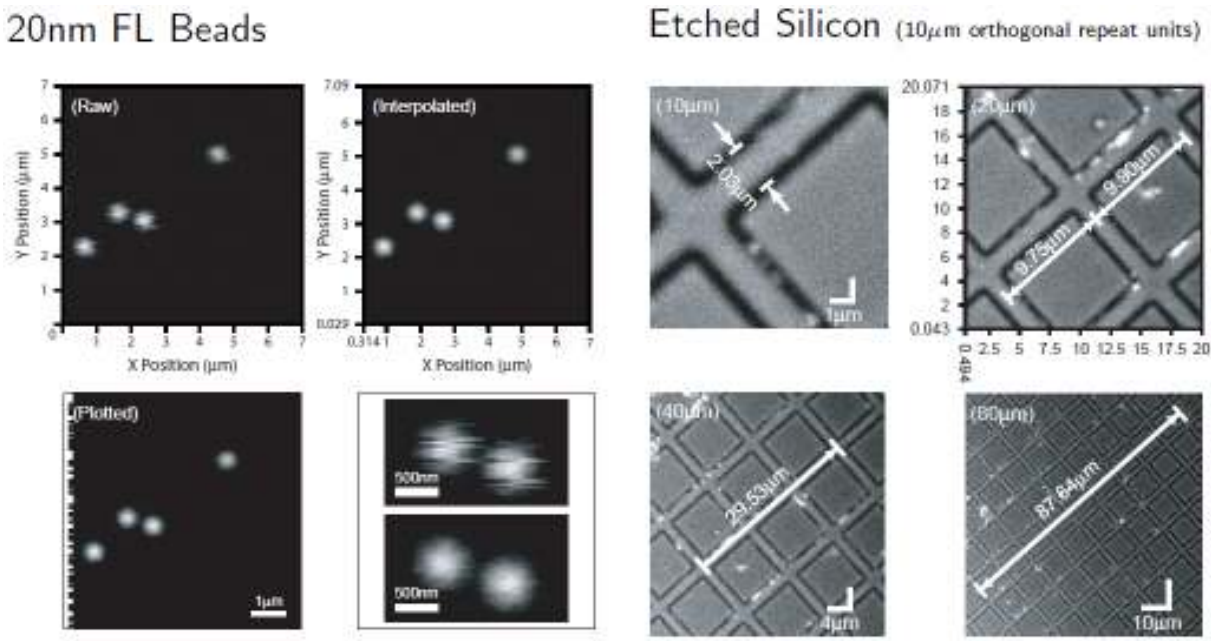

Figure 15. Scan stage fluorescence (left) and reflectance (right) calibration standard (left).

For assessment of the SF and FL capabilities of the instrument, a somewhat more complicated series of standards were created. These standards were composed of a series of etched void structures in a thin gold layer deposited on glass (Figure 16). The gold is known to generate a broad non-resonant SF background signal, and can be used to simultaneously generate a laser reflectance image in the confocal FL detection path (Figure 17). Alternatively a single layer of octadecane thiol (ODT) (bound to gold) was used to generate a well known SF signal.

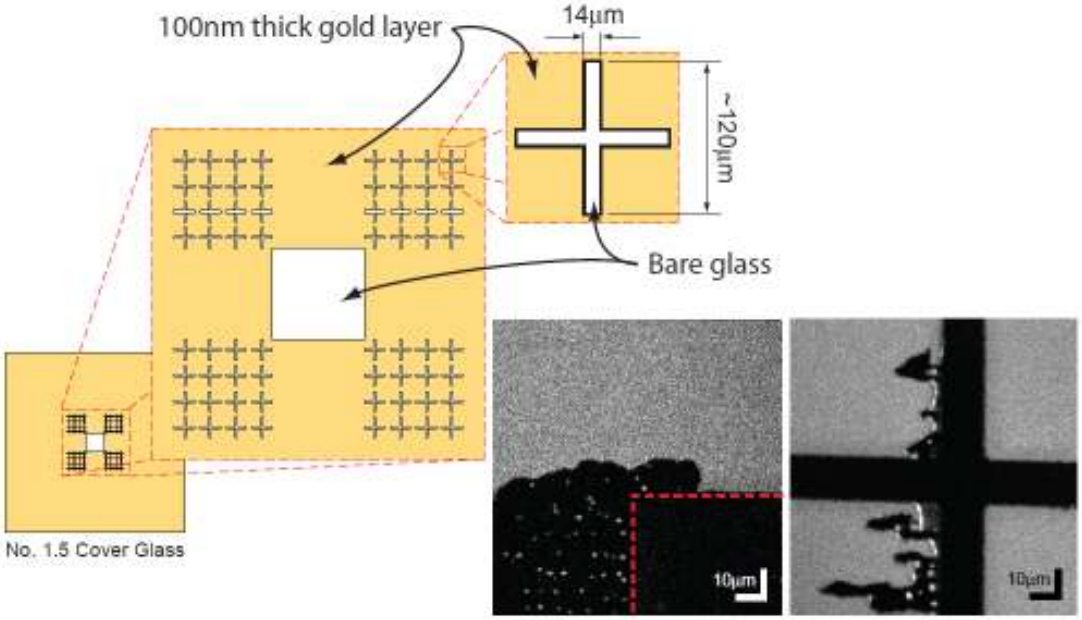

Figure 16. Gold patterned SF/FL standard. The image insets show the effect of laser ablation when the instrument is operated at elevated pump power.

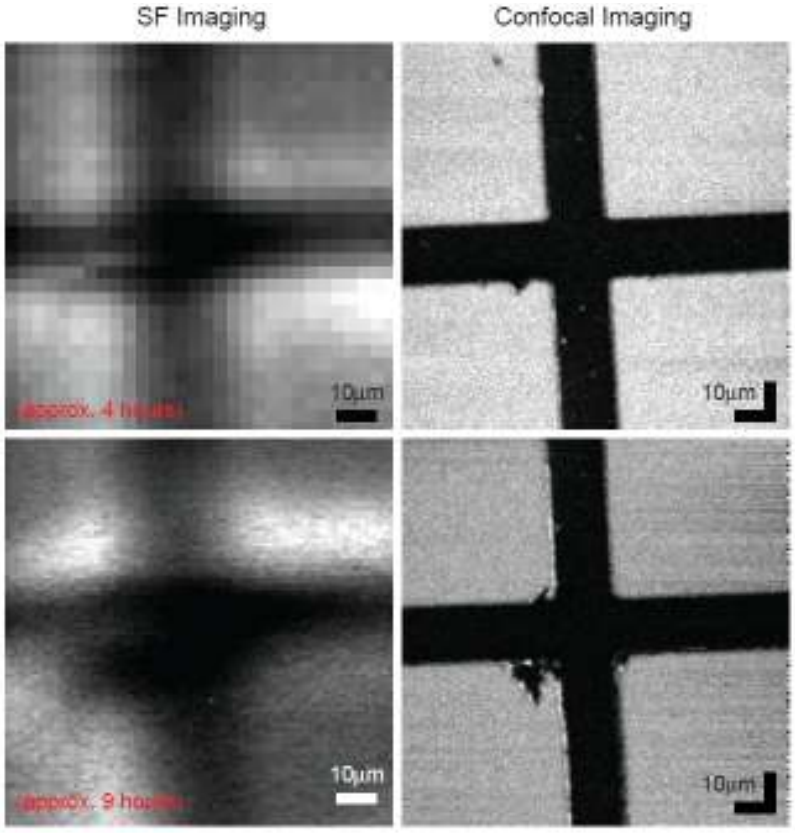

Figure 17. Simultaneous SF (ODT) and FL images acquired for the patterned gold standard (top). The same sample is reimaged at increased pixel resolution (bottom).

V. CAPABILITIES AND SAMPLE DATA

A. Spectral and Confocal Imaging Results

In addition to the patterned gold substrate described above, a second biologically interesting test sample was constructed consisting of a fluorescently labeled phase separated lipid monolayer deposited directly on the afore mentioned CaF_2 prism. Fabrication of this sample followed from an investigation of phase separation in lipid monolayers. 1,2-dilauroyl-*sn*-glycero-3-phosphocholine (DLPC), with a main phase transition temperature of -1°C, and 1,2-distearoyl(d70) *sn*glycero- 3-phosphocholine (perdeuterated DSPC, referred to as dDSPC herein), main phase transition temperature of 55°C, were mixed, doped with the fluorophore 1,2-dimyristoyl*sn*- glycero-3-phosphoethanolamine-N-(lissamine rhodamine B sulfonyl) (ammonium salt) (Rho-PE)(Avanti Polar Lipids, 810157), and deposited via the Langmuir-Blodgett technique. Wide field microscopy revealed apparent domain formation presumed to be that of solid phase (at room temperature) dDSPC, while the DLPC (liquid phase at room temperature) appeared uniformly distributed outside the domains (Lin *et al.*, 2006; Ratto & Longo, 2002) with the Rho-PE separating into the liquid phase DLPC (Crane & Tamm, 2004). Deposition conditions (subphase temperature, and deposition pressure), Rho-PE concentration, presence/concentration of cholesterol, and dDSPC to DLPC ratios were varied and their affects on domain size tracked. Ultimately a 1:1 DLPC to dDSPC mixture doped with 0.0005mol% Rho-PE and deposited at 35mN/m with a subphase temperature of 26°C was found to yield

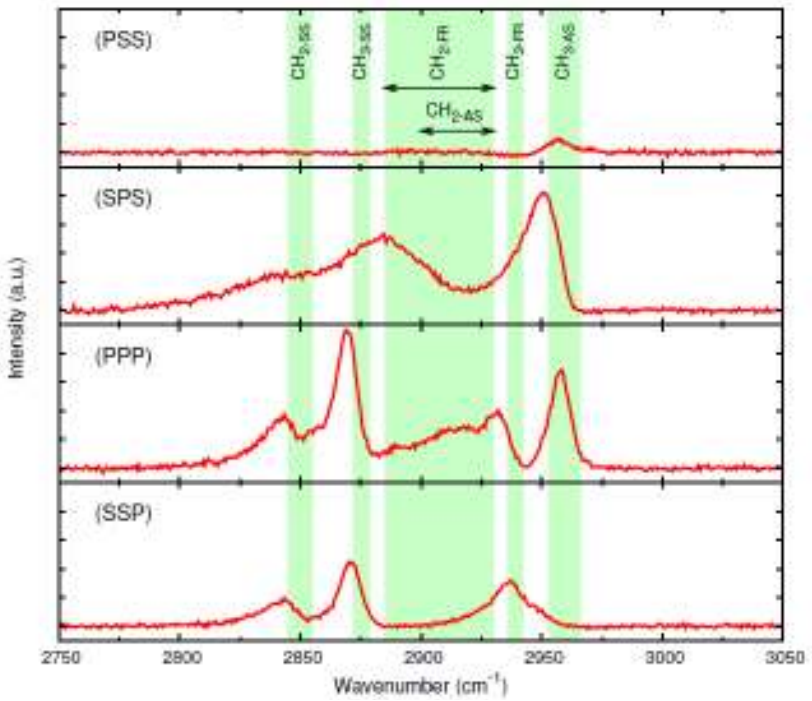

Figure 18. Background subtracted SFS-TIR spectra of a DLPC monolayer at the air-solid interface. All four spectra were acquired under identical conditions while the SF excitation polarizations were varied (1 min. integration time). The intensity on each y-axis is identical allowing comparison of the relative intensities of polarization combinations. The shaded boxes indicate the high and low limits for peak assignments found in literature where the vibrational modes are indicated at the top of the plot. The CH2−*FR* and CH2−*AS* modes overlap and the ranges of each have been indicated with arrows.

clusters of large phase separated solid phase dDSPC domains, while the Rho-PE remained mixed within the liquid phase DLPC. As perdeuterated material is inactive in the CH stretching region, the phase separated dDSPC will not generate SF signal. Because Rho-PE resides in the DLPC, which is active in the CH stretching region, this sample should yield matching SF and FL images with domains easily visualized by both. As such 1:1 DLPC to dDSPC, with 0.0005mol% Rho-PE monolayers, deposited by LB deposition with the above mentioned trough parameters were fabricated on the CaF_2 equilateral prism for instrumental validation and testing.

Example TIR spectra of DLPC, in the CH region, are presented in Figure 18. Spectra show excellent signal to noise despite a relatively short integration time (1 min.). The peaks evident in the spectra of Figure 18 are seen in the spectra of individual pixels, in the spectral images and should be considered representative. Although the peaks are close to the literature values they clearly fall on the edges of the respective ranges given by the high and low values as presented in Figure 18. Aside from the possibility that this is related to the spectral/temporal profile and delay of the SFS excitation pulses, two obvious factors can account for variation in the vibrational modes: the presence of Rho-PE and depositing the DLPC while in the fluid phase, as opposed to the highly ordered solid phase. A less ordered environment would clearly result in different interaction forces subsequently altering the vibrational modes of the methyl groups. In fact, the presence of methylene peaks in the spectra presented in Figure 18 is clear evidence of a less than ideally ordered monolayer.

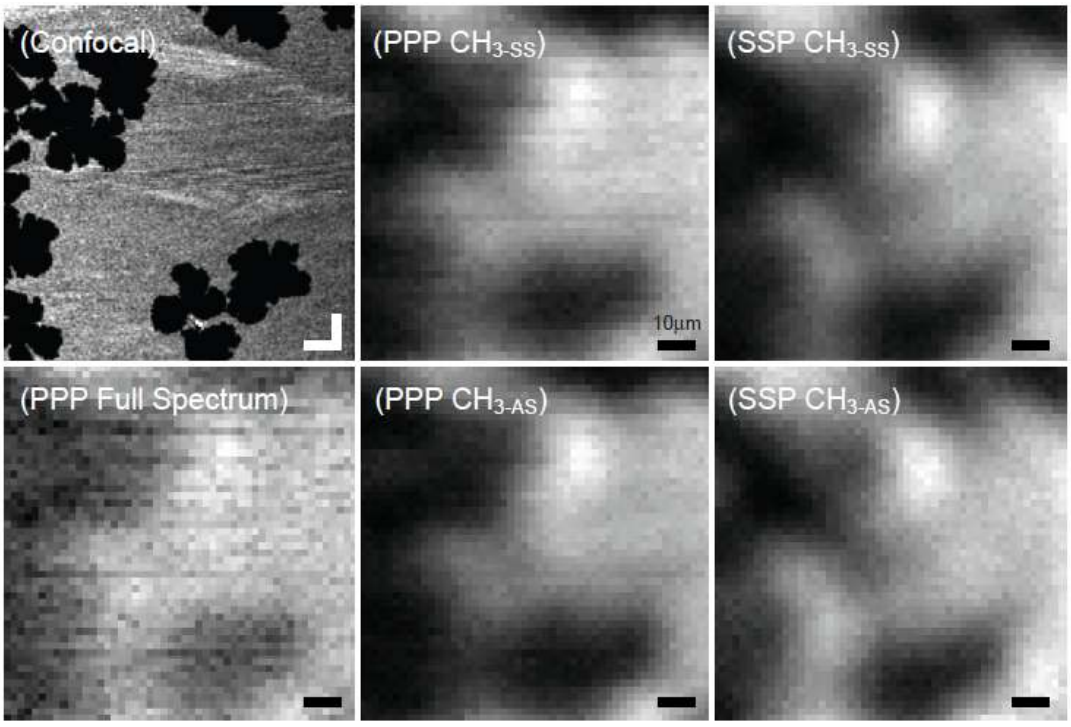

Figure 19. (A) Confocal image of DLPC/dDSPC monolayer on a CaF2 prism and the same area imaged using SF microscopy (B)-(F). Specifically (B) presents the results of integrating the entire spectrum at each pixel to assign a pixel value while (C) and (D) utilize the methyl symmetric and asymmetric stretch modes, using the PPP polarization combination, respectively. Images (E) and (F) likewise show the methyl symmetric and asymmetric stretches respectively with the SSP polarization combination employed. Scale bars are all 10μm.

Images from SF-TIR and confocal FL acquisitions are presented in Figure 19 and clearly demonstrate SF images that closely match the corresponding confocal FL images. In some cases the images are of slightly differing regions, however, features seen in the confocal images are clearly distinguishable in the accompanying SF images. Each pixel in the SF images can be derived from a full SF spectrum acquired at that location on the sample, or generated from specific spectral regions. Thus we may choose which spectral features should be used to set the pixel values. In all the SF images presented here each pixel value results from integration of either the CH3 symmetric or asymmetric stretch mode (with a width of 0.5nm centered around the peak's maximum value). Although the image is discernable for the entire SF spectrum (integrated) it is not particularly clear in contrast to images derived from the same data but with either the methyl symmetric stretch or asymmetric stretch integration used for the pixel value. Figure 19 also shows a detectable difference between images acquired using either the PPP or

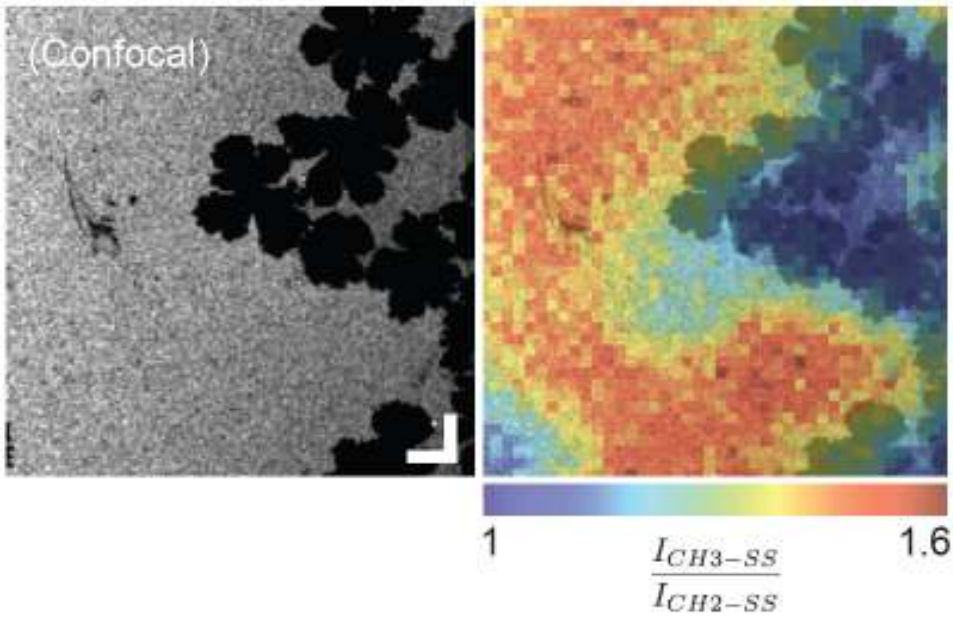

Figure 20. Confocal FL image of phase segregated Rho-PE (left). (Right) Hybrid image of SF determined lipid order (colorized) overlapped with FL data.

SSP polarization combinations. This suggests that not only is spatially resolved vibrational information present but further information, e.g. the spatial distribution of mean tilt angles, can be elucidated. All images are displayed on a linear scale ranging from the image's maximum (white) to minimum (black) value.

Possibly the best demonstration of the utility of the hybrid microscope is the simultaneous display of SF and FL information. This is accomplished, for example by comparing the intensity of CH_3 and CH_2 modes (a measure of relative order), and overlapping this information with the confocal (Rho-PE) data, as shown in Figure 20. Immediately, previously unforeseen spatial correlations, and interesting anti-correlations between phase separated and ordered regions are observed. The specific implications of this data are still being

considered (manuscript in progress). The data in Figure 20 are unique to this instrument and suggests successful completion of this MRI project. Future experiments will generate data of this form for other scientifically relevant sample types.

B. Instrument Resolution

The SFS-VIS has been observed to be well above the diffraction limit and subsequently its size could be measured direct or indirectly, e.g. photo bleaching a uniform dye film or by imaging with a CCD camera. However, the SFS imaging resolution is not a function of the SFS-VIS beam alone. Clearly the overlapping SFS-IR and -VIS beams define the spatial sensitivity of the system, the effective SFS excitation area. Were the SFS-VIS and SFS-IR beam sizes both known a reasonable estimate of the signal generating region could be made. This could, in turn, allow for an estimation of the SFS imaging resolution. Unfortunately direct measurement of the focused SFS-IR beam is not possible. Here we employ three methods for spectral imaging resolution estimation: an adapted knife edge method, simulation of an SF image with defined step edges, and finally direct visualization of the SFS-VIS beam. The results of this analysis are shown in Figures 21 and 22.

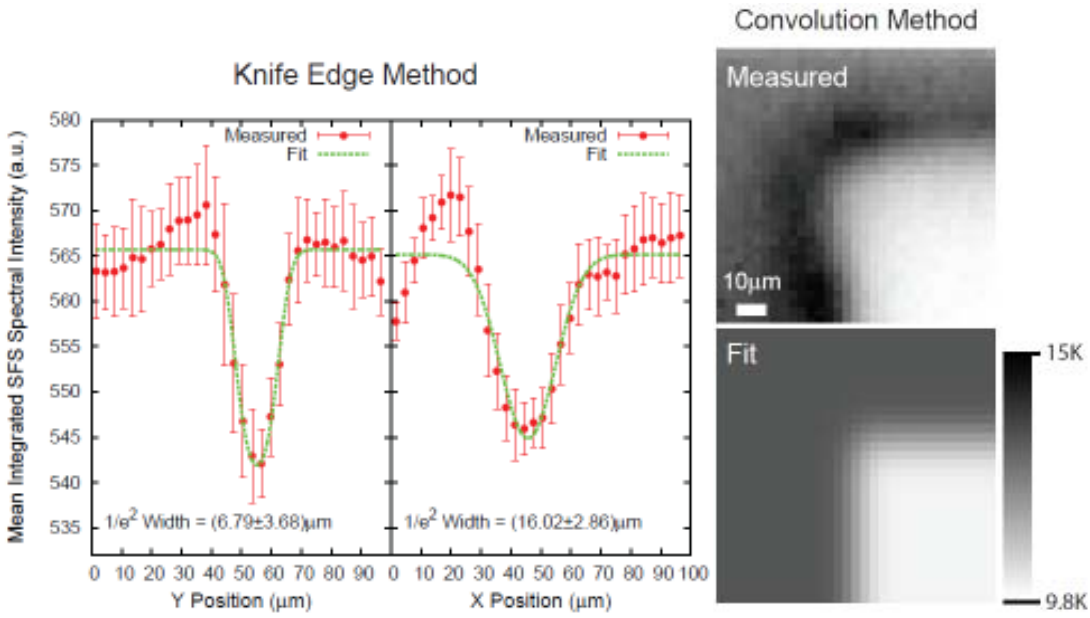

Figure 21. Line feature scan through SFS excitation beams fit with Equation (X) for the (A) Y and (B) X dimensions. Fitting yields 1/e2 radii of (16.02±2.86)μm and (6.79±3.68)μm in the X and Y dimensions respectively which is consistent with the observed elongated dimension of the SFS-VIS beam in the X dimension.

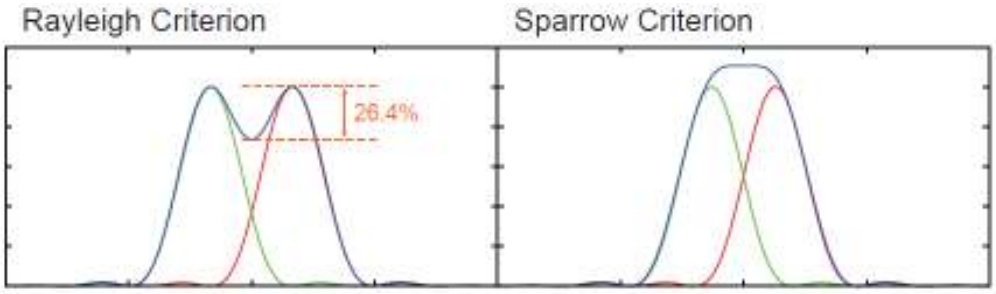

Method	Dimension	Diameter (μm)	Rayleigh (μm)	Sparrow (μm)
Convolved	X	12.77±1.11	17.88	14.06
	Y	12.55±1.12	17.57	13.854
Knife Edge	X	16.02±2.86	22.43	17.68
	Y	6.79±3.68	9.51	7.49
SFS-VIS Fit	X	22.37±5.05	31.32	24.69
	Y	16.62±7.40	23.27	18.348

Figure 22. Line feature scan through SFS excitation beams fit with Equation (X) for the (A) Y and (B) X dimensions. Fitting yields 1/e2 radii of (16.02±2.86)μm and (6.79±3.68)μm in the X and Y dimensions respectively which is consistent with the observed elongated dimension of the SFS-VIS beam in the X dimension.

VI. CONCLUSIONS AND FUTURE PLANS

Here we have detailed the construction and function of a hybrid SF/ FL spectral imaging sample scanning microscope as applied in both a reflection and TIR geometry. A number of test samples were investigated the results of which clearly illustrate the power of this new hybrid instrument. This one-of-a-kind instrument is now capable of generating unique data combining the capabilities of SF and FL and represents successful completion of this MRI project.

Although the proof of principle is now clear, a number of improvements would further benefit the system. On exiting the SSPS, clear spatial irregularities can be easily seen in SFS-VIS mode. Attempts were made at spatial filtering using high energy pin holes (5-50μm) but were found to have negligible affect (they either burned or were to large). As such implementation of a polarization preserving, low dispersion single mode, fiber optic could clean up the beam profile while simultaneously providing a simple method for delivering the beam to the hybrid microscope with greatly reduced risk of laser eye damage (the fiber would provide a closed beam path and allow the beam to be conveniently launched and sized on the microscope breadboard, additionally reducing table clutter).

While the Princeton Instruments EMCCD camera has proven sufficient for TIR- SFS collection, it lacks the extremely fast electronic shutter employed on the PI-Max camera. The PTG timing option on the PI-Max camera allows extremely low shutter and trigger delay times, on the order of hundreds of nanoseconds. Typically shutter times employed on the Neivandt SFS system are 250μs. The SSPS output is in the picosecond regime while the SFS-IR pulse width remains in the femtosecond. Clearly, even thought the PI-Max camera is shuttered on the scale of nanoseconds its exposure time is still three orders of magnitude larger than SF emission duration

per pulse. Unfortunately the ProEM camera employed for the hybrid microscope's spectral detection lacks the fast shuttering capabilities of the PI-Max camera. The ProEM camera runs in shutter mode, most often with exposure times above 1 second (certianly faster exposure speeds can be set but the ProEM camera cannot achive the 1kHz frame that would be required regardless of exposure time). In this case the ratio of shutter open time to actually signal generation time is extremely large. For an exposure time of 1 second with a 1kHz pulse repetition we assume signal is generated for 1 picosecond for each pulse, meaning SF light is collected by the camera for only 0.000001% of the exposure time. The remaining 99.999999% of the exposure provides no further signal but does allow collection of background noise. Switching to a fast electronically shuttered camera has the potential to greatly reduce the noise collected during spectral acquisition which, in turn, could allow for shorter acquisition times and subsequently much shorter spectral imaging times. The scanning apparatus employed here is limited to scanning a 100μm square. Although this is ideal for many samples, there are likely as many other systems for which a large scan area would be more applicable. In light of the instrument's current resolution a larger scanning area may prove a better match. Replacing the course, manually posi- tioned, XY stock Olympus scan stage with a stepper motor driven stage would allow for easy large area SF imaging. Additionally, the existing scan stage could be easily mounted on top of a large scanning stage for high resolution investigations of ROIs without the loss of FL imaging capabilities. This would allow conformational order over very large sample areas to be studied (something not currently found in the literature).

VII. BROADER IMPACTS / OUTREACH ACTIVITIES

To date 16 undergraduate students and 4 graduate students have been involved in this project. The graduate students involved have now completed advanced science degrees in Physics and Chemical Engineering. The 16 undergraduate students are pursuing bachelors degrees in Physics, Chemical Engineering, and Biological Engineering.

In conjunction with this cutting edge project educational and outreach programs were developed demonstrating to an audience of high school students and educators the capabilities of the proposed instrument as well as the importance of new instrument development to the broader research community. Through this program nearly 150 high school students have participated in a one day directed research experience, and 4 high school students and 2 science teachers participated in a two month NSF supported research program, and an additional 6 high school students have participate in related research based on an internal matching grant.

Over two summers (2008, 2009) a Master of Science and Teaching (MST) Student (Erik DeSilva) was hired in conjunction with this MRI development project to specifically develop 1) course curricula/teaching modules for a new Biological Engineering Instrumentation and Advanced Methods Course, 2) development of high school outreach activities and curricula including on-campus research experiences (BEAR Program http://www.umche.maine.edu/bear/). Funding for this position was provided by UMaine Sponsored Programs in response to the proposed MRI funded outreach and educational activities. In addition, this student has completed a high school classroom teaching module which he has implemented on a trial basis.

Also completed are the two halves of the online description of the technology development, including the underlying photophysics, associated with this project. This can be found online at: http://www.physics.umaine.edu/FPALM_SFS_NOV09/sfs.html.

REFERENCES

[i] Florsheimer, M.; Brillert, C.; Fuchs, H. "Chemical imaging of interfaces by sum frequency microscopy" *Langmuir* **1999**, *15*:5437-39.

[ii] Florsheimer, M.; Brillert, C.; Fuchs, H. "Chemical imaging of interfaces by sum-frequency generation" *Materials Science & Engineering C-Biomimetic and Supramolecular Systems* **1999**, *8-9*:335-41.

[iii] Kuhnke, K.; Hoffmann, D. M. P.; Wu, X. C.; Bittner, A. M.; Kern, K. "Chemical imaging of interfaces by sum-frequency generation microscopy: Application to patterned self-assembled monolayers" *Applied Physics Letters* **2003**, *83*:3830-32.

[iv] Cimatu, K.; Baldelli, S. "Sum Frequency Generation Imaging Microscopy of CO on Platinum" *Journal of the American Chemical Society.* **2006**, 128: 16016-16017.

[v] Cimatu, K.; Baldelli, S. "Sum Frequency Generation Microscopy fo Microcontact-Printed Mixed Self-Assembled Monolayers" *Journal of Physical Chemistry. B* **2006**, 110: 1807-1813.

Final Report on NSF Award No. CHE-0722759: MRI: Development of a Hybrid Scanning Fluorescence and Sum Frequency Spectroscopy Imaging Microscope

Edward S. Allgeyer[2], Samuel T. Hess[2], Michael D. Mason[1], David J. Neivandt[1], Sarah M. Sterling[1], Mudalige Gunewardene[2]

[1]Department of Chemical and Biological Engineering, University of Maine, Orono, ME 04469
[2]Department of Physics and Astronomy, University of Maine, Orono, ME 04469

Abstract

This MRI project was focused on developing a hybrid scanning fluorescence (FL) and sum-frequency (SF) vibrational spectroscopic microscope. Now completed, the microscope will expand the capabilities of the nation's research infrastructure by combining the benefits of two powerful imaging and spectroscopic techniques. This combination enables the direct correlation between localized or distributed photophysical (FL) molecular properties and the structure of the environment (SF). In its current form the instrument has diffraction limited resolution in the fluorescence channel (~250 nm), and ~10 μm resolution in the sum-frequency channel. The instrument is capable of obtaining 2D (or 3D) image sets comprised of single pixel fluorescence information and complete (1024 pixel) high resolution (< 0.1 cm^{-1}) Sum-Frequency spectra. An additional point probe mode was included which allows for high temporal resolution (<1 ns) fluorescence detection with single molecule sensitivity and simultaneous high spectral resolution sum-frequency detection. The 'particle-in-a-bath' capabilities of the proposed instrument will have utility in biology, biochemistry, materials science, chemistry and physics. For example, it is anticipated that future research conducted with this new instrument will provide breakthroughs in our understanding of membrane and film organization at the molecular level. Sample data illustrating the power of our instrument is presented. Much of the final project description presented here has been excerpted from the outstanding PhD thesis of the primary graduate student working on this project (Edward S. Allgeyer).[1]

I. INTRODUCTION

To further advance the research and educational capabilities of the University of Maine and the Institute for Molecular Biophysics (IMB), we proposed to capitalize on our expertise in sum-frequency (SF) spectroscopy and fluorescence (FL) imaging to develop an instrument with unique capabilities crucial to the study of a broad range of systems from materials to bio-membranes. Ideally, this imaging spectrometer would measure molecular conformations, photophysical properties, and dynamics in a temporal regime which is inaccessible, yet entirely complementary, to existing instrumentation available for our current research efforts.

Sum Frequency (SF) is a vibrational technique based on non-linear optical mixing of photons of two different energies. SF provides detailed structural information on an ensemble of molecules at an interface within an optically-defined sample volume, including absolute orientation and conformational configuration. SF has been used to analyze thin film systems in a number of instrumental geometries including transmitting[i,ii] and reflective substrates.[iii] For example, in two recent publications by Cimatu and Baldelli, SF was used to observe the spatial distribution of CO on platinum surfaces[iv] and chemically distinct regions of self-assembled alkane-thiol monolayers.[v] Fluorescence (FL) spectroscopy

complements SF by providing access to single-molecule properties of individual species within an ensemble of molecules on 10^{-12} s to $>10^{2}$ s timescales. Ideally, both FL and SF methodologies would be employed simultaneously yielding localized dynamics of the single fluorophore (FL), or multiple fluorophores, and spatially correlated structural information about the local surroundings (SF). Additionally, the ability to select phase or structure specific fluorescent molecules allows one to correlate spatial and temporal fluorescence information with structural information regarding the surroundings. This *'particle-in-a-bath'* approach has found limited implementation due to differing optical requirements and inherent difficulties in distinguishing between the two signals; the MRI instrument developed by our group circumvents these issues by exploiting fundamental differences in the optical nature of SF and FL.

In the following sections we describe the individual Fluorescence and Sum-frequency components of the MRI instrument separately, and as a combined tool. It is important to note that our instrument has all of the capabilities of separate FL and SF equipment in addition to the expanded capabilities arising from this unique combination.

II. FLUORESCENCE COMPONENTS

A. Fluorescence Microscope Core

At the core of the combined Sum-frequency and Fluorescence instrument is a standard Olympus IX71 inverted microscope base as shown in Figure 1A. This base was chosen primarily due to its flexibility for multiple light source inputs and signal collection points. This base is widely used for either laser scanning or sample scanning confocal fluorescence microscopy (SCFM). The relatively open inverted design was chosen to allow for Sum-Frequency signal acquisition to occur from the top (epi-) and fluorescence signal acquisition to occur from either the bottom or the top (transmission or reflection modes).

Typical with all SCFM instruments, a laser is directed into the back aperture of a microscope objective which focuses the beam with a tight waist at the focal plane positioned inside the sample. Scattered or emitted light is collected by the same objective and focussed onto a pin hole placed confocally with the illumination spot in the image plane. The confocal pin hole discriminates against light originating from regions of the sample above or below the focal plane or laterally adjacent to the beam waist. This is geometrically apparent as the dotted rays in Figure 1B which are defocused when they reach the pin hole and are largely blocked, although some background light is admitted. Light which does pass the pin hole is detected with an avalanche photodiode (APD) whose signal is recorded by a computer. An image is collected point-wise by either raster scanning the sample and recording the detected light for each illuminated position. Collecting an image at varying axial sample positions generates a stack of 2-dimensional images that may be reconstructed to form a 3-dimensional image.

Although the confocal aperture provides a modest increase in lateral resolution its distinct advantage over wide field illumination and collection is the enormous increase in background suppression yielding greatly improved depth discrimination (Diaspro, 2007); the confocal pin hole restricts imaging to only a small sample slice. Certainly the modest improvement in lateral resolution, up to a factor of $\sqrt{2}$ (Sandison & Webb, 1994; Sandison *et al.*, 1995) is advantageous but alone is not enough to have propelled confocal microscopy into its present position as a virtual standard. Rather the 2-3 orders of magnitude increase in the signal to background ratio (Sandison & Webb, 1994; Sandison *et al.*, 1995), allowing for 3D sectioning and improved image quality, is responsible. Because of its greatly improved surface specificity, it is a clear choice for pairing with interface specific techniques such as sum frequency spectroscopy.

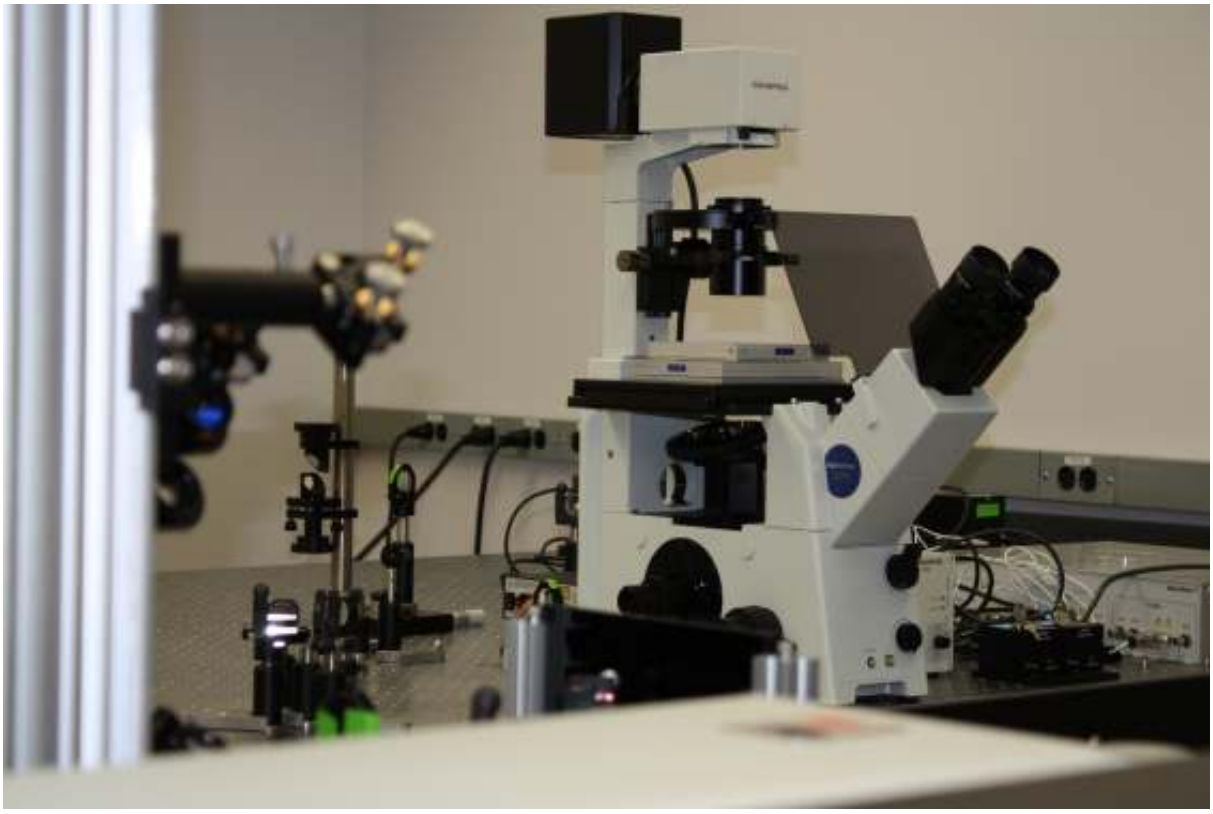

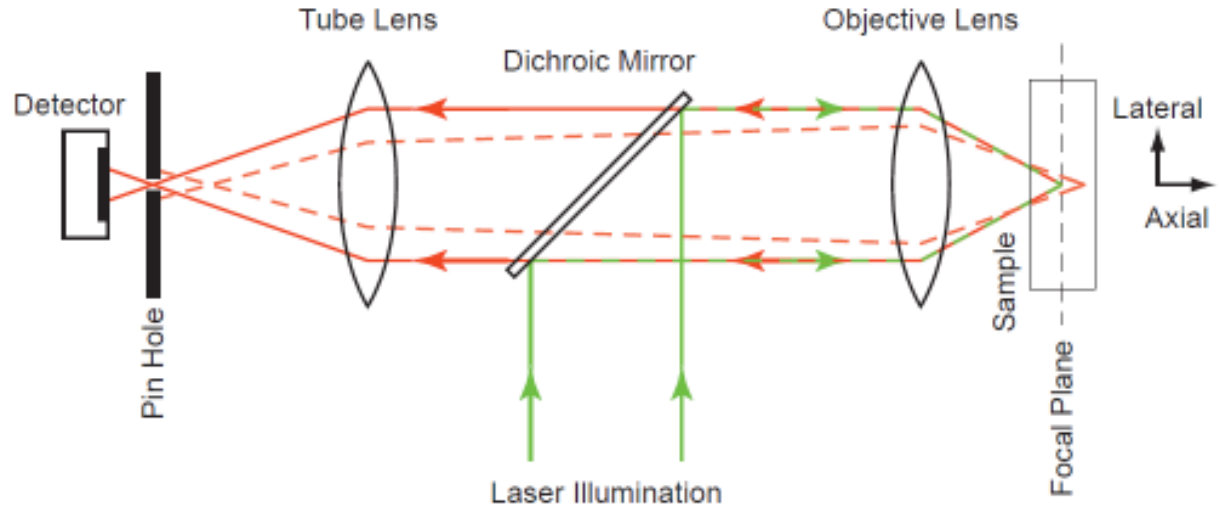

Figure 1. (Top) Basic illustration of a confocal microscope. Laser illumination is directed into the back aperture of a microscope objective with a dichroic mirror and focused inside the sample for excitation. Light is collected with the same objective lens, passed through the dichroic mirror, and is focused by the tube lens through a pin hole onto a photodetector (APD). Light originating outside the focal region (dotted rays) is defocused at the pin hole and largely blocked. (Bottom) Photo of the Olympus microscope body during the initial construction phase of the FL/SF combined instrument.

B. Low Drift Stage and Objective Holder

While the as-purchased XY-translation stage of the Olympus IX71 inverted microscope is considered to have excellent position stability, the rigorous demands of the combined SF and FL instrument required further refinements. Specifically, the z-position of the sample, relative to the excitation and collection optics, is critical to maintain stability in the SF signal and to ensure spatial correlation between the SF and FL information. As such, the factory shipped XY translation stage and objective turret were removed and replaced with a custom built isolation stage and objective mount (Figure 2A). All components of this custom stage were produced at UMaine.

In place of the original XY stage a 12.7mm thick 178 by 240mm block of aluminum was employed. A 32mm square was milled in the middle of the plate to accommodate our custom objective holder (detailed later) and four M6 clearance holes were drilled allowing the plate to be mounted on the IX71 base in place of the Olympus XY stage. Four holes were drilled and tapped for 1/4-20 screw size allowing for the attachment of a large aperture high performance two axis translation stage (Newport Corporation, 406) and our objective holder. Mounted on top of the aluminum plate is the afore mentioned large aperture Newport course XY stage. This stage has a 57.15mm diameter aperture to accommodate our objective holder and 13mm of travel in the X and Y directions allowing the sample to be manually positioned. A three axis piezo scan stage (Mad City Labs, Nano-T115) was mounted, via a connecting plate, on top of the Newport XY stage. This software controlled stage provides the XY motion required for sample scanning during FL and SF data acquisition. Finally, an acrylic sample cell holder that thermally insulates the scan stage from the sample cell sits atop the piezo scan stage.

The objective holder consists of an externally threaded 28.757mm outside diameter stainless steel rod, a brass mounting plate, and a brass lock ring. The brass mounting plate and lock ring have internal threads mated to the external threads of the rod. The stainless steel rod is 88.9mm long and has 76.2mm of external 44 threads per inch (tpi) threads (giving a 577μm axial advance per revolution). The inner diameter of the rod is 0.8 inch with internal RMS threads (20.32mm diameter and 36 tpi) at one end allowing attachment of a microscope objective. The brass mounting plate is attached to the top of the large aluminum plate while the stainless steel rod and lock ring thread in from beneath. Rotation of the threaded rod, accessed from under the aluminum plate, allows the microscope objective to be moved up and down. The lock ring allows the position of the objective to be fixed and the high tpi provides the necessary axial resolution for the objective. Fine tuning of the focus is easily accomplished with the Z-axis of the piezo scan stage. A schematic of the stage and objective holder is given in Figure 2A. With the setup described the sample cell is fixed to the top of the scan stage and the position of the objective relative to the sample is held constant once the lock ring is tightened. Thus, for a given piezo z-position, the critical feature of a fixed distance between the sample and objective is fulfilled while the Newport XY translation stage allows for the equally critical feature of course sample positioning. This level of position stability is often overlooked in fluorescence confocal imaging, and is critical for signal stability in SF techniques involving sample scanning.

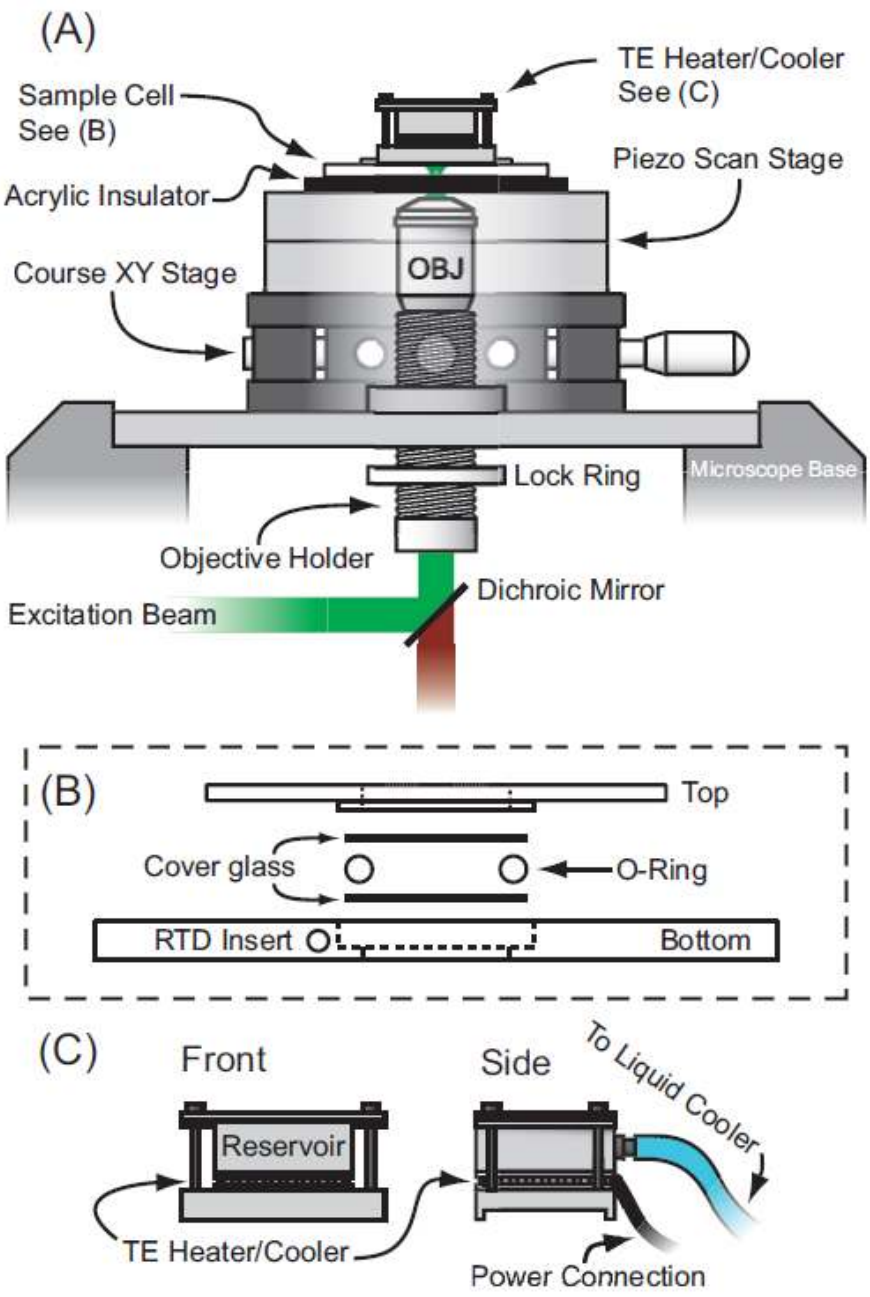

Figure 2. (A) Stage and objective holder as detailed in the text. (B) Liquid sample cell forming a cover glass o-ring sandwich for planar membrane systems. (C) TE heater/cooler sandwiched between circulating liquid reservoir and an aluminum plate that friction fits on top of the sample cell presented in (B).

C. Liquid cell and heater/cooler stage

As many of the samples of interest require a liquid environment as custom liquid sample cell was constructed. The custom built sample cell is composed of two 300 series stainless steel plates, one with a boss (top), and the other with a matching pocket (bottom) as show in Figure 2B. The lower portion of the sample cell is a 4.7625mm thick stainless steel bar comprised of a 22x22mm pocket milled in the center, two 4-40 clearance holes for direct mounting to the scan stage, and a 7.9375mm aperture to accommodate the microscope objective. The upper portion of the sample cell has a boss that fits inside the pocket of the lower portion. The depth of the pocket and height of the boss have been chosen so two No. 1.5 microscope cover slips may sandwich a PTFE coated o-ring inside the cavity and compress the o-ring by approximately 5%. The top portion of the sample cell attaches to the lower portion using four 4-40 stainless steel screws. Stainless steel is employed throughout to allow all parts to be rigorously cleaned. A 3.175mm hole machined into the side of the lower plate of the sample cell houses a friction-fit removable brass rod that penetrates to within 1.5mm of the liquid cavity. A 1.2mm hole machined longitudinally into the brass rod houses a thermistor (RTD) (TE Technology, MP-2444) mounted with thermal paste. This allows easy removal of the RTD rod unit for cleaning and sample mounting while providing accurate temperature data of the liquid cavity environment.

For measurements requiring temperature control a peltier-thermoelectric (TE) heater/cooler (TE Technology, TE-127-1.0-0.8) is sandwiched between an aluminum reservoir with liquid input and output ports and an aluminum block machined to fit on top of the sample cell as shown in Fig. 2C. The aluminum reservoir is connected to a circulating liquid cooler (Thermaltake, BigWater 780e ESA) to dissipate heat or cool one side of the TE heater/cooler. The fully assembled sample cell with the TE heater/cooler weighs 196g just under the maximum recommended vertical load of the scan stage of 200g.

Proportional-integral-derivative (PID) control (TE Technology, TC-36-25-RS232) was initially used to regulate the temperature of the TE heater/cooler and sample cell. After judicious determination of PID parameters, the PID controller was able to control the sample cell's temperature to within a tenth of a degree Celsius of the set point, however, doing so required the controller to modulate the TE heater/cooler's power. It was quickly noted, however, that the cycling of the power to the TE heater/cooler, although providing a relatively constant temperature, produced a change in the detected count rate from control samples (detailed later) as may be seen in Fig. 3 (the definite cause of this affect remains undetermined). This effect produced gross distortions in measured correlation curves and, subsequently, PID control was eliminated in favor of a constant power heating scheme. The controller was set to a constant power and the resulting steady state temperature was observed and recorded using a custom LabVIEW interface across a range of experimentally relevant temperatures. The results were fit using a second order polynomial allowing the power needed to achieve a desired temperature to be predicted. This scheme resulted in average steady state temperatures with standard deviations of only a few hundredths of a degree although the time necessary to reach the desired temperature was longer than that observed using PID control.

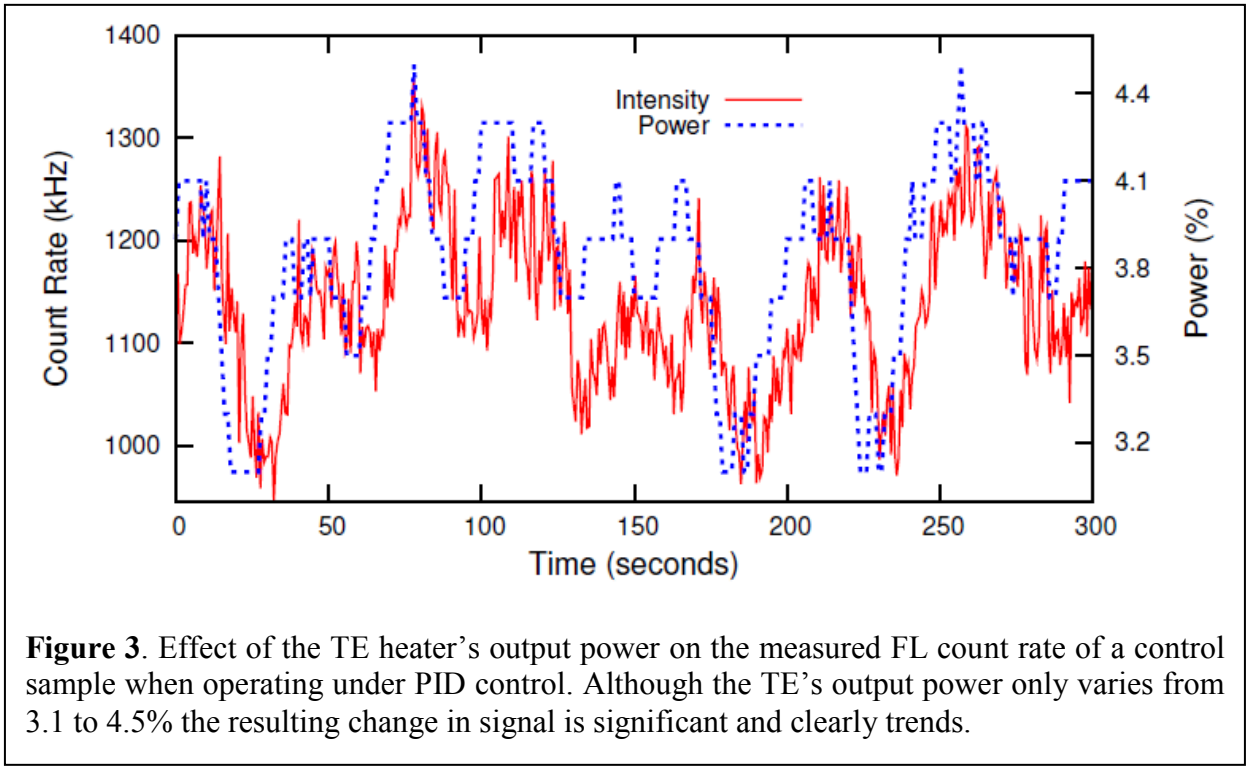

Figure 3. Effect of the TE heater's output power on the measured FL count rate of a control sample when operating under PID control. Although the TE's output power only varies from 3.1 to 4.5% the resulting change in signal is significant and clearly trends.

D. Stage and cell evaluation

Evaluation of the sample cell and stage's stability was carried out by loading the sample cell with two No. 1.5 coverslips and a PTFE coated o-ring but with liquid omitted from the cavity. The sample cell was mounted on the scan stage and the inner surface of the bottom coverslip was brought into focus using a 60X 1.2 N.A. UPlanApo/IR water immersion objective (Olympus) by monitoring the scattered laser light from the glass/air interface. Excitation and collection followed a standard confocal geometry using a 50μm diameter fiber in place of a pin hole and a fiber-coupled avalanche photo diode (APD) as the detector. Once the objective was brought into position, the brass lock ring was secured and a custom LabVIEW program was used to monitor the APD count rate and control the position of the piezo scan stage. The sample cell was scanned through the axial range of the scan stage, the APD count rate at each position was saved, fit to a Gaussian, and the center position of the fitted Gaussian recorded. The software was then set to scan the sample cell through the initial center position every 5 minutes. Scanning was performed from 3μm below to 3μm above the initial center position, in 500nm steps, and the APD count rate at each position was recorded along with the time at which each scan began. The fitted center position for each scan along with the time stamp allowed the position as a function of time to be tracked. Axial scanning of the sample cell using the custom stage setup yielded an average drift rate of 3.47±0.22 nm/min. A typical result is presented in Figure 4A. Similarly, the scan stage and sample cell were mounted on the factory shipped XY stage and the objective was mounted on the original objective turret, and the scan repeated. This yielded an average drift rate of (7.25±1.06)nm/min, as shown in Figure 4B, which is a factor of two larger than our custom setup. Furthermore, Figure 4A also presents occasional mechanical instabilities beyond the

reported average rate were observed suggesting that the stability of the stock stage and turret have the potential to heavily affect measurements on planar systems without operator awareness.

The same stability verification method was also employed to evaluate typical sample mounting methods relative to our custom sample cell. Here, cover glass was mounted to welled slide glass using wax and nail polish. The welled slide glass was inverted and held on the scan stage using clips typically found on microscope stages for said purpose. Typical results from investigating the stability of wax and nail polish sealed cover glass are shown in Fig. 4B along with the stability of our custom setup for comparison. Finally, a No. 1.5 bottom thickness 8-chambered well (Nunc, Lab-Tek II) was tested and the results are also presented in Fig. 4B. As can be seen in Fig. 4B the wax and nail polish sealed welled slide glass, as well as the 8-chamber well, are relatively unstable when compared with our custom setup.

As is clearly evidenced in Fig. 4 by comparing data presented in parts (A) and (B), although our custom stage setup does provide a factor of two decrease in axial drift, relative to the conventional system, it is clear that the custom sample cell employed herein plays an even more critical role. For typical z-scan step sizes (200-300nm) we find the sample′s maximum axial speed is 20.4μm/s (1.22mm/min) and likely not a cause of instability.

Both nail polish and wax seals have been observed to allow air bubbles into the sealed sample well if left for as little as 12 hours. This suggests that the wax and nail polish may form an unreliable seal and allow liquid to evaporate. In equivalent unsealed samples, we observe that as samples dry the loss of liquid due to evaporation causes a visually apparent concave deformation in the cover glass. If the cover glass, which supports the sample, is deforming as a function of time this will clearly affect the absolute position of the sample from scan to scan. This is in contrast to our custom sample cell which allows samples to be examined promptly prior to the potential formation of air bubbles and without having to wait for nail polish or wax to dry. Bubbles have been observed to form in our custom sample cell but only after a few days. More importantly, our sample holder is physically attached to the scan stage using two 4-40 machine screws. This ensures good rigidity between the sample cell and scan stage whereas in the case of conventional microscope stage clips the sample is held by pressure and direct attachment of the sample to the stage is not possible.

To test the imaging stability of our setup a dilute 3nM solution of 200nm fluorescent beads (Invitrogen, F8784) were dried on a No. 1.5 cover glass and mounted in the sample cell. The sample cell was mounted on the piezo scan stage and the beads were brought into focus. An EMCCD camera (Andor, Luca) was used to capture an image of the beads every five minutes for 75 minutes after the initial focus was achieved. Initial and final images are shown in Fig. 2.4. Features in each image were fit to a 2D Gaussian using a custom MatLab script and the resulting $1=e^2$ radius of each feature was stored (features with fitted $1/e^2$ radii larger than would be expected for this imaging system and features not well spatially separated were excluded). Over the 75 minute period the average fitted $1=e^2$ radius increased by (209.4±137)nm (or (2.6±1)nm/min.) indicating the viability of this system for long term imaging.

In all the custom built scan stage and sample cell were proven to have stability far superior to that observed for the as-delivered stage, and typical sample mounting methods, respectively. Due to the z-stability requirements of the combined SF and FL technique this was a necessary achievement of this MRI project.

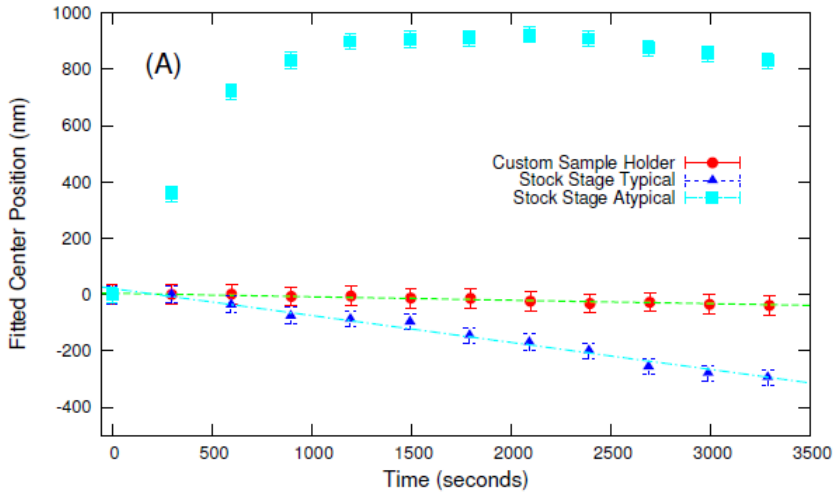

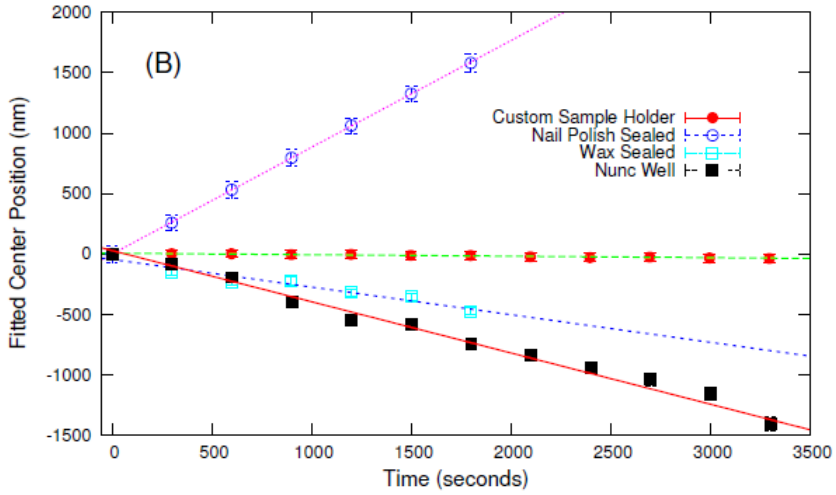

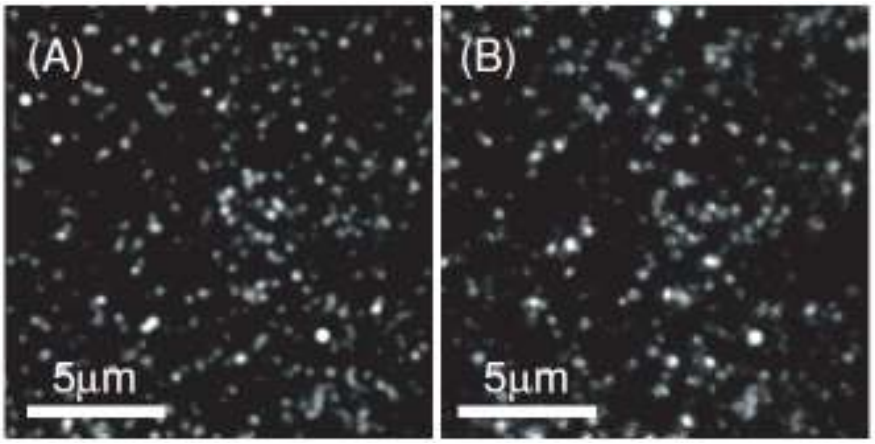

Figure 4. (Top) (A) Axial stability of the custom setup described here is compared with a typical and a typical result from a stock stage and turret. (B) Stability of our sample cell compared with nail polish and wax sealed coverglass and an 8 chamber well. (Bottom) Images of drop cast 200nm beads imaged (A) after initial focus and (B) 75 minutes later.

III. SUM-FREQUENCY COMPONENTS

A. Sum Frequency Basics

Sum frequency spectroscopy (SFS), an application of sum frequency generation (SFG), employs nonlinear optics for the elucidation of interfacial chemical, vibrational, orientation, and conformational information. SFG is produced by spatially and temporally overlapping two electric fields resulting in the creation of a third electric field with angular frequency equal to the sum the to exciting fields: $\omega_{SF} = \omega_1 + \omega_2$. Although the mixing of electric fields from any source, in principle, will produce SFG, in practice the power densities needed and phase matching requirements prohibit detectable SF from being generated by virtually anything other than pulsed lasers. Employing collimated laser excitation further aides in SF detection as the resulting light is emitted as a beam whose angle of emission may be calculated directly. For this reason SFS instruments are universally constructed with one goal: focusing pulsed, collimated, and coherent light onto an interface. A basic SF experimental setup is depicted in Figure 5 where both the SFS-VIS and SFS-IR beams are shown propagating in the positive *z* direction (co-propagating). Note also in Figure 5 indication of electric field polarization in the plane normal to the interface is referred to as *p*-polarized while electric field polarization parallel to the interface is *s*. Interfaces are of paramount importance as under the dipole approximation SFG is forbidden in bulk media with inversion symmetry. However, when inversion symmetry of isotropic centrosymmetric media is broken at an interface the interfacial molecules become sum frequency (SF) active giving SFS its inherent surface specificity.

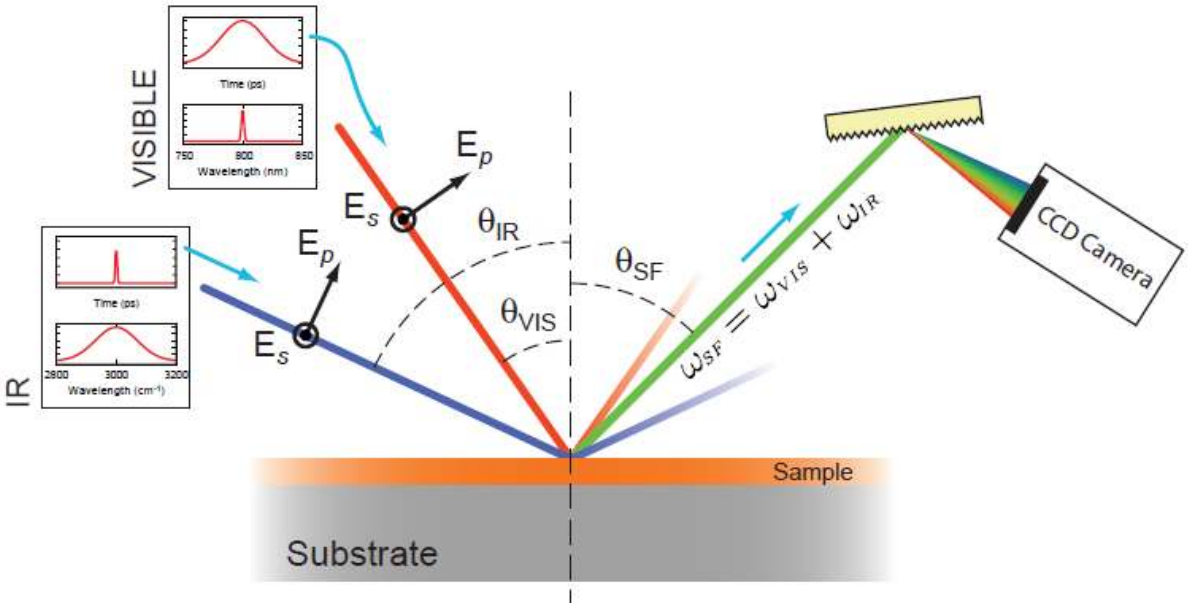

Figure 5. Basic SF experimental geometry. Two pulsed beams meet at an interface and generate SF. (B) Energy level diagram of SFG. Excitation of a vibrational mode is induced via an IR photon (broadband source). A second visible wavelength photon (monochromatic) excites to a virtual level and the photon emitted upon relaxation has an angular frequency equal to the sum of the incident angular frequencies. Complete SF spectra are dispersed from a grating onto a CCD detector in a single shot.

B. Stand alone sum frequency instrumentation

One of the primary goals of this MRI project was to construct the hybrid SF/FL microscope making use of an existing SF (non-imaging) instrument (Neivandt Lab), while maintaining its existing functionality as a user friendly non-spatially resolved spectrometer. However, the rigorous power and spectral demands of the hybrid instrument, as well as the stability required for SF light source switching between the two, required significant changes in configuration of the existing instrument. As such, contruction of the hybrid microscope began with the complete rebuild of the existing spectrometer and the installation of a new optical parametric amplifier (OPA). The basic layout of the updated SF instrument is shown in Figure 6 and a photo is shown in Figure 7.

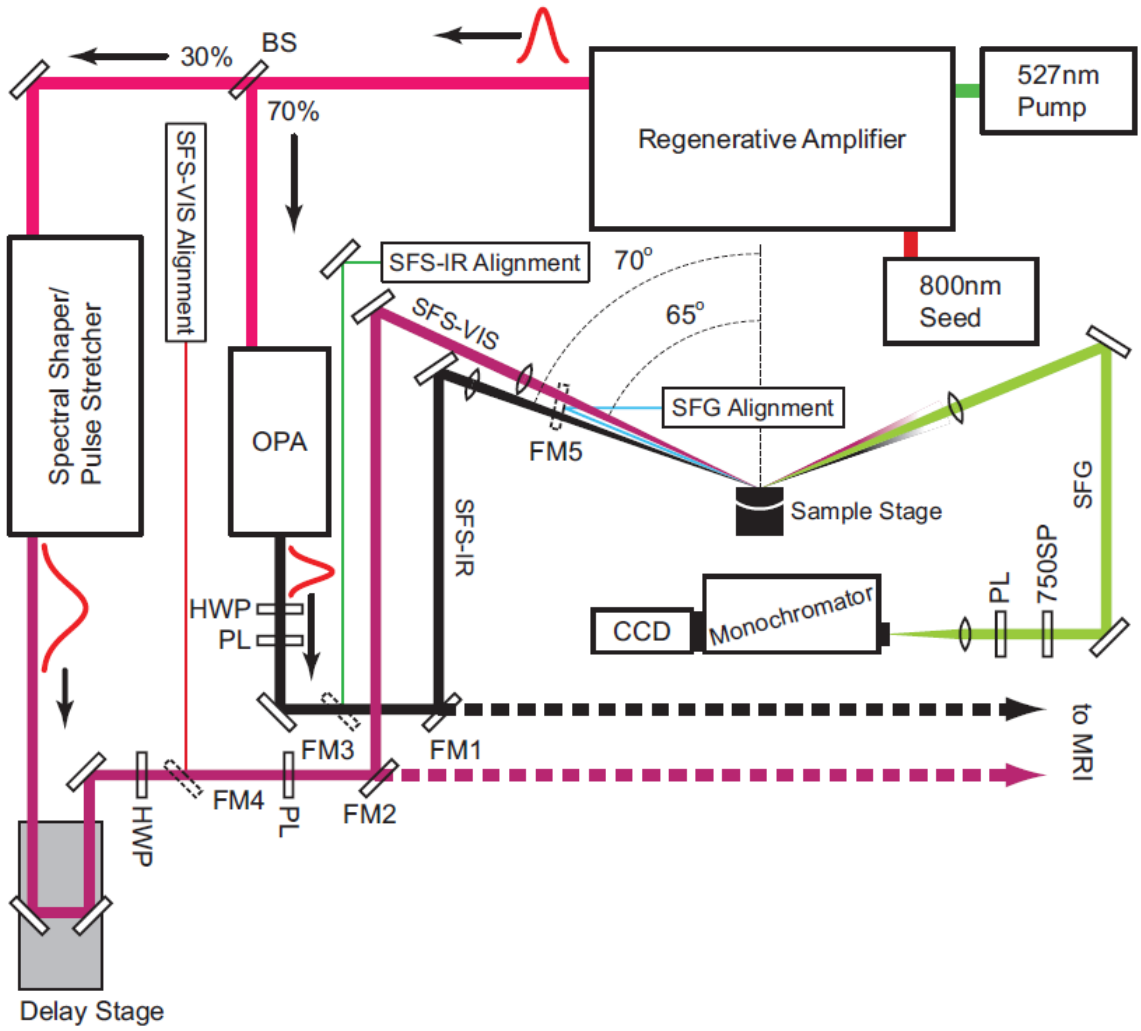

Figure 6. Layout of the rebuilt Neivandt spectrometer detail within the thesis text. FM1-5 are flip mirrors with FM1-2 used to direct the SFG excitation beams to either the Neivandt spectrometer (solid lines) or to the MRI instrument (dotted lines). FM3-4 allow the SFG excitation beams to be replaced with their respective alignment beams while FM5 serves the same function for the SFG signal beam. Abbreviations used are beam splitter (BS), half wave plate (HWP), polarizer (PL), 750nm short pass filter (750SP), and optical parametric amplifier (OPA).

Figure 7. Photo of rebuilt SF spectrometer (FL arm not shown).

In addition to a complete rebuild, optical elements were added to the beam paths to allow for redirection of the light sources to the hybrid instrument. As indicated in Figure 6 three flip mirrors (dotted outlines, FM3-5) may direct three alignment lasers to follow the optical path of the SFS excitation beams and the SFG beam. These are extremely necessary as directly viewing the SFS-VIS beam is hazardous, and the SFS-IR beam is not visible to humans. Two additional flip mirrors (FM1 and FM2) either reflect the excitation beams to the Neivandt sample stage or pass them to the hybrid MRI microscope.

Because the hybrid microscopy and SF excitation lasers reside on separate optical tables an investigation of beam stability on the MRI table, relative to the Neivandt table, was performed. If the SFS excitation beams were found to be excessively unstable, or wander significantly on short time scales, additional stabilization would be required. Beam stability across the two tables was assessed using the SFS-IR alignment laser. The SFS-IR alignment laser was allowed to trace the path of the SFS-IR beam onto the MRI table and the stability was assessed by imaging with a CCD camera at three locations along the beam path. At each of the three camera positions along the beam path, the CCD was set to image the SFS-IR alignment laser every two seconds for fifteen minutes. Image analysis was used to determine the mean and time-dependent angular displacement ((3.23±1.91)μrads, (2.72±1.60)μrads, and (3.38±1.85)μrads, respectively). Based on these results no further stabilization was implemented.

IV. COMBINED SF AND FL INSTRUMENT

A. Hardware

As mentioned above, an inverted microscope base (Olympus, IX71) serves as the hybrid microscope's main body with FL excitation and collection from below and SFS excitation and collection from above. The overall instrumental setup is presented in Figures 8 and 9. FL excitation beams pass through a computer controlled shutter and into the rear port of the IX71. From there a dichroic mirror directs the beam into the back aperture of the microscope objective focusing it to a diffraction limited spot at the sample while a flipper mounted lens at the rear port allows wide-field illumination for sample positioning. Due to the longer working distance requirements imposed by the sample holder an Olympus 40X 0.65NA PLAN N infinity corrected objective lens corrected for No. 1.5 thickness cover glass is employed. FL is collected through the same objective, passes through the dichroic mirror and a bandpass filter, and out the side port of the microscope. Collected FL is sent directly to a fiber coupled APD, via a flipper mirror, to an EMCCD camera for wide field imaging/sample positioning. Atop the microscope body and course XY scan stage resides a high resolution piezo scan stage (Nano T115; Mad City Labs; Madison, Wisconsin). The scan stage is operated in closed loop mode and is controlled by computer. The scan stage has 100μm of travel in X and Y (lateral) directions and a maximum 50μm range in Z (axial) with 0.2 and 0.4nm resolution respectively. The piezo scan stage scans the sample for both FL and SF imaging.

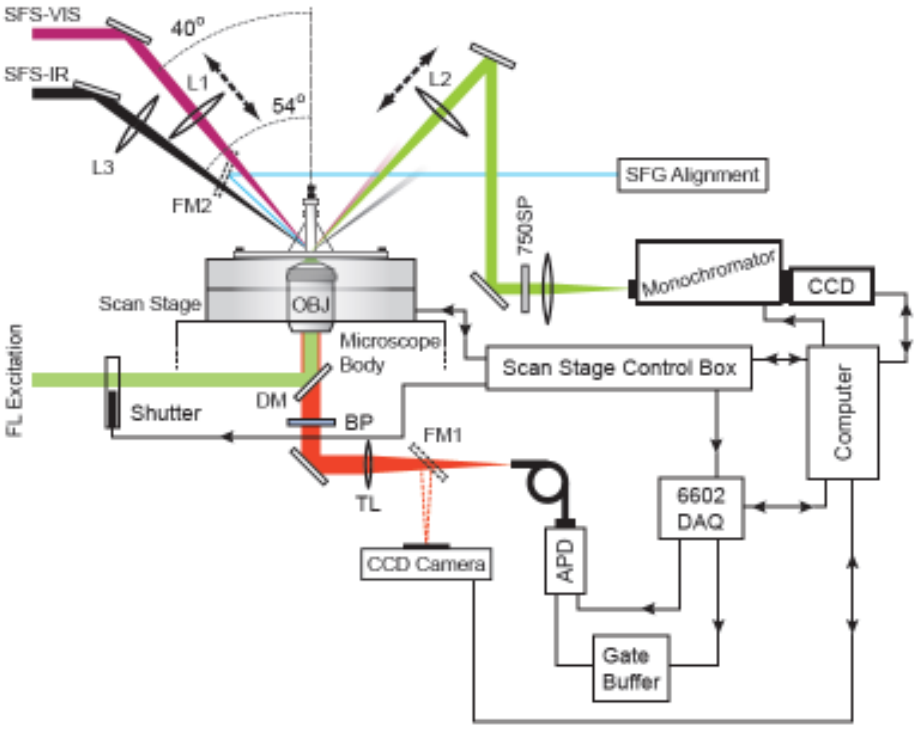

Figure 8. Hybrid SF/FL microscope hardware setup.

Figure 9. Photo of hybrid SF/FL microscope hardware setup.

Visible in Figure 9 are vertical breadboards coupled to the IX71 base which facilitates SFS excitation and collection. The beams are directed up while en route from the Neivandt to hybrid microscope table. Both beams are directed to the center of the sample stage, accounting for deviations due the equilateral prism (described below), and are focused by a 150mm focal length CaF2 lens and an uncoated 100mm focal length BK7 lens for SFS-IR and -VIS respectively. The SFS-VIS focus lens is additionally mounted on an axial translator for fine focus adjustments. (It was experimentally determined that SFS-IR focus is also critical for strong SFG, an additional axial translator for this lens would be a good future addition). For work at the air-solid interface SFS-TIR theory suggests incident beam angles at, or just below, the critical angle will maximize SFG. As such an SFS-VIS incident angle of 40° with respect to the table normal, resulting in an internal incident angle of 46° at the CaF_2 air interface (2° below the critical angle), was employed. Hardware mounting limitations resulted in the SFS-IR beam incident at approximately 53° with respect to the table normal resulting in an internal incident angle 10° beyond its critical angle in CaF_2.

SFG signal was collected by at 175mm focal length BK7 lens positioned at the detection angle predicted by the K-matching condition, one focal length away from the sample. Like the SFS-VIS lens the SFG collection lens is mounted for axial translation and collection optimization. The collected SF signal is directed through a 700 short pass filter (Part number;

Thorlabs; Newton, NJ) and focused with a 100mm focal length lens the entrance slit of a spectrograph consisting of a monochromator (2300, Princeton Instruments) and an EMCDD camera (1024 ProEM, Princeton Instruments). A flipper mirror in the excitation path allows an additional laser to reflect from a metalic substrate, in place of the prism, and into the detection path, simulating the SFG's path, for alignment.

B. TIR-SFS/FL Sample Holder

Like Raman, SFG is a relatively weak phenomena and direct detection without en- hancement is rarely employed. The two most common enhancement mechanisms for SFS are reflective metallic substrates, similar to SERS in Raman, and total internal reflection. These modes thus dictate sample cell design. We require something amenable to confocal fluorescence from below (due to the inverted microscope base) and SF excitation from above. Clearly enhancement from a thick metallic substrate would be a poor choice as it excludes FL imaging, leaving TIR as the viable choice. The ability to image using SFG further requires an experimental geometry amenable to sample scanning eliminating two obvious prism choices, hemi-cylinder and hemi-spherical. An equilateral prism, however, should meet the design criteria; it allows for TIR and sample scanning without grossly affecting the SFS excitation beam's incident positions on its inner surface. Thus an equilateral 1" CaF_2 prism (ISP Optics, Irvington, New York) is employed for SFS imaging. A custom sample cell for prism TIR, from above, and confocal imaging, from below, was fabricated as illustrated in Figure 10.

The use of TIR and the prism interface, is a departure from the original proposal were a much more complicated assembly of CaF_2 meniscus lenses was proposed as a means of improving resolution of the SF method. While this approach still remains possible, it was necessarily abandoned due to the general lack of availability of the necessary optical elements following closing of the few commercial vendors. While the TIR/prism method exhibits limited spatial resolution, the dramatic reduction in background and increase in signal allows for more rapid image acquisition, a significant downside of the originally proposed design.

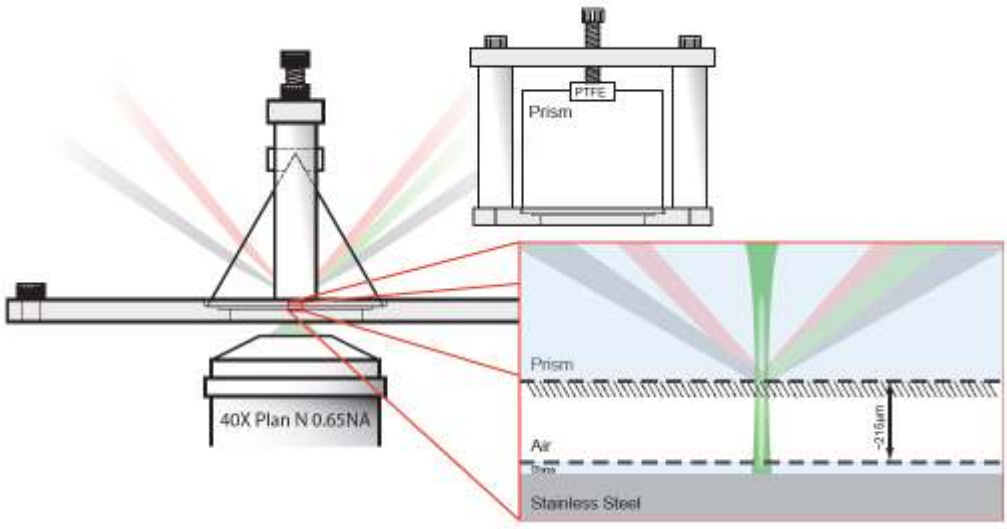

Figure 10. Side view of the custom TIR-SFS/FL sample holder (A) and 90° rotated from (A) side view.

B. Software

The basic data acquisition approach of the hybrid microscope is one of synchronous point-by-point data acquisition, as illustrated in Figure 11. Briefly, 2D images are obtained by raster scanning the sample through a series of software controlled positions, collecting SF and FL information at each location. Unlike traditional FL imaging, each pixel has multidimensional data which is post processed by the user. Control of the microscope is accomplished with a custom built LabVIEW control program. Much effort has been expended to make the MRI control program intuitive and simple. Whenever possible operations have been automated and all initialization/ shutdown routines are performed without the need for user input. The program is composed of one primary interface screen with two additional screens, one for CCD camera and monochromator setup/control (Figure 14) and the other for manual stage positioning, live count rate from the APD, and sample focusing (Figure 13). Unlike many LabVIEW programs that employ an infinite loop to keep the program running, which unnecessarily hogs processor time and slows the computer down, the hybrid microscope's control software uses event based architecture.

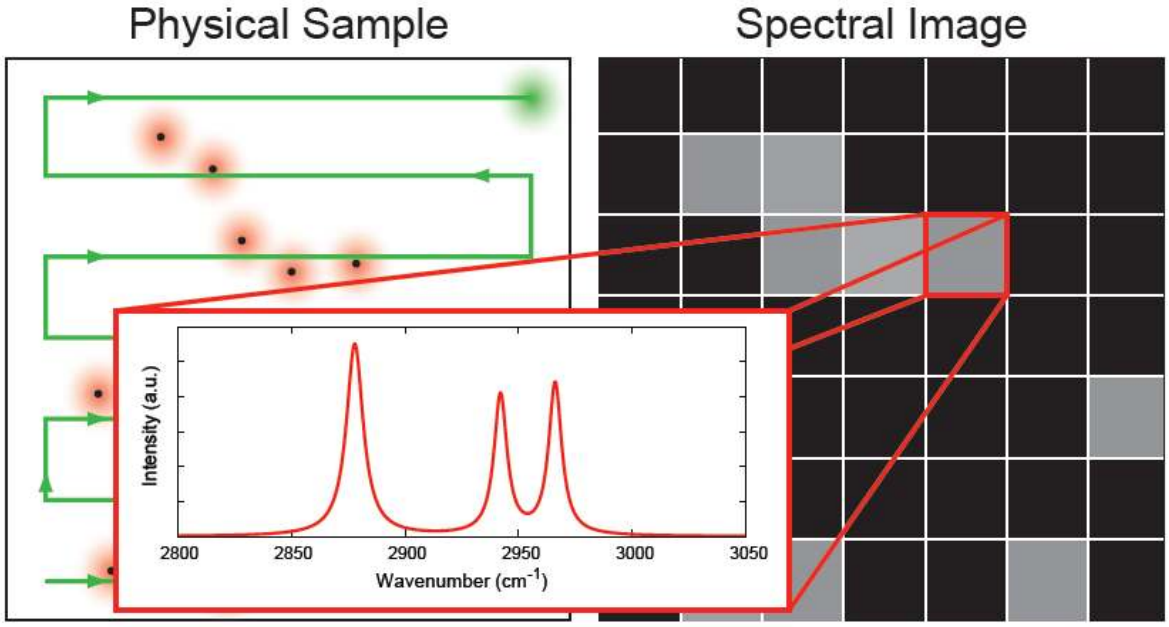

Figure 11. Depiction of sample raster scanning and data acquisition of the MRI hybrid instrument.

At the center of the primary screen is a large display showing acquired images and real-time acquisition progress (Figure 12). Above the primary image display is a plot that dynamically changes based on the acquisition being performed; it automatically shows the confocal line scans or SF spectra as they are being acquired, for example. To the left of the central display are indicators allowing easy checking of relevant setup parameters. These show if

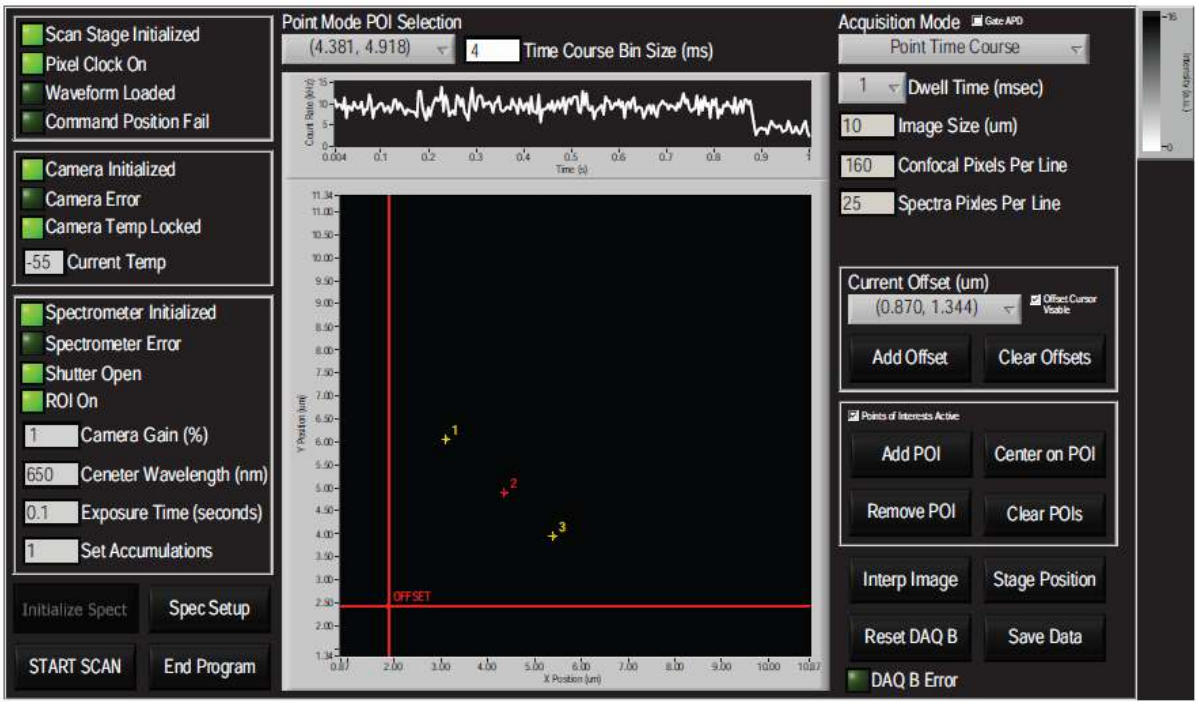

Figure 12. Primary acquisition display screen.

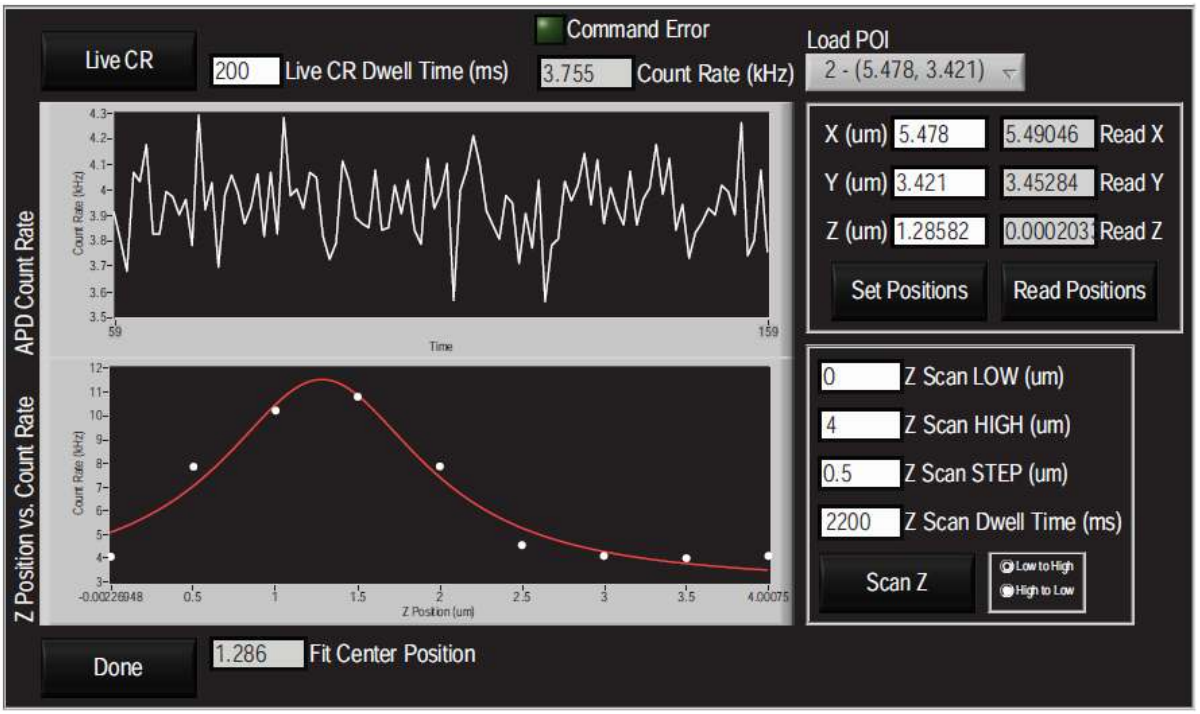

Figure 13. Manual stage positioning, live count rate from the APD, and sample focusing control panel.

the scan stage has been initialized, if the pixel clock is on, if the waveform is loaded, if the stage has failed to reach the commanded position, if the camera is initialized, if the camera temperature is stable, what the current camera temperature is, if the camera, spectrometer, or if the data acquisition (DAQ) board have reported errors, if the camera shutter is open, if a specific region-of-interest (ROI) has been set on the CCD, what the camera's reported EM gain is, the current CCD exposure time and accumulations, and the spectrometer's reported center wavelength. To the right of the primary display a drop down menu allows selection of the acquisition mode and numeric input fields allow specification of imaging parameters. Currently, the supported acquisition modes are confocal imaging, spectral imaging, confocal and spectral imaging, point time course and point spectum modes. These modes, along with the function of the primary and secondary screen's remaining elements will be detailed in the rest of this section (the only element not covered is the "Reset DAQ B" button which simply resets the DAQ board should an error arise).

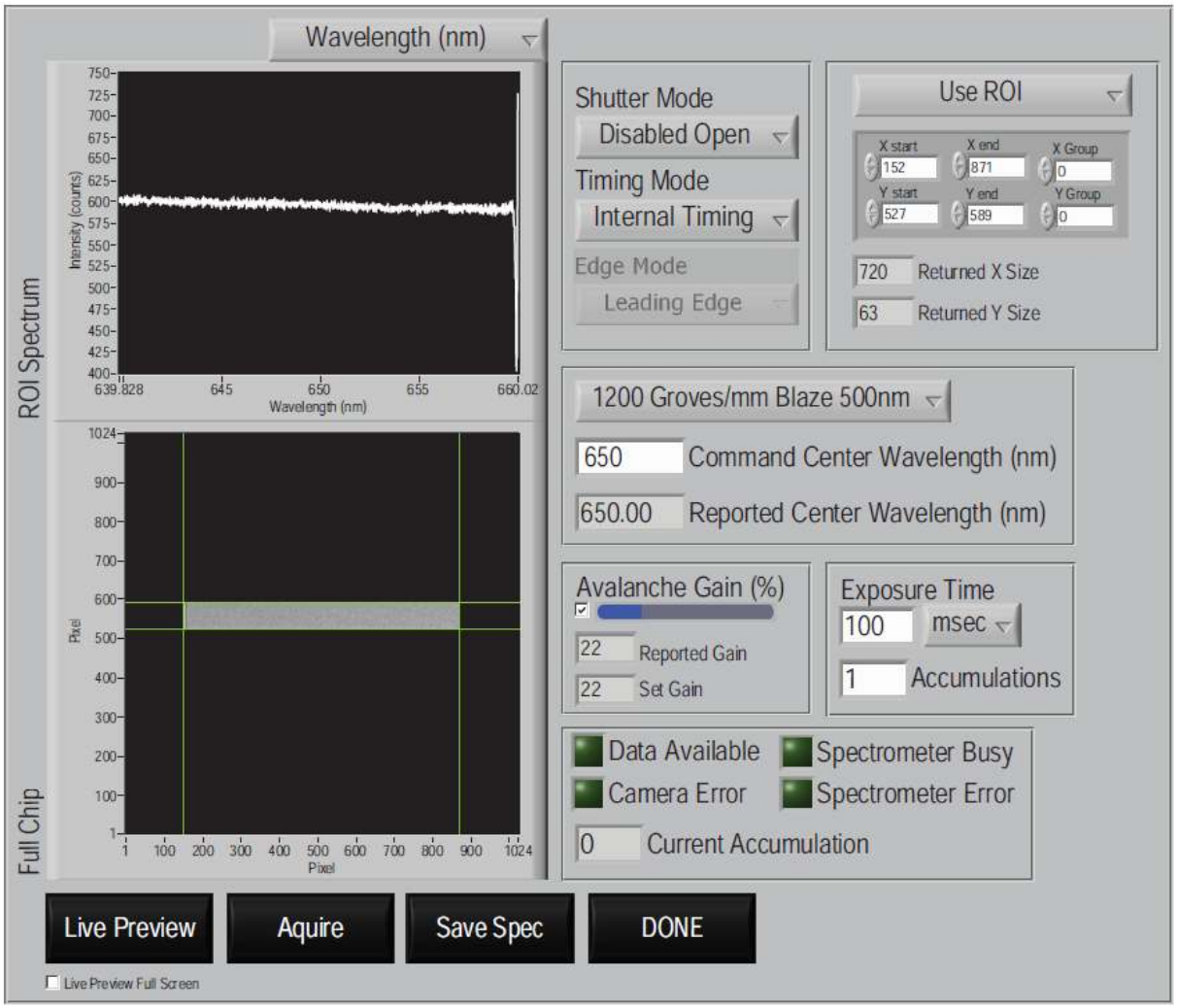

Figure 14. CCD camera and monochromator setup/control display.

C. Metrics / Standards

Calibration of the scan stage was verified by confocal reflectance imaging of a scanning electron microscope calibration standard (C1500-AB, SPI Supplies, West Chester, Pennsylvania) (Figure 15). This calibration sample is fabricated from pure silicon with a uniform lattice of orthogonal 1.9μm±5% wide grooves etched by electron beam lithography and spaced 10μm apart. Pure flat silicon is highly reflective and imaging was accomplished by collecting a small amount of reflected laser light from the sample. Interpolated images of the SPI standard are presented in Figure (3.11) and suggest the scan stage and all image acquisition components function correctly. As an additional test 20nm fluorescent beads (F8784, Invitrogen, Carlsbad, California) were imaged via wide-field excitation using a CCD camera and fluorescent confocal microscopy as presented in Figure 15. Good agreement between the confocal and wide-field images is clear from Figure (3.12) further demonstrating correct operation of the confocal imaging setup. Despite correct functioning confocal scanning hardware the potential affects of imaging with the highly sensitive APD while the SFS excitation beams are also incident on the sample must be considered.

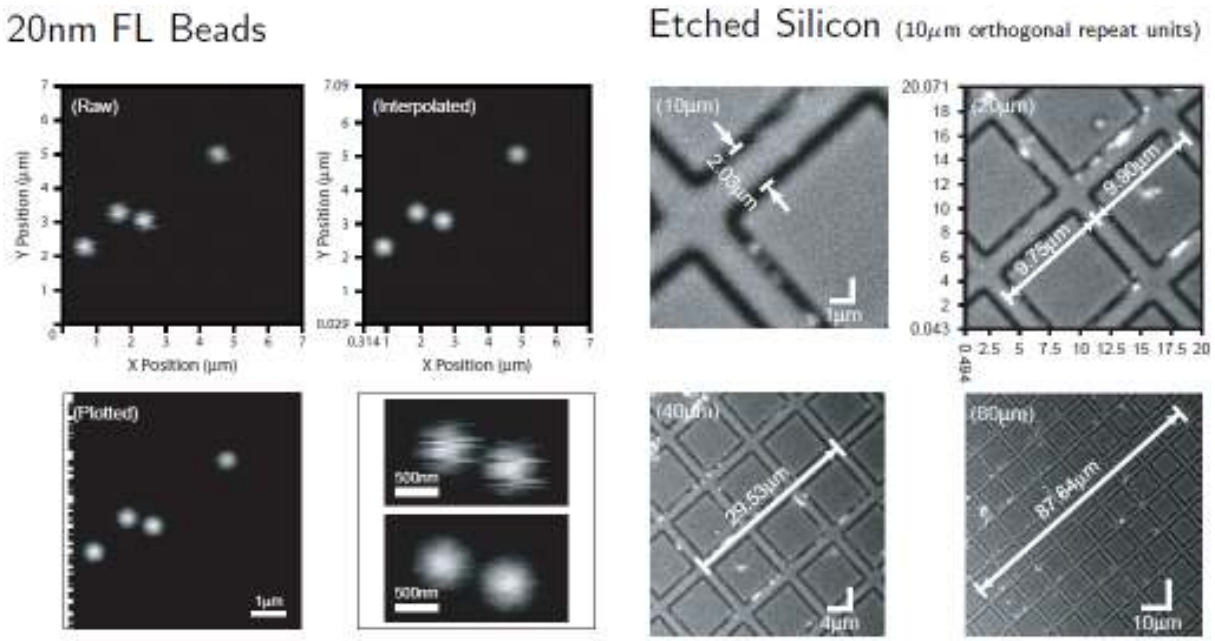

Figure 15. Scan stage fluorescence (left) and reflectance (right) calibration standard (left).

For assessment of the SF and FL capabilities of the instrument, a somewhat more complicated series of standards were created. These standards were composed of a series of etched void structures in a thin gold layer deposited on glass (Figure 16). The gold is known to generate a broad non-resonant SF background signal, and can be used to simultaneously generate a laser reflectance image in the confocal FL detection path (Figure 17). Alternatively a single layer of octadecane thiol (ODT) (bound to gold) was used to generate a well known SF signal.

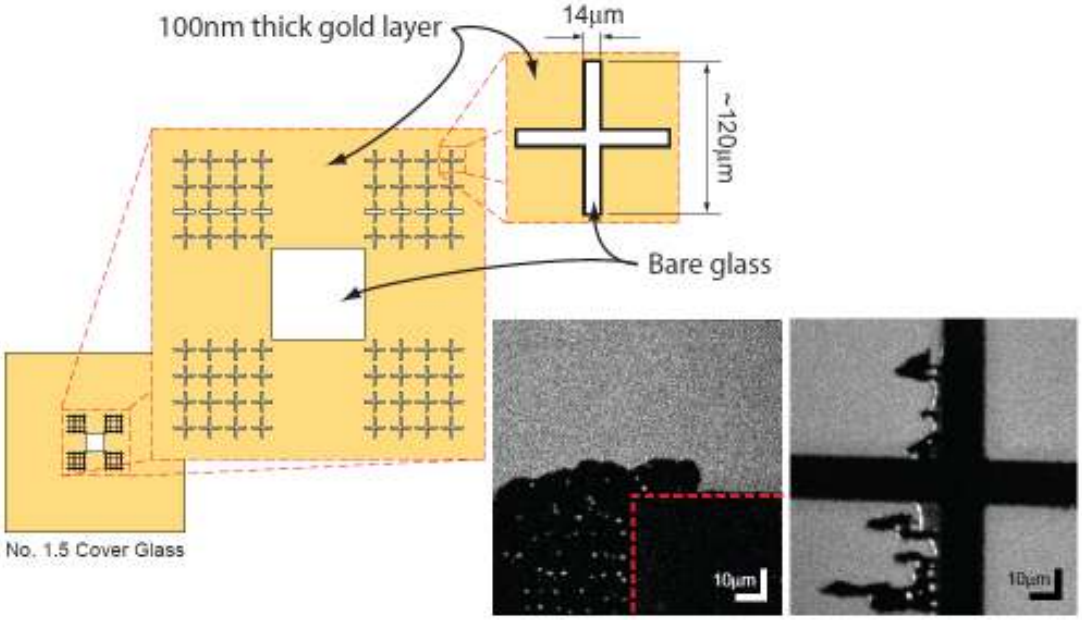

Figure 16. Gold patterned SF/FL standard. The image insets show the effect of laser ablation when the instrument is operated at elevated pump power.

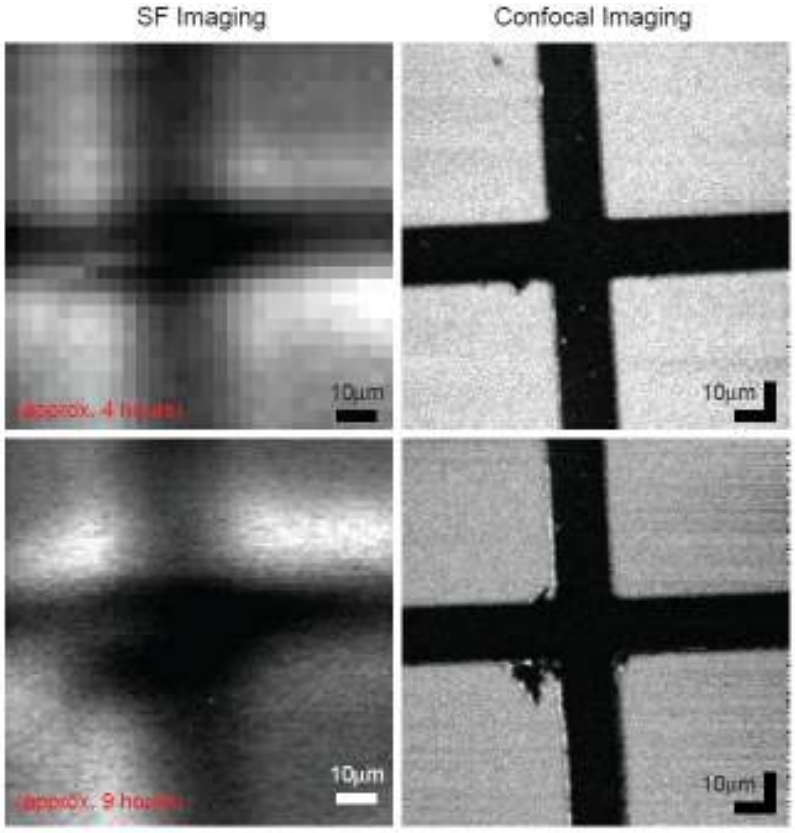

Figure 17. Simultaneous SF (ODT) and FL images acquired for the patterned gold standard (top). The same sample is reimaged at increased pixel resolution (bottom).

V. CAPABILITIES AND SAMPLE DATA

A. Spectral and Confocal Imaging Results

In addition to the patterned gold substrate described above, a second biologically interesting test sample was constructed consisting of a fluorescently labeled phase separated lipid monolayer deposited directly on the afore mentioned CaF_2 prism. Fabrication of this sample followed from an investigation of phase separation in lipid monolayers. 1,2-dilauroyl-*sn*-glycero-3-phosphocholine (DLPC), with a main phase transition temperature of -1°C, and 1,2-distearoyl(d70) *sn*glycero- 3-phosphocholine (perdeuterated DSPC, referred to as dDSPC herein), main phase transition temperature of 55°C, were mixed, doped with the fluorophore 1,2-dimyristoyl*sn*- glycero-3-phosphoethanolamine-N-(lissamine rhodamine B sulfonyl) (ammonium salt) (Rho-PE)(Avanti Polar Lipids, 810157), and deposited via the Langmuir-Blodgett technique. Wide field microscopy revealed apparent domain formation presumed to be that of solid phase (at room temperature) dDSPC, while the DLPC (liquid phase at room temperature) appeared uniformly distributed outside the domains (Lin *et al.*, 2006; Ratto & Longo, 2002) with the Rho-PE separating into the liquid phase DLPC (Crane & Tamm, 2004). Deposition conditions (subphase temperature, and deposition pressure), Rho-PE concentration, presence/concentration of cholesterol, and dDSPC to DLPC ratios were varied and their affects on domain size tracked. Ultimately a 1:1 DLPC to dDSPC mixture doped with 0.0005mol% Rho-PE and deposited at 35mN/m with a subphase temperature of 26°C was found to yield

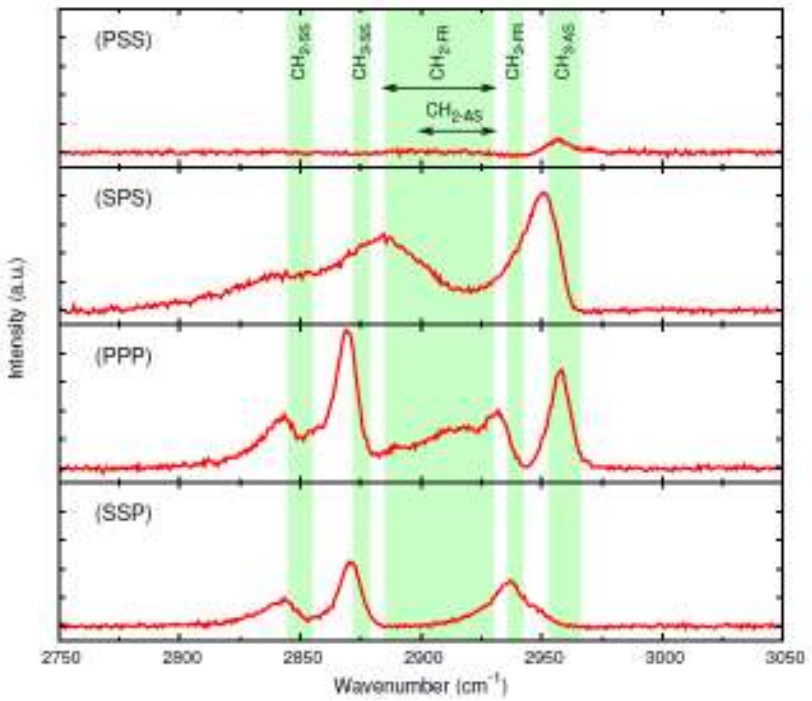

Figure 18. Background subtracted SFS-TIR spectra of a DLPC monolayer at the air-solid interface. All four spectra were acquired under identical conditions while the SF excitation polarizations were varied (1 min. integration time). The intensity on each y-axis is identical allowing comparison of the relative intensities of polarization combinations. The shaded boxes indicate the high and low limits for peak assignments found in literature where the vibrational modes are indicated at the top of the plot. The CH2−*FR* and CH2−*AS* modes overlap and the ranges of each have been indicated with arrows.

clusters of large phase separated solid phase dDSPC domains, while the Rho-PE remained mixed within the liquid phase DLPC. As perdeuterated material is inactive in the CH stretching region, the phase separated dDSPC will not generate SF signal. Because Rho-PE resides in the DLPC, which is active in the CH stretching region, this sample should yield matching SF and FL images with domains easily visualized by both. As such 1:1 DLPC to dDSPC, with 0.0005mol% Rho-PE monolayers, deposited by LB deposition with the above mentioned trough parameters were fabricated on the CaF_2 equilateral prism for instrumental validation and testing.

Example TIR spectra of DLPC, in the CH region, are presented in Figure 18. Spectra show excellent signal to noise despite a relatively short integration time (1 min.). The peaks evident in the spectra of Figure 18 are seen in the spectra of individual pixels, in the spectral images and should be considered representative. Although the peaks are close to the literature values they clearly fall on the edges of the respective ranges given by the high and low values as presented in Figure 18. Aside from the possibility that this is related to the spectral/temporal profile and delay of the SFS excitation pulses, two obvious factors can account for variation in the vibrational modes: the presence of Rho-PE and depositing the DLPC while in the fluid phase, as opposed to the highly ordered solid phase. A less ordered environment would clearly result in different interaction forces subsequently altering the vibrational modes of the methyl groups. In fact, the presence of methylene peaks in the spectra presented in Figure 18 is clear evidence of a less than ideally ordered monolayer.

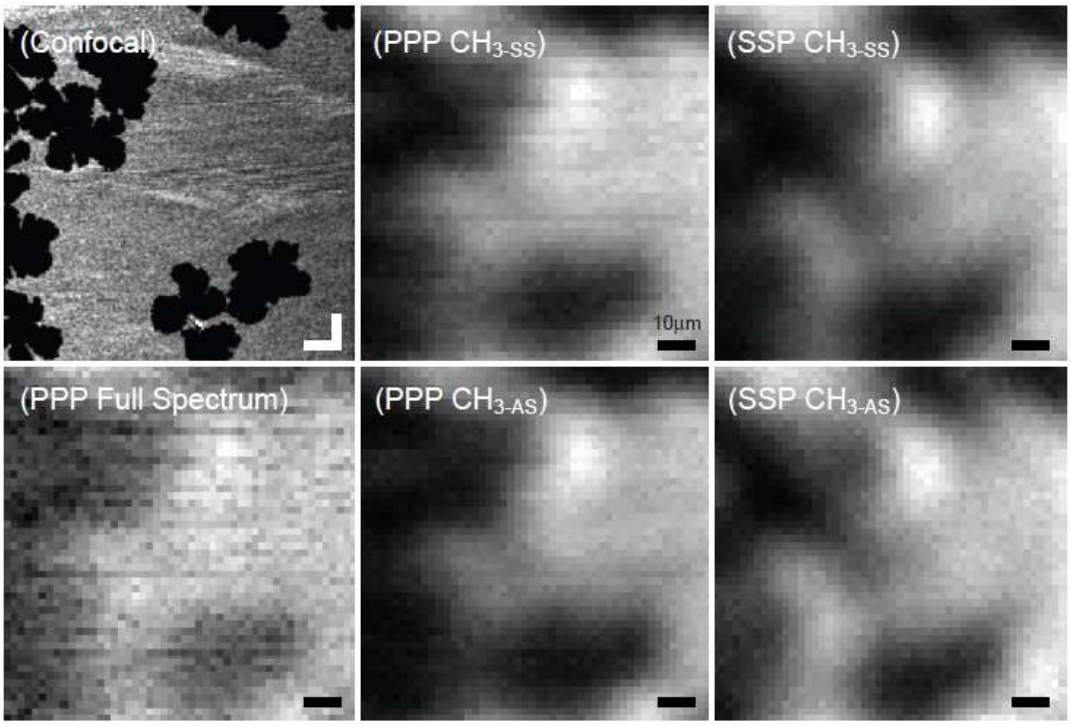

Figure 19. (A) Confocal image of DLPC/dDSPC monolayer on a CaF2 prism and the same area imaged using SF microscopy (B)-(F). Specifically (B) presents the results of integrating the entire spectrum at each pixel to assign a pixel value while (C) and (D) utilize the methyl symmetric and asymmetric stretch modes, using the PPP polarization combination, respectively. Images (E) and (F) likewise show the methyl symmetric and asymmetric stretches respectively with the SSP polarization combination employed. Scale bars are all 10μm.

Images from SF-TIR and confocal FL acquisitions are presented in Figure 19 and clearly demonstrate SF images that closely match the corresponding confocal FL images. In some cases the images are of slightly differing regions, however, features seen in the confocal images are clearly distinguishable in the accompanying SF images. Each pixel in the SF images can be derived from a full SF spectrum acquired at that location on the sample, or generated from specific spectral regions. Thus we may choose which spectral features should be used to set the pixel values. In all the SF images presented here each pixel value results from integration of either the CH3 symmetric or asymmetric stretch mode (with a width of 0.5nm centered around the peak's maximum value). Although the image is discernable for the entire SF spectrum (integrated) it is not particularly clear in contrast to images derived from the same data but with either the methyl symmetric stretch or asymmetric stretch integration used for the pixel value. Figure 19 also shows a detectable difference between images acquired using either the PPP or

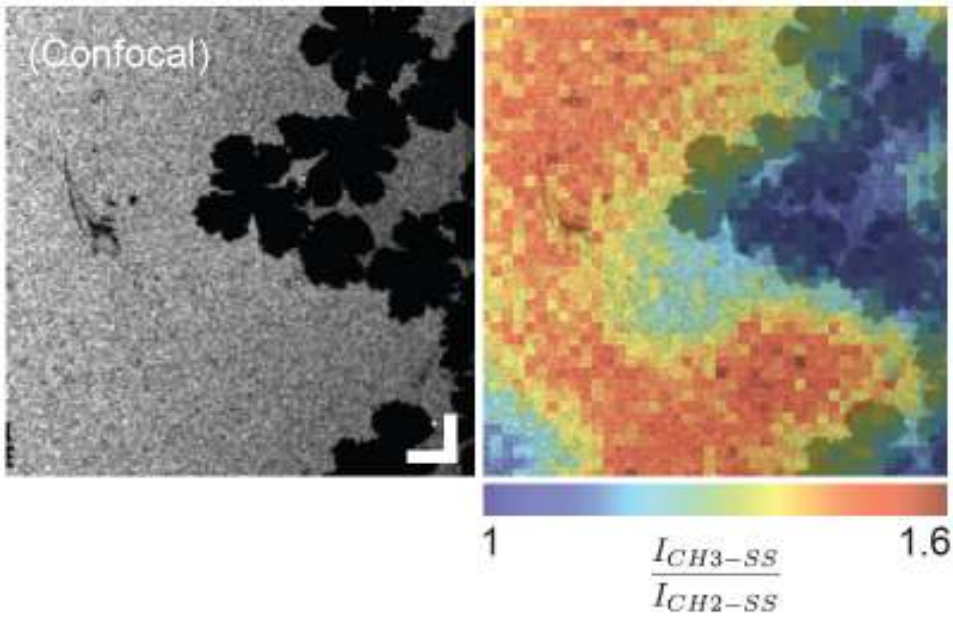

Figure 20. Confocal FL image of phase segregated Rho-PE (left). (Right) Hybrid image of SF determined lipid order (colorized) overlapped with FL data.

SSP polarization combinations. This suggests that not only is spatially resolved vibrational information present but further information, e.g. the spatial distribution of mean tilt angles, can be elucidated. All images are displayed on a linear scale ranging from the image's maximum (white) to minimum (black) value.

Possibly the best demonstration of the utility of the hybrid microscope is the simultaneous display of SF and FL information. This is accomplished, for example by comparing the intensity of CH_3 and CH_2 modes (a measure of relative order), and overlapping this information with the confocal (Rho-PE) data, as shown in Figure 20. Immediately, previously unforeseen spatial correlations, and interesting anti-correlations between phase separated and ordered regions are observed. The specific implications of this data are still being

considered (manuscript in progress). The data in Figure 20 are unique to this instrument and suggests successful completion of this MRI project. Future experiments will generate data of this form for other scientifically relevant sample types.

B. Instrument Resolution

The SFS-VIS has been observed to be well above the diffraction limit and subsequently its size could be measured direct or indirectly, e.g. photo bleaching a uniform dye film or by imaging with a CCD camera. However, the SFS imaging resolution is not a function of the SFS-VIS beam alone. Clearly the overlapping SFS-IR and -VIS beams define the spatial sensitivity of the system, the effective SFS excitation area. Were the SFS-VIS and SFS-IR beam sizes both known a reasonable estimate of the signal generating region could be made. This could, in turn, allow for an estimation of the SFS imaging resolution. Unfortunately direct measurement of the focused SFS-IR beam is not possible. Here we employ three methods for spectral imaging resolution estimation: an adapted knife edge method, simulation of an SF image with defined step edges, and finally direct visualization of the SFS-VIS beam. The results of this analysis are shown in Figures 21 and 22.

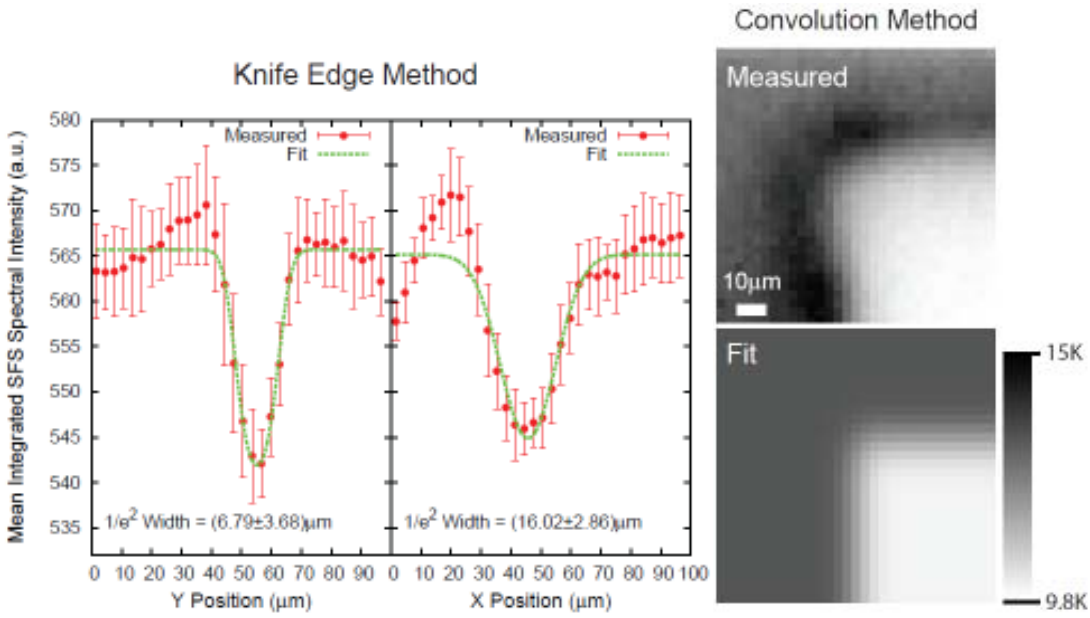

Figure 21. Line feature scan through SFS excitation beams fit with Equation (X) for the (A) Y and (B) X dimensions. Fitting yields 1/e2 radii of (16.02±2.86)μm and (6.79±3.68)μm in the X and Y dimensions respectively which is consistent with the observed elongated dimension of the SFS-VIS beam in the X dimension.

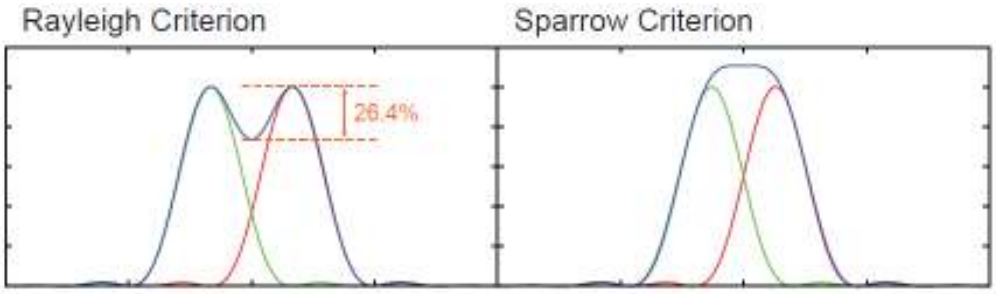

Method	Dimension	Diameter (μm)	Rayleigh (μm)	Sparrow (μm)
Convolved	X	12.77±1.11	17.88	14.06
	Y	12.55±1.12	17.57	13.854
Knife Edge	X	16.02±2.86	22.43	17.68
	Y	6.79±3.68	9.51	7.49
SFS-VIS Fit	X	22.37±5.05	31.32	24.69
	Y	16.62±7.40	23.27	18.348

Figure 22. Line feature scan through SFS excitation beams fit with Equation (X) for the (A) Y and (B) X dimensions. Fitting yields 1/e2 radii of (16.02±2.86)μm and (6.79±3.68)μm in the X and Y dimensions respectively which is consistent with the observed elongated dimension of the SFS-VIS beam in the X dimension.

VI. CONCLUSIONS AND FUTURE PLANS

Here we have detailed the construction and function of a hybrid SF/ FL spectral imaging sample scanning microscope as applied in both a reflection and TIR geometry. A number of test samples were investigated the results of which clearly illustrate the power of this new hybrid instrument. This one-of-a-kind instrument is now capable of generating unique data combining the capabilities of SF and FL and represents successful completion of this MRI project.

Although the proof of principle is now clear, a number of improvements would further benefit the system. On exiting the SSPS, clear spatial irregularities can be easily seen in SFS-VIS mode. Attempts were made at spatial filtering using high energy pin holes (5-50μm) but were found to have negligible affect (they either burned or were to large). As such implementation of a polarization preserving, low dispersion single mode, fiber optic could clean up the beam profile while simultaneously providing a simple method for delivering the beam to the hybrid microscope with greatly reduced risk of laser eye damage (the fiber would provide a closed beam path and allow the beam to be conveniently launched and sized on the microscope breadboard, additionally reducing table clutter).

While the Princeton Instruments EMCCD camera has proven sufficient for TIR- SFS collection, it lacks the extremely fast electronic shutter employed on the PI-Max camera. The PTG timing option on the PI-Max camera allows extremely low shutter and trigger delay times, on the order of hundreds of nanoseconds. Typically shutter times employed on the Neivandt SFS system are 250μs. The SSPS output is in the picosecond regime while the SFS-IR pulse width remains in the femtosecond. Clearly, even thought the PI-Max camera is shuttered on the scale of nanoseconds its exposure time is still three orders of magnitude larger than SF emission duration

per pulse. Unfortunately the ProEM camera employed for the hybrid microscope's spectral detection lacks the fast shuttering capabilities of the PI-Max camera. The ProEM camera runs in shutter mode, most often with exposure times above 1 second (certianly faster exposure speeds can be set but the ProEM camera cannot achive the 1kHz frame that would be required regardless of exposure time). In this case the ratio of shutter open time to actually signal generation time is extremely large. For an exposure time of 1 second with a 1kHz pulse repetition we assume signal is generated for 1 picosecond for each pulse, meaning SF light is collected by the camera for only 0.000001% of the exposure time. The remaining 99.999999% of the exposure provides no further signal but does allow collection of background noise. Switching to a fast electronically shuttered camera has the potential to greatly reduce the noise collected during spectral acquisition which, in turn, could allow for shorter acquisition times and subsequently much shorter spectral imaging times. The scanning apparatus employed here is limited to scanning a 100μm square. Although this is ideal for many samples, there are likely as many other systems for which a large scan area would be more applicable. In light of the instrument's current resolution a larger scanning area may prove a better match. Replacing the course, manually posi- tioned, XY stock Olympus scan stage with a stepper motor driven stage would allow for easy large area SF imaging. Additionally, the existing scan stage could be easily mounted on top of a large scanning stage for high resolution investigations of ROIs without the loss of FL imaging capabilities. This would allow conformational order over very large sample areas to be studied (something not currently found in the literature).

VII. BROADER IMPACTS / OUTREACH ACTIVITIES

To date 16 undergraduate students and 4 graduate students have been involved in this project. The graduate students involved have now completed advanced science degrees in Physics and Chemical Engineering. The 16 undergraduate students are pursuing bachelors degrees in Physics, Chemical Engineering, and Biological Engineering.

In conjunction with this cutting edge project educational and outreach programs were developed demonstrating to an audience of high school students and educators the capabilities of the proposed instrument as well as the importance of new instrument development to the broader research community. Through this program nearly 150 high school students have participated in a one day directed research experience, and 4 high school students and 2 science teachers participated in a two month NSF supported research program, and an additional 6 high school students have participate in related research based on an internal matching grant.

Over two summers (2008, 2009) a Master of Science and Teaching (MST) Student (Erik DeSilva) was hired in conjunction with this MRI development project to specifically develop 1) course curricula/teaching modules for a new Biological Engineering Instrumentation and Advanced Methods Course, 2) development of high school outreach activities and curricula including on-campus research experiences (BEAR Program http://www.umche.maine.edu/bear/). Funding for this position was provided by UMaine Sponsored Programs in response to the proposed MRI funded outreach and educational activities. In addition, this student has completed a high school classroom teaching module which he has implemented on a trial basis.

Also completed are the two halves of the online description of the technology development, including the underlying photophysics, associated with this project. This can be found online at: http://www.physics.umaine.edu/FPALM_SFS_NOV09/sfs.html.

REFERENCES

[i] Florsheimer, M.; Brillert, C.; Fuchs, H. "Chemical imaging of interfaces by sum frequency microscopy" *Langmuir* **1999**, *15*:5437-39.

[ii] Florsheimer, M.; Brillert, C.; Fuchs, H. "Chemical imaging of interfaces by sum-frequency generation" *Materials Science & Engineering C-Biomimetic and Supramolecular Systems* **1999**, *8-9*:335-41.

[iii] Kuhnke, K.; Hoffmann, D. M. P.; Wu, X. C.; Bittner, A. M.; Kern, K. "Chemical imaging of interfaces by sum-frequency generation microscopy: Application to patterned self-assembled monolayers" *Applied Physics Letters* **2003**, *83*:3830-32.

[iv] Cimatu, K.; Baldelli, S. "Sum Frequency Generation Imaging Microscopy of CO on Platinum" *Journal of the American Chemical Society.* **2006**, 128: 16016-16017.

[v] Cimatu, K.; Baldelli, S. "Sum Frequency Generation Microscopy fo Microcontact-Printed Mixed Self-Assembled Monolayers" *Journal of Physical Chemistry. B* **2006**, 110: 1807-1813.

Final Report on NSF Award No. CHE-0722759: MRI: Development of a Hybrid Scanning Fluorescence and Sum Frequency Spectroscopy Imaging Microscope

Edward S. Allgeyer[2], Samuel T. Hess[2], Michael D. Mason[1], David J. Neivandt[1], Sarah M. Sterling[1], Mudalige Gunewardene[2]

[1]Department of Chemical and Biological Engineering, University of Maine, Orono, ME 04469
[2]Department of Physics and Astronomy, University of Maine, Orono, ME 04469

Abstract

This MRI project was focused on developing a hybrid scanning fluorescence (FL) and sum-frequency (SF) vibrational spectroscopic microscope. Now completed, the microscope will expand the capabilities of the nation's research infrastructure by combining the benefits of two powerful imaging and spectroscopic techniques. This combination enables the direct correlation between localized or distributed photophysical (FL) molecular properties and the structure of the environment (SF). In its current form the instrument has diffraction limited resolution in the fluorescence channel (~250 nm), and ~10 μm resolution in the sum-frequency channel. The instrument is capable of obtaining 2D (or 3D) image sets comprised of single pixel fluorescence information and complete (1024 pixel) high resolution (< 0.1 cm^{-1}) Sum-Frequency spectra. An additional point probe mode was included which allows for high temporal resolution (<1 ns) fluorescence detection with single molecule sensitivity and simultaneous high spectral resolution sum-frequency detection. The 'particle-in-a-bath' capabilities of the proposed instrument will have utility in biology, biochemistry, materials science, chemistry and physics. For example, it is anticipated that future research conducted with this new instrument will provide breakthroughs in our understanding of membrane and film organization at the molecular level. Sample data illustrating the power of our instrument is presented. Much of the final project description presented here has been excerpted from the outstanding PhD thesis of the primary graduate student working on this project (Edward S. Allgeyer).[1]

I. INTRODUCTION

To further advance the research and educational capabilities of the University of Maine and the Institute for Molecular Biophysics (IMB), we proposed to capitalize on our expertise in sum-frequency (SF) spectroscopy and fluorescence (FL) imaging to develop an instrument with unique capabilities crucial to the study of a broad range of systems from materials to bio-membranes. Ideally, this imaging spectrometer would measure molecular conformations, photophysical properties, and dynamics in a temporal regime which is inaccessible, yet entirely complementary, to existing instrumentation available for our current research efforts.

Sum Frequency (SF) is a vibrational technique based on non-linear optical mixing of photons of two different energies. SF provides detailed structural information on an ensemble of molecules at an interface within an optically-defined sample volume, including absolute orientation and conformational configuration. SF has been used to analyze thin film systems in a number of instrumental geometries including transmitting[i,ii] and reflective substrates.[iii] For example, in two recent publications by Cimatu and Baldelli, SF was used to observe the spatial distribution of CO on platinum surfaces[iv] and chemically distinct regions of self-assembled alkane-thiol monolayers.[v] Fluorescence (FL) spectroscopy

complements SF by providing access to single-molecule properties of individual species within an ensemble of molecules on 10^{-12} s to $>10^{2}$ s timescales. Ideally, both FL and SF methodologies would be employed simultaneously yielding localized dynamics of the single fluorophore (FL), or multiple fluorophores, and spatially correlated structural information about the local surroundings (SF). Additionally, the ability to select phase or structure specific fluorescent molecules allows one to correlate spatial and temporal fluorescence information with structural information regarding the surroundings. This *'particle-in-a-bath'* approach has found limited implementation due to differing optical requirements and inherent difficulties in distinguishing between the two signals; the MRI instrument developed by our group circumvents these issues by exploiting fundamental differences in the optical nature of SF and FL.

In the following sections we describe the individual Fluorescence and Sum-frequency components of the MRI instrument separately, and as a combined tool. It is important to note that our instrument has all of the capabilities of separate FL and SF equipment in addition to the expanded capabilities arising from this unique combination.

II. FLUORESCENCE COMPONENTS

A. Fluorescence Microscope Core

At the core of the combined Sum-frequency and Fluorescence instrument is a standard Olympus IX71 inverted microscope base as shown in Figure 1A. This base was chosen primarily due to its flexibility for multiple light source inputs and signal collection points. This base is widely used for either laser scanning or sample scanning confocal fluorescence microscopy (SCFM). The relatively open inverted design was chosen to allow for Sum-Frequency signal acquisition to occur from the top (epi-) and fluorescence signal acquisition to occur from either the bottom or the top (transmission or reflection modes).

Typical with all SCFM instruments, a laser is directed into the back aperture of a microscope objective which focuses the beam with a tight waist at the focal plane positioned inside the sample. Scattered or emitted light is collected by the same objective and focussed onto a pin hole placed confocally with the illumination spot in the image plane. The confocal pin hole discriminates against light originating from regions of the sample above or below the focal plane or laterally adjacent to the beam waist. This is geometrically apparent as the dotted rays in Figure 1B which are defocused when they reach the pin hole and are largely blocked, although some background light is admitted. Light which does pass the pin hole is detected with an avalanche photodiode (APD) whose signal is recorded by a computer. An image is collected point-wise by either raster scanning the sample and recording the detected light for each illuminated position. Collecting an image at varying axial sample positions generates a stack of 2-dimensional images that may be reconstructed to form a 3-dimensional image.

Although the confocal aperture provides a modest increase in lateral resolution its distinct advantage over wide field illumination and collection is the enormous increase in background suppression yielding greatly improved depth discrimination (Diaspro, 2007); the confocal pin hole restricts imaging to only a small sample slice. Certainly the modest improvement in lateral resolution, up to a factor of $\sqrt{2}$ (Sandison & Webb, 1994; Sandison *et al.*, 1995) is advantageous but alone is not enough to have propelled confocal microscopy into its present position as a virtual standard. Rather the 2-3 orders of magnitude increase in the signal to background ratio (Sandison & Webb, 1994; Sandison *et al.*, 1995), allowing for 3D sectioning and improved image quality, is responsible. Because of its greatly improved surface specificity, it is a clear choice for pairing with interface specific techniques such as sum frequency spectroscopy.

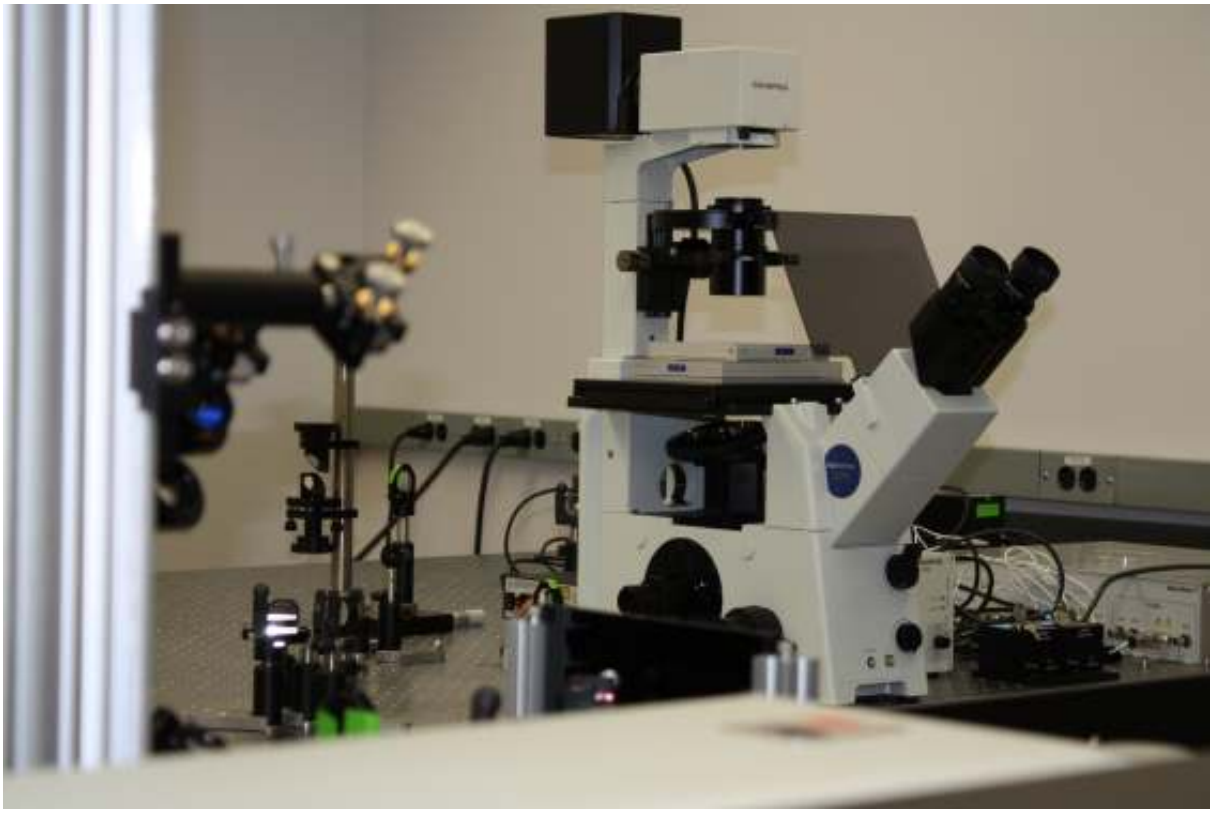

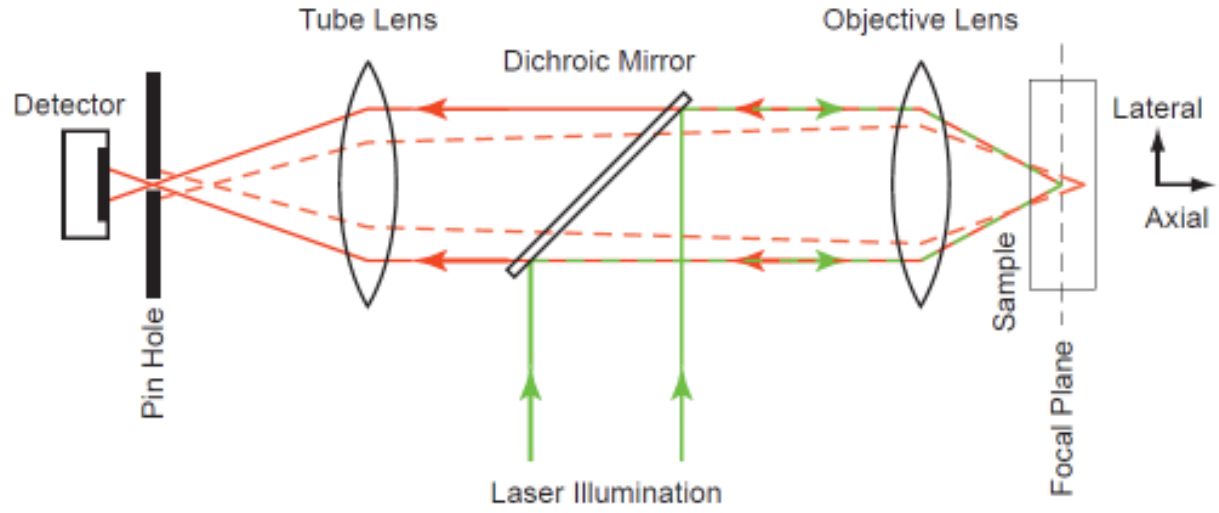

Figure 1. (Top) Basic illustration of a confocal microscope. Laser illumination is directed into the back aperture of a microscope objective with a dichroic mirror and focused inside the sample for excitation. Light is collected with the same objective lens, passed through the dichroic mirror, and is focused by the tube lens through a pin hole onto a photodetector (APD). Light originating outside the focal region (dotted rays) is defocused at the pin hole and largely blocked. (Bottom) Photo of the Olympus microscope body during the initial construction phase of the FL/SF combined instrument.

B. Low Drift Stage and Objective Holder

While the as-purchased XY-translation stage of the Olympus IX71 inverted microscope is considered to have excellent position stability, the rigorous demands of the combined SF and FL instrument required further refinements. Specifically, the z-position of the sample, relative to the excitation and collection optics, is critical to maintain stability in the SF signal and to ensure spatial correlation between the SF and FL information. As such, the factory shipped XY translation stage and objective turret were removed and replaced with a custom built isolation stage and objective mount (Figure 2A). All components of this custom stage were produced at UMaine.

In place of the original XY stage a 12.7mm thick 178 by 240mm block of aluminum was employed. A 32mm square was milled in the middle of the plate to accommodate our custom objective holder (detailed later) and four M6 clearance holes were drilled allowing the plate to be mounted on the IX71 base in place of the Olympus XY stage. Four holes were drilled and tapped for 1/4-20 screw size allowing for the attachment of a large aperture high performance two axis translation stage (Newport Corporation, 406) and our objective holder. Mounted on top of the aluminum plate is the afore mentioned large aperture Newport course XY stage. This stage has a 57.15mm diameter aperture to accommodate our objective holder and 13mm of travel in the X and Y directions allowing the sample to be manually positioned. A three axis piezo scan stage (Mad City Labs, Nano-T115) was mounted, via a connecting plate, on top of the Newport XY stage. This software controlled stage provides the XY motion required for sample scanning during FL and SF data acquisition. Finally, an acrylic sample cell holder that thermally insulates the scan stage from the sample cell sits atop the piezo scan stage.

The objective holder consists of an externally threaded 28.757mm outside diameter stainless steel rod, a brass mounting plate, and a brass lock ring. The brass mounting plate and lock ring have internal threads mated to the external threads of the rod. The stainless steel rod is 88.9mm long and has 76.2mm of external 44 threads per inch (tpi) threads (giving a 577μm axial advance per revolution). The inner diameter of the rod is 0.8 inch with internal RMS threads (20.32mm diameter and 36 tpi) at one end allowing attachment of a microscope objective. The brass mounting plate is attached to the top of the large aluminum plate while the stainless steel rod and lock ring thread in from beneath. Rotation of the threaded rod, accessed from under the aluminum plate, allows the microscope objective to be moved up and down. The lock ring allows the position of the objective to be fixed and the high tpi provides the necessary axial resolution for the objective. Fine tuning of the focus is easily accomplished with the Z-axis of the piezo scan stage. A schematic of the stage and objective holder is given in Figure 2A. With the setup described the sample cell is fixed to the top of the scan stage and the position of the objective relative to the sample is held constant once the lock ring is tightened. Thus, for a given piezo z-position, the critical feature of a fixed distance between the sample and objective is fulfilled while the Newport XY translation stage allows for the equally critical feature of course sample positioning. This level of position stability is often overlooked in fluorescence confocal imaging, and is critical for signal stability in SF techniques involving sample scanning.

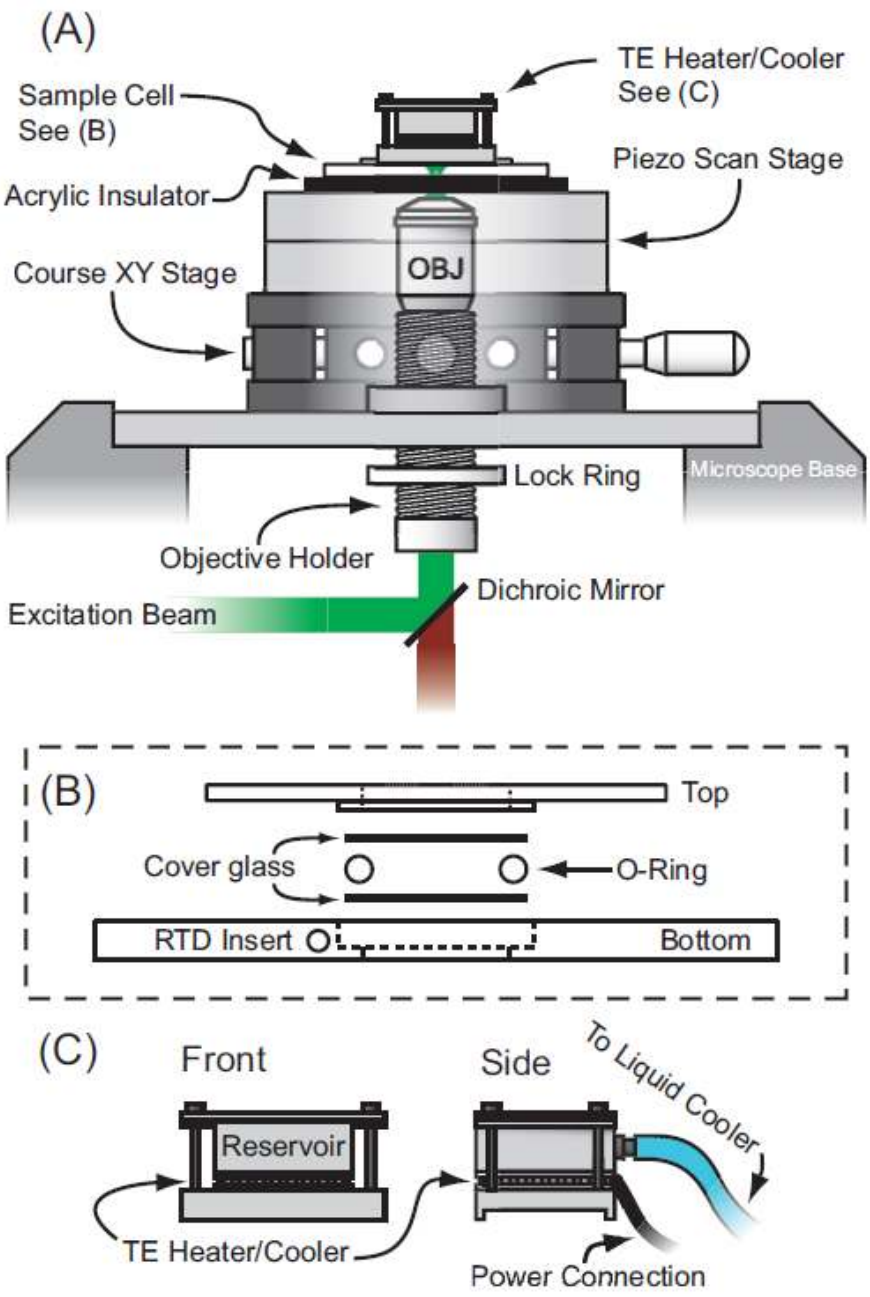

Figure 2. (A) Stage and objective holder as detailed in the text. (B) Liquid sample cell forming a cover glass o-ring sandwich for planar membrane systems. (C) TE heater/cooler sandwiched between circulating liquid reservoir and an aluminum plate that friction fits on top of the sample cell presented in (B).

C. Liquid cell and heater/cooler stage

As many of the samples of interest require a liquid environment as custom liquid sample cell was constructed. The custom built sample cell is composed of two 300 series stainless steel plates, one with a boss (top), and the other with a matching pocket (bottom) as show in Figure 2B. The lower portion of the sample cell is a 4.7625mm thick stainless steel bar comprised of a 22x22mm pocket milled in the center, two 4-40 clearance holes for direct mounting to the scan stage, and a 7.9375mm aperture to accommodate the microscope objective. The upper portion of the sample cell has a boss that fits inside the pocket of the lower portion. The depth of the pocket and height of the boss have been chosen so two No. 1.5 microscope cover slips may sandwich a PTFE coated o-ring inside the cavity and compress the o-ring by approximately 5%. The top portion of the sample cell attaches to the lower portion using four 4-40 stainless steel screws. Stainless steel is employed throughout to allow all parts to be rigorously cleaned. A 3.175mm hole machined into the side of the lower plate of the sample cell houses a friction-fit removable brass rod that penetrates to within 1.5mm of the liquid cavity. A 1.2mm hole machined longitudinally into the brass rod houses a thermistor (RTD) (TE Technology, MP-2444) mounted with thermal paste. This allows easy removal of the RTD rod unit for cleaning and sample mounting while providing accurate temperature data of the liquid cavity environment.

For measurements requiring temperature control a peltier-thermoelectric (TE) heater/cooler (TE Technology, TE-127-1.0-0.8) is sandwiched between an aluminum reservoir with liquid input and output ports and an aluminum block machined to fit on top of the sample cell as shown in Fig. 2C. The aluminum reservoir is connected to a circulating liquid cooler (Thermaltake, BigWater 780e ESA) to dissipate heat or cool one side of the TE heater/cooler. The fully assembled sample cell with the TE heater/cooler weighs 196g just under the maximum recommended vertical load of the scan stage of 200g.

Proportional-integral-derivative (PID) control (TE Technology, TC-36-25-RS232) was initially used to regulate the temperature of the TE heater/cooler and sample cell. After judicious determination of PID parameters, the PID controller was able to control the sample cell's temperature to within a tenth of a degree Celsius of the set point, however, doing so required the controller to modulate the TE heater/cooler's power. It was quickly noted, however, that the cycling of the power to the TE heater/cooler, although providing a relatively constant temperature, produced a change in the detected count rate from control samples (detailed later) as may be seen in Fig. 3 (the definite cause of this affect remains undetermined). This effect produced gross distortions in measured correlation curves and, subsequently, PID control was eliminated in favor of a constant power heating scheme. The controller was set to a constant power and the resulting steady state temperature was observed and recorded using a custom LabVIEW interface across a range of experimentally relevant temperatures. The results were fit using a second order polynomial allowing the power needed to achieve a desired temperature to be predicted. This scheme resulted in average steady state temperatures with standard deviations of only a few hundredths of a degree although the time necessary to reach the desired temperature was longer than that observed using PID control.

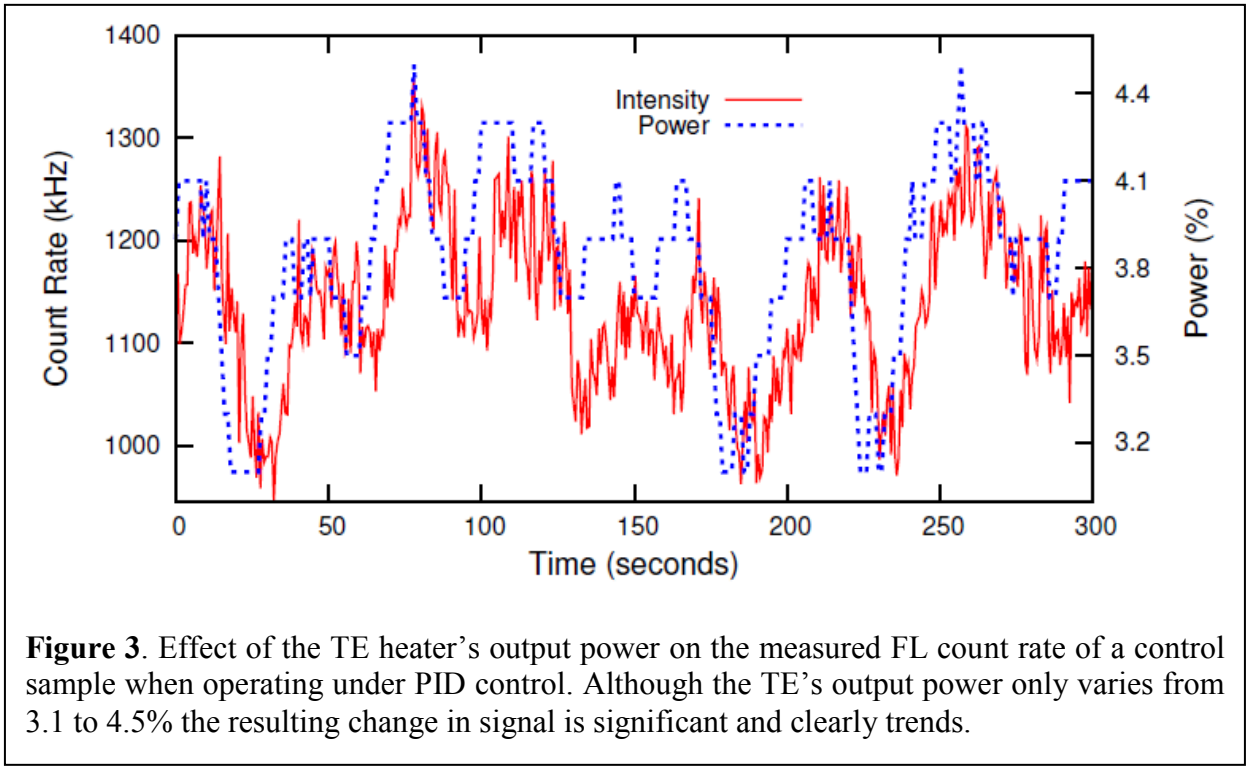

Figure 3. Effect of the TE heater's output power on the measured FL count rate of a control sample when operating under PID control. Although the TE's output power only varies from 3.1 to 4.5% the resulting change in signal is significant and clearly trends.

D. Stage and cell evaluation

Evaluation of the sample cell and stage's stability was carried out by loading the sample cell with two No. 1.5 coverslips and a PTFE coated o-ring but with liquid omitted from the cavity. The sample cell was mounted on the scan stage and the inner surface of the bottom coverslip was brought into focus using a 60X 1.2 N.A. UPlanApo/IR water immersion objective (Olympus) by monitoring the scattered laser light from the glass/air interface. Excitation and collection followed a standard confocal geometry using a 50μm diameter fiber in place of a pin hole and a fiber-coupled avalanche photo diode (APD) as the detector. Once the objective was brought into position, the brass lock ring was secured and a custom LabVIEW program was used to monitor the APD count rate and control the position of the piezo scan stage. The sample cell was scanned through the axial range of the scan stage, the APD count rate at each position was saved, fit to a Gaussian, and the center position of the fitted Gaussian recorded. The software was then set to scan the sample cell through the initial center position every 5 minutes. Scanning was performed from 3μm below to 3μm above the initial center position, in 500nm steps, and the APD count rate at each position was recorded along with the time at which each scan began. The fitted center position for each scan along with the time stamp allowed the position as a function of time to be tracked. Axial scanning of the sample cell using the custom stage setup yielded an average drift rate of 3.47±0.22 nm/min. A typical result is presented in Figure 4A. Similarly, the scan stage and sample cell were mounted on the factory shipped XY stage and the objective was mounted on the original objective turret, and the scan repeated. This yielded an average drift rate of (7.25±1.06)nm/min, as shown in Figure 4B, which is a factor of two larger than our custom setup. Furthermore, Figure 4A also presents occasional mechanical instabilities beyond the

reported average rate were observed suggesting that the stability of the stock stage and turret have the potential to heavily affect measurements on planar systems without operator awareness.

The same stability verification method was also employed to evaluate typical sample mounting methods relative to our custom sample cell. Here, cover glass was mounted to welled slide glass using wax and nail polish. The welled slide glass was inverted and held on the scan stage using clips typically found on microscope stages for said purpose. Typical results from investigating the stability of wax and nail polish sealed cover glass are shown in Fig. 4B along with the stability of our custom setup for comparison. Finally, a No. 1.5 bottom thickness 8-chambered well (Nunc, Lab-Tek II) was tested and the results are also presented in Fig. 4B. As can be seen in Fig. 4B the wax and nail polish sealed welled slide glass, as well as the 8-chamber well, are relatively unstable when compared with our custom setup.

As is clearly evidenced in Fig. 4 by comparing data presented in parts (A) and (B), although our custom stage setup does provide a factor of two decrease in axial drift, relative to the conventional system, it is clear that the custom sample cell employed herein plays an even more critical role. For typical z-scan step sizes (200-300nm) we find the sample′s maximum axial speed is 20.4μm/s (1.22mm/min) and likely not a cause of instability.

Both nail polish and wax seals have been observed to allow air bubbles into the sealed sample well if left for as little as 12 hours. This suggests that the wax and nail polish may form an unreliable seal and allow liquid to evaporate. In equivalent unsealed samples, we observe that as samples dry the loss of liquid due to evaporation causes a visually apparent concave deformation in the cover glass. If the cover glass, which supports the sample, is deforming as a function of time this will clearly affect the absolute position of the sample from scan to scan. This is in contrast to our custom sample cell which allows samples to be examined promptly prior to the potential formation of air bubbles and without having to wait for nail polish or wax to dry. Bubbles have been observed to form in our custom sample cell but only after a few days. More importantly, our sample holder is physically attached to the scan stage using two 4-40 machine screws. This ensures good rigidity between the sample cell and scan stage whereas in the case of conventional microscope stage clips the sample is held by pressure and direct attachment of the sample to the stage is not possible.

To test the imaging stability of our setup a dilute 3nM solution of 200nm fluorescent beads (Invitrogen, F8784) were dried on a No. 1.5 cover glass and mounted in the sample cell. The sample cell was mounted on the piezo scan stage and the beads were brought into focus. An EMCCD camera (Andor, Luca) was used to capture an image of the beads every five minutes for 75 minutes after the initial focus was achieved. Initial and final images are shown in Fig. 2.4. Features in each image were fit to a 2D Gaussian using a custom MatLab script and the resulting $1=e^2$ radius of each feature was stored (features with fitted $1/e^2$ radii larger than would be expected for this imaging system and features not well spatially separated were excluded). Over the 75 minute period the average fitted $1=e^2$ radius increased by (209.4±137)nm (or (2.6±1)nm/min.) indicating the viability of this system for long term imaging.

In all the custom built scan stage and sample cell were proven to have stability far superior to that observed for the as-delivered stage, and typical sample mounting methods, respectively. Due to the z-stability requirements of the combined SF and FL technique this was a necessary achievement of this MRI project.

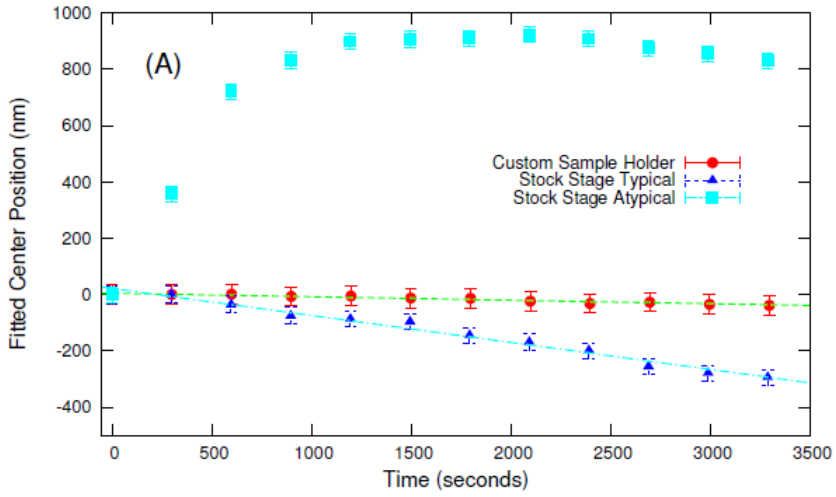

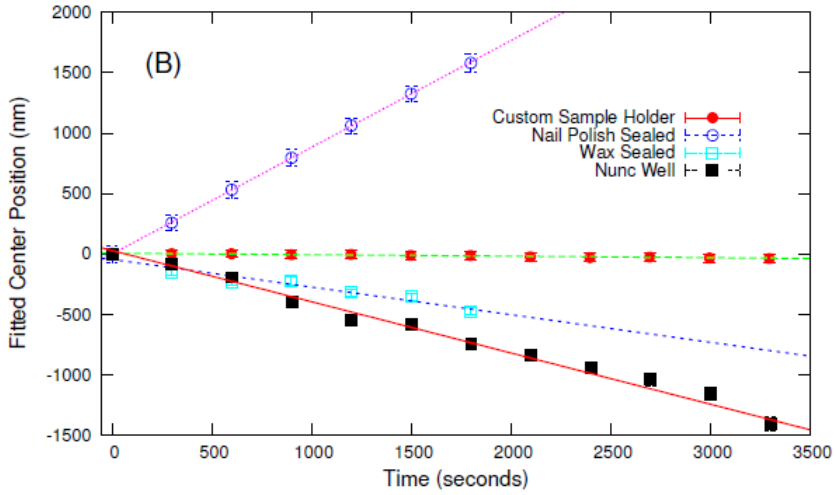

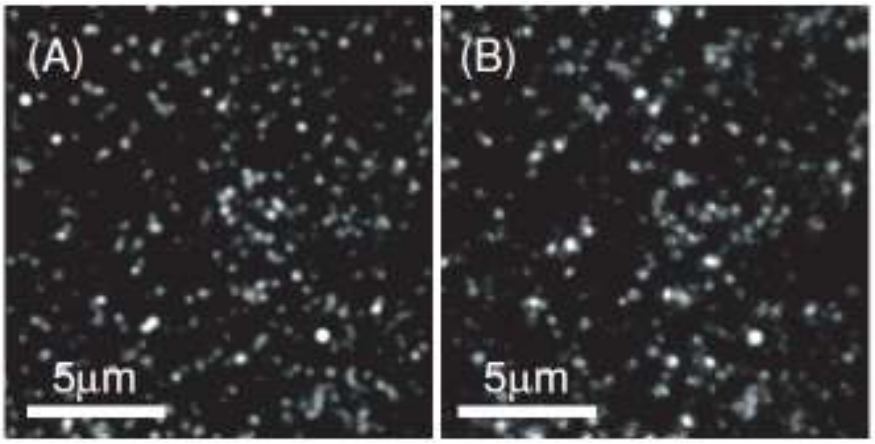

Figure 4. (Top) (A) Axial stability of the custom setup described here is compared with a typical and a typical result from a stock stage and turret. (B) Stability of our sample cell compared with nail polish and wax sealed coverglass and an 8 chamber well. (Bottom) Images of drop cast 200nm beads imaged (A) after initial focus and (B) 75 minutes later.

III. SUM-FREQUENCY COMPONENTS

A. Sum Frequency Basics

Sum frequency spectroscopy (SFS), an application of sum frequency generation (SFG), employs nonlinear optics for the elucidation of interfacial chemical, vibrational, orientation, and conformational information. SFG is produced by spatially and temporally overlapping two electric fields resulting in the creation of a third electric field with angular frequency equal to the sum the to exciting fields: $\omega_{SF} = \omega_1 + \omega_2$. Although the mixing of electric fields from any source, in principle, will produce SFG, in practice the power densities needed and phase matching requirements prohibit detectable SF from being generated by virtually anything other than pulsed lasers. Employing collimated laser excitation further aides in SF detection as the resulting light is emitted as a beam whose angle of emission may be calculated directly. For this reason SFS instruments are universally constructed with one goal: focusing pulsed, collimated, and coherent light onto an interface. A basic SF experimental setup is depicted in Figure 5 where both the SFS-VIS and SFS-IR beams are shown propagating in the positive *z* direction (co-propagating). Note also in Figure 5 indication of electric field polarization in the plane normal to the interface is referred to as *p*-polarized while electric field polarization parallel to the interface is *s*. Interfaces are of paramount importance as under the dipole approximation SFG is forbidden in bulk media with inversion symmetry. However, when inversion symmetry of isotropic centrosymmetric media is broken at an interface the interfacial molecules become sum frequency (SF) active giving SFS its inherent surface specificity.

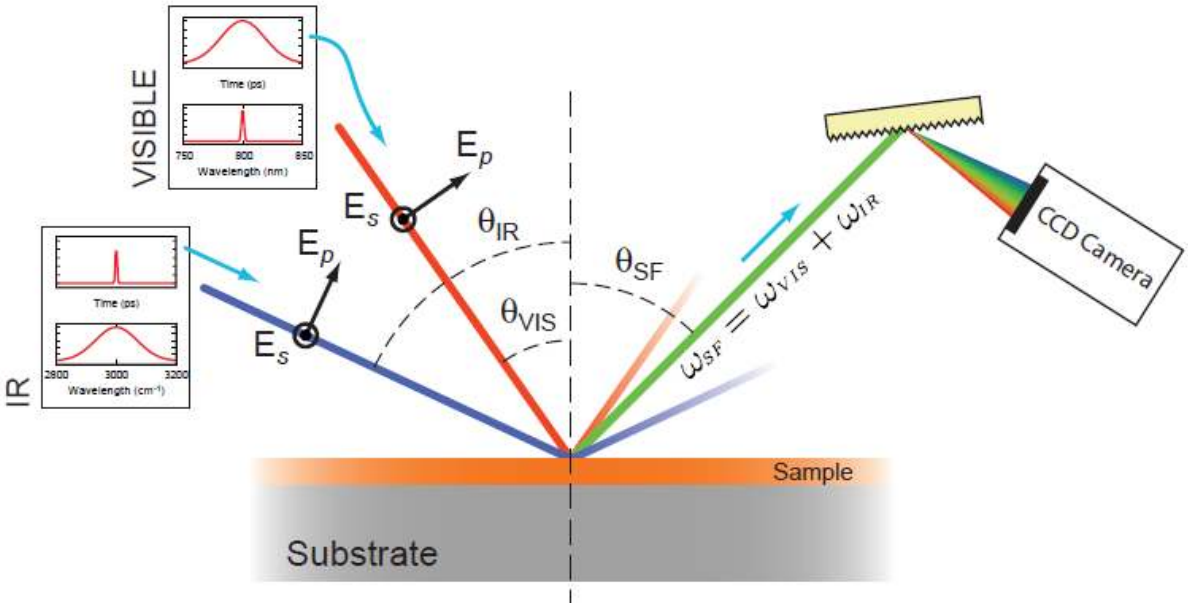

Figure 5. Basic SF experimental geometry. Two pulsed beams meet at an interface and generate SF. (B) Energy level diagram of SFG. Excitation of a vibrational mode is induced via an IR photon (broadband source). A second visible wavelength photon (monochromatic) excites to a virtual level and the photon emitted upon relaxation has an angular frequency equal to the sum of the incident angular frequencies. Complete SF spectra are dispersed from a grating onto a CCD detector in a single shot.

B. Stand alone sum frequency instrumentation

One of the primary goals of this MRI project was to construct the hybrid SF/FL microscope making use of an existing SF (non-imaging) instrument (Neivandt Lab), while maintaining its existing functionality as a user friendly non-spatially resolved spectrometer. However, the rigorous power and spectral demands of the hybrid instrument, as well as the stability required for SF light source switching between the two, required significant changes in configuration of the existing instrument. As such, contruction of the hybrid microscope began with the complete rebuild of the existing spectrometer and the installation of a new optical parametric amplifier (OPA). The basic layout of the updated SF instrument is shown in Figure 6 and a photo is shown in Figure 7.

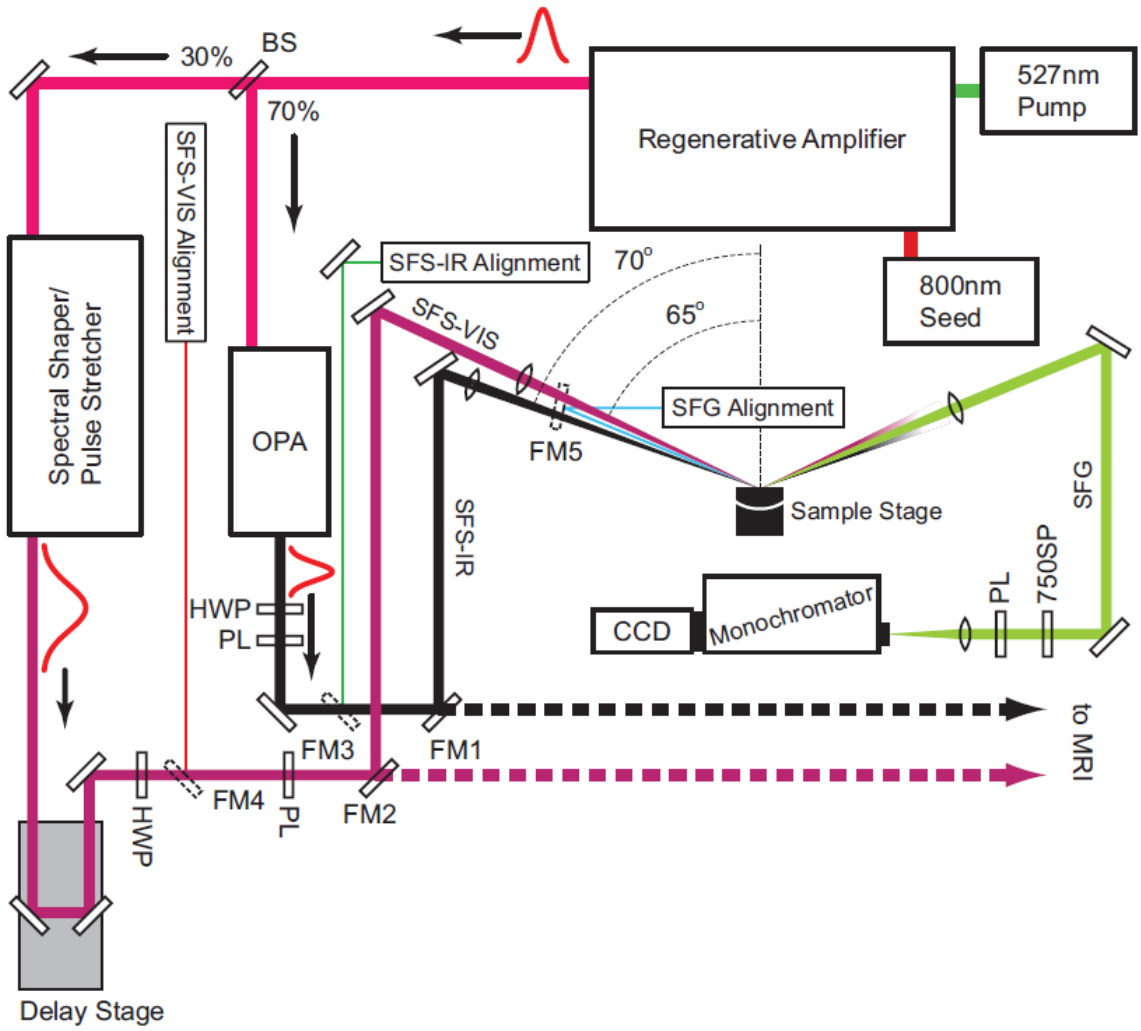

Figure 6. Layout of the rebuilt Neivandt spectrometer detail within the thesis text. FM1-5 are flip mirrors with FM1-2 used to direct the SFG excitation beams to either the Neivandt spectrometer (solid lines) or to the MRI instrument (dotted lines). FM3-4 allow the SFG excitation beams to be replaced with their respective alignment beams while FM5 serves the same function for the SFG signal beam. Abbreviations used are beam splitter (BS), half wave plate (HWP), polarizer (PL), 750nm short pass filter (750SP), and optical parametric amplifier (OPA).

Figure 7. Photo of rebuilt SF spectrometer (FL arm not shown).

In addition to a complete rebuild, optical elements were added to the beam paths to allow for redirection of the light sources to the hybrid instrument. As indicated in Figure 6 three flip mirrors (dotted outlines, FM3-5) may direct three alignment lasers to follow the optical path of the SFS excitation beams and the SFG beam. These are extremely necessary as directly viewing the SFS-VIS beam is hazardous, and the SFS-IR beam is not visible to humans. Two additional flip mirrors (FM1 and FM2) either reflect the excitation beams to the Neivandt sample stage or pass them to the hybrid MRI microscope.

Because the hybrid microscopy and SF excitation lasers reside on separate optical tables an investigation of beam stability on the MRI table, relative to the Neivandt table, was performed. If the SFS excitation beams were found to be excessively unstable, or wander significantly on short time scales, additional stabilization would be required. Beam stability across the two tables was assessed using the SFS-IR alignment laser. The SFS-IR alignment laser was allowed to trace the path of the SFS-IR beam onto the MRI table and the stability was assessed by imaging with a CCD camera at three locations along the beam path. At each of the three camera positions along the beam path, the CCD was set to image the SFS-IR alignment laser every two seconds for fifteen minutes. Image analysis was used to determine the mean and time-dependent angular displacement ((3.23±1.91)μrads, (2.72±1.60)μrads, and (3.38±1.85)μrads, respectively). Based on these results no further stabilization was implemented.

IV. COMBINED SF AND FL INSTRUMENT

A. Hardware

As mentioned above, an inverted microscope base (Olympus, IX71) serves as the hybrid microscope's main body with FL excitation and collection from below and SFS excitation and collection from above. The overall instrumental setup is presented in Figures 8 and 9. FL excitation beams pass through a computer controlled shutter and into the rear port of the IX71. From there a dichroic mirror directs the beam into the back aperture of the microscope objective focusing it to a diffraction limited spot at the sample while a flipper mounted lens at the rear port allows wide-field illumination for sample positioning. Due to the longer working distance requirements imposed by the sample holder an Olympus 40X 0.65NA PLAN N infinity corrected objective lens corrected for No. 1.5 thickness cover glass is employed. FL is collected through the same objective, passes through the dichroic mirror and a bandpass filter, and out the side port of the microscope. Collected FL is sent directly to a fiber coupled APD, via a flipper mirror, to an EMCCD camera for wide field imaging/sample positioning. Atop the microscope body and course XY scan stage resides a high resolution piezo scan stage (Nano T115; Mad City Labs; Madison, Wisconsin). The scan stage is operated in closed loop mode and is controlled by computer. The scan stage has 100μm of travel in X and Y (lateral) directions and a maximum 50μm range in Z (axial) with 0.2 and 0.4nm resolution respectively. The piezo scan stage scans the sample for both FL and SF imaging.

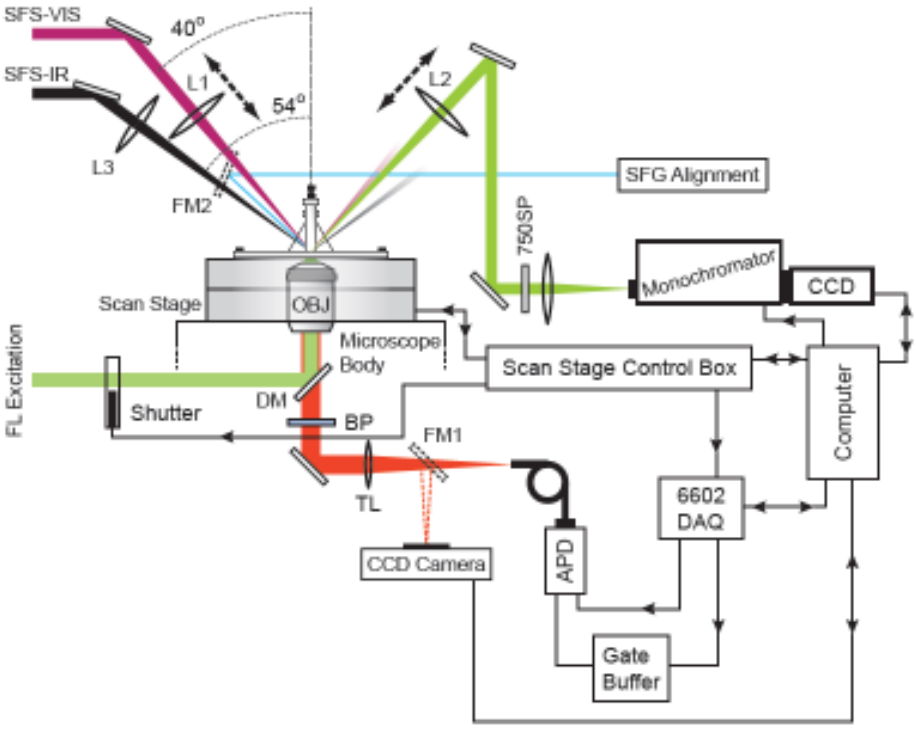

Figure 8. Hybrid SF/FL microscope hardware setup.

Figure 9. Photo of hybrid SF/FL microscope hardware setup.

Visible in Figure 9 are vertical breadboards coupled to the IX71 base which facilitates SFS excitation and collection. The beams are directed up while en route from the Neivandt to hybrid microscope table. Both beams are directed to the center of the sample stage, accounting for deviations due the equilateral prism (described below), and are focused by a 150mm focal length CaF2 lens and an uncoated 100mm focal length BK7 lens for SFS-IR and -VIS respectively. The SFS-VIS focus lens is additionally mounted on an axial translator for fine focus adjustments. (It was experimentally determined that SFS-IR focus is also critical for strong SFG, an additional axial translator for this lens would be a good future addition). For work at the air-solid interface SFS-TIR theory suggests incident beam angles at, or just below, the critical angle will maximize SFG. As such an SFS-VIS incident angle of 40° with respect to the table normal, resulting in an internal incident angle of 46° at the CaF_2 air interface (2° below the critical angle), was employed. Hardware mounting limitations resulted in the SFS-IR beam incident at approximately 53° with respect to the table normal resulting in an internal incident angle 10° beyond its critical angle in CaF_2.

SFG signal was collected by at 175mm focal length BK7 lens positioned at the detection angle predicted by the K-matching condition, one focal length away from the sample. Like the SFS-VIS lens the SFG collection lens is mounted for axial translation and collection optimization. The collected SF signal is directed through a 700 short pass filter (Part number;

Thorlabs; Newton, NJ) and focused with a 100mm focal length lens the entrance slit of a spectrograph consisting of a monochromator (2300, Princeton Instruments) and an EMCDD camera (1024 ProEM, Princeton Instruments). A flipper mirror in the excitation path allows an additional laser to reflect from a metalic substrate, in place of the prism, and into the detection path, simulating the SFG's path, for alignment.

B. TIR-SFS/FL Sample Holder

Like Raman, SFG is a relatively weak phenomena and direct detection without en- hancement is rarely employed. The two most common enhancement mechanisms for SFS are reflective metallic substrates, similar to SERS in Raman, and total internal reflection. These modes thus dictate sample cell design. We require something amenable to confocal fluorescence from below (due to the inverted microscope base) and SF excitation from above. Clearly enhancement from a thick metallic substrate would be a poor choice as it excludes FL imaging, leaving TIR as the viable choice. The ability to image using SFG further requires an experimental geometry amenable to sample scanning eliminating two obvious prism choices, hemi-cylinder and hemi-spherical. An equilateral prism, however, should meet the design criteria; it allows for TIR and sample scanning without grossly affecting the SFS excitation beam's incident positions on its inner surface. Thus an equilateral 1" CaF_2 prism (ISP Optics, Irvington, New York) is employed for SFS imaging. A custom sample cell for prism TIR, from above, and confocal imaging, from below, was fabricated as illustrated in Figure 10.

The use of TIR and the prism interface, is a departure from the original proposal were a much more complicated assembly of CaF_2 meniscus lenses was proposed as a means of improving resolution of the SF method. While this approach still remains possible, it was necessarily abandoned due to the general lack of availability of the necessary optical elements following closing of the few commercial vendors. While the TIR/prism method exhibits limited spatial resolution, the dramatic reduction in background and increase in signal allows for more rapid image acquisition, a significant downside of the originally proposed design.

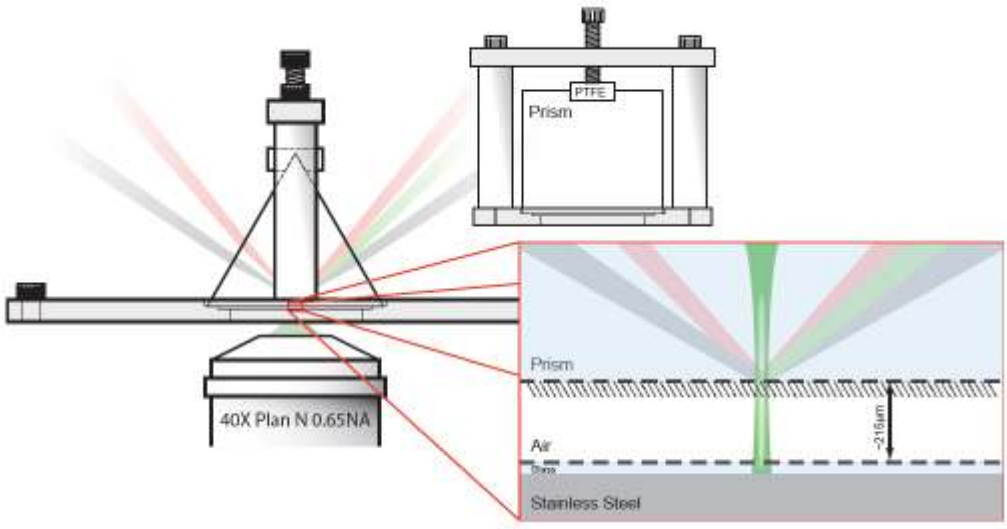

Figure 10. Side view of the custom TIR-SFS/FL sample holder (A) and 90° rotated from (A) side view.

B. Software

The basic data acquisition approach of the hybrid microscope is one of synchronous point-by-point data acquisition, as illustrated in Figure 11. Briefly, 2D images are obtained by raster scanning the sample through a series of software controlled positions, collecting SF and FL information at each location. Unlike traditional FL imaging, each pixel has multidimensional data which is post processed by the user. Control of the microscope is accomplished with a custom built LabVIEW control program. Much effort has been expended to make the MRI control program intuitive and simple. Whenever possible operations have been automated and all initialization/ shutdown routines are performed without the need for user input. The program is composed of one primary interface screen with two additional screens, one for CCD camera and monochromator setup/control (Figure 14) and the other for manual stage positioning, live count rate from the APD, and sample focusing (Figure 13). Unlike many LabVIEW programs that employ an infinite loop to keep the program running, which unnecessarily hogs processor time and slows the computer down, the hybrid microscope's control software uses event based architecture.

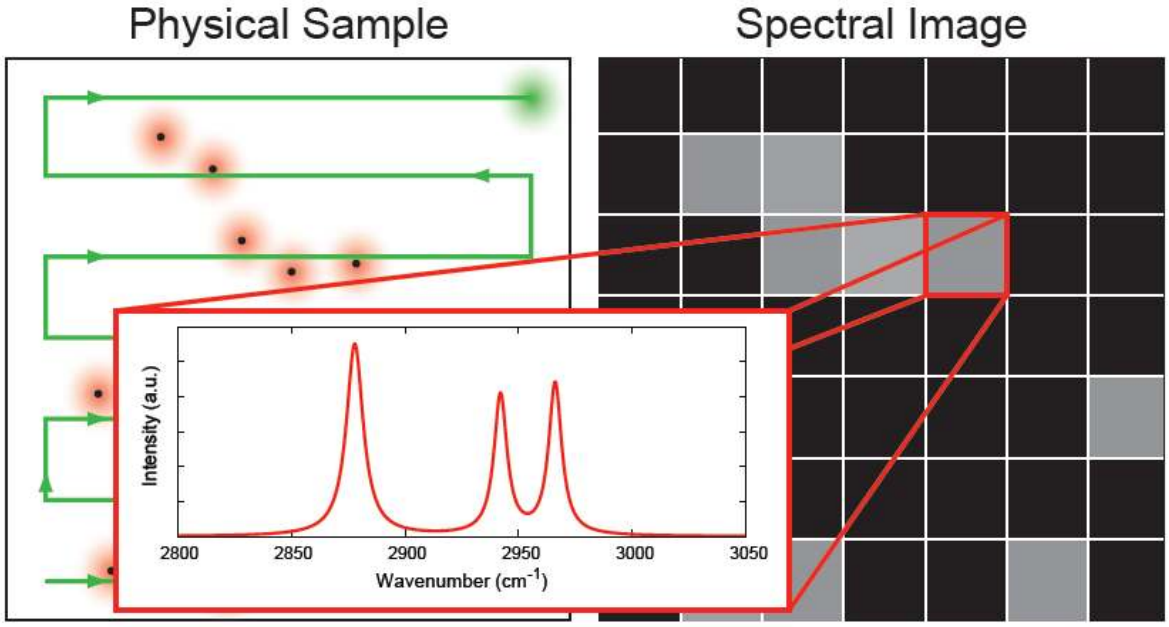

Figure 11. Depiction of sample raster scanning and data acquisition of the MRI hybrid instrument.

At the center of the primary screen is a large display showing acquired images and real-time acquisition progress (Figure 12). Above the primary image display is a plot that dynamically changes based on the acquisition being performed; it automatically shows the confocal line scans or SF spectra as they are being acquired, for example. To the left of the central display are indicators allowing easy checking of relevant setup parameters. These show if

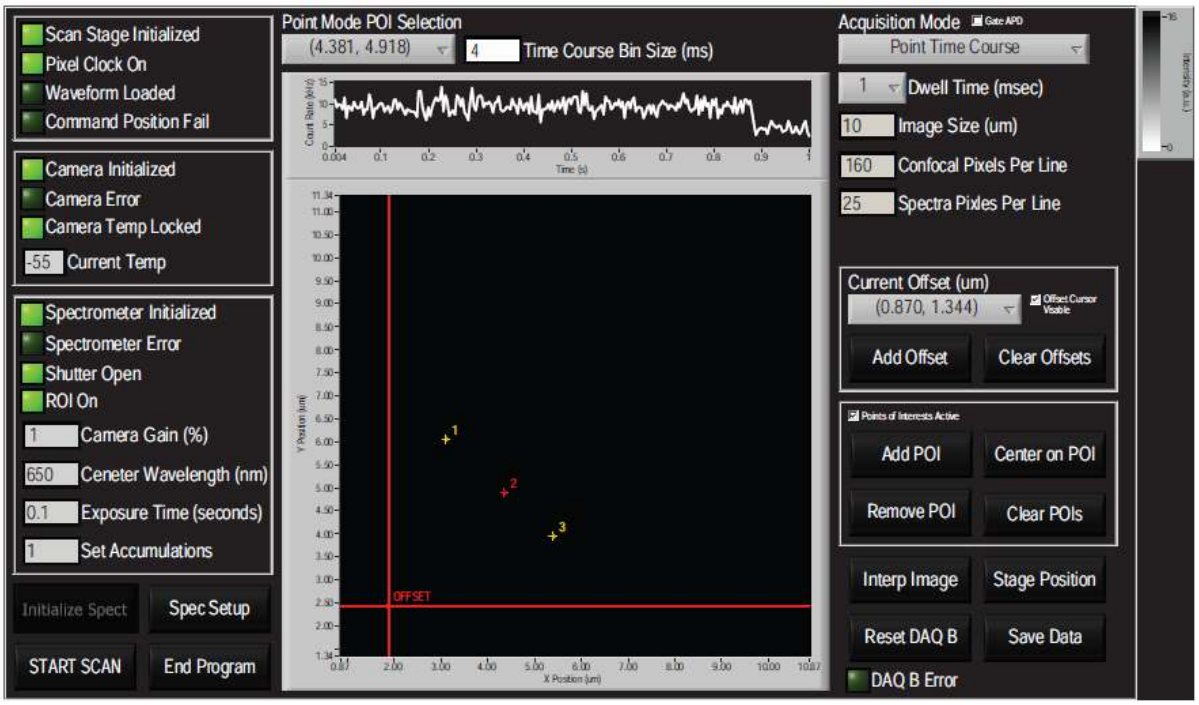

Figure 12. Primary acquisition display screen.

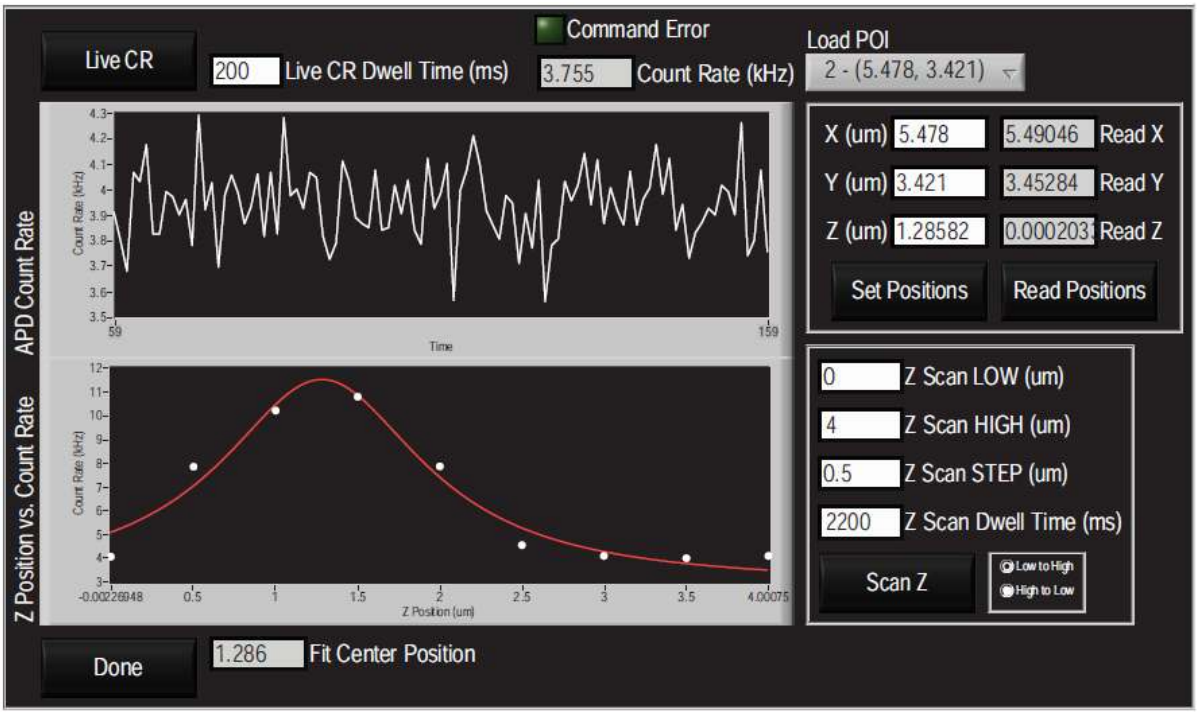

Figure 13. Manual stage positioning, live count rate from the APD, and sample focusing control panel.

the scan stage has been initialized, if the pixel clock is on, if the waveform is loaded, if the stage has failed to reach the commanded position, if the camera is initialized, if the camera temperature is stable, what the current camera temperature is, if the camera, spectrometer, or if the data acquisition (DAQ) board have reported errors, if the camera shutter is open, if a specific region-of-interest (ROI) has been set on the CCD, what the camera's reported EM gain is, the current CCD exposure time and accumulations, and the spectrometer's reported center wavelength. To the right of the primary display a drop down menu allows selection of the acquisition mode and numeric input fields allow specification of imaging parameters. Currently, the supported acquisition modes are confocal imaging, spectral imaging, confocal and spectral imaging, point time course and point spectum modes. These modes, along with the function of the primary and secondary screen's remaining elements will be detailed in the rest of this section (the only element not covered is the "Reset DAQ B" button which simply resets the DAQ board should an error arise).

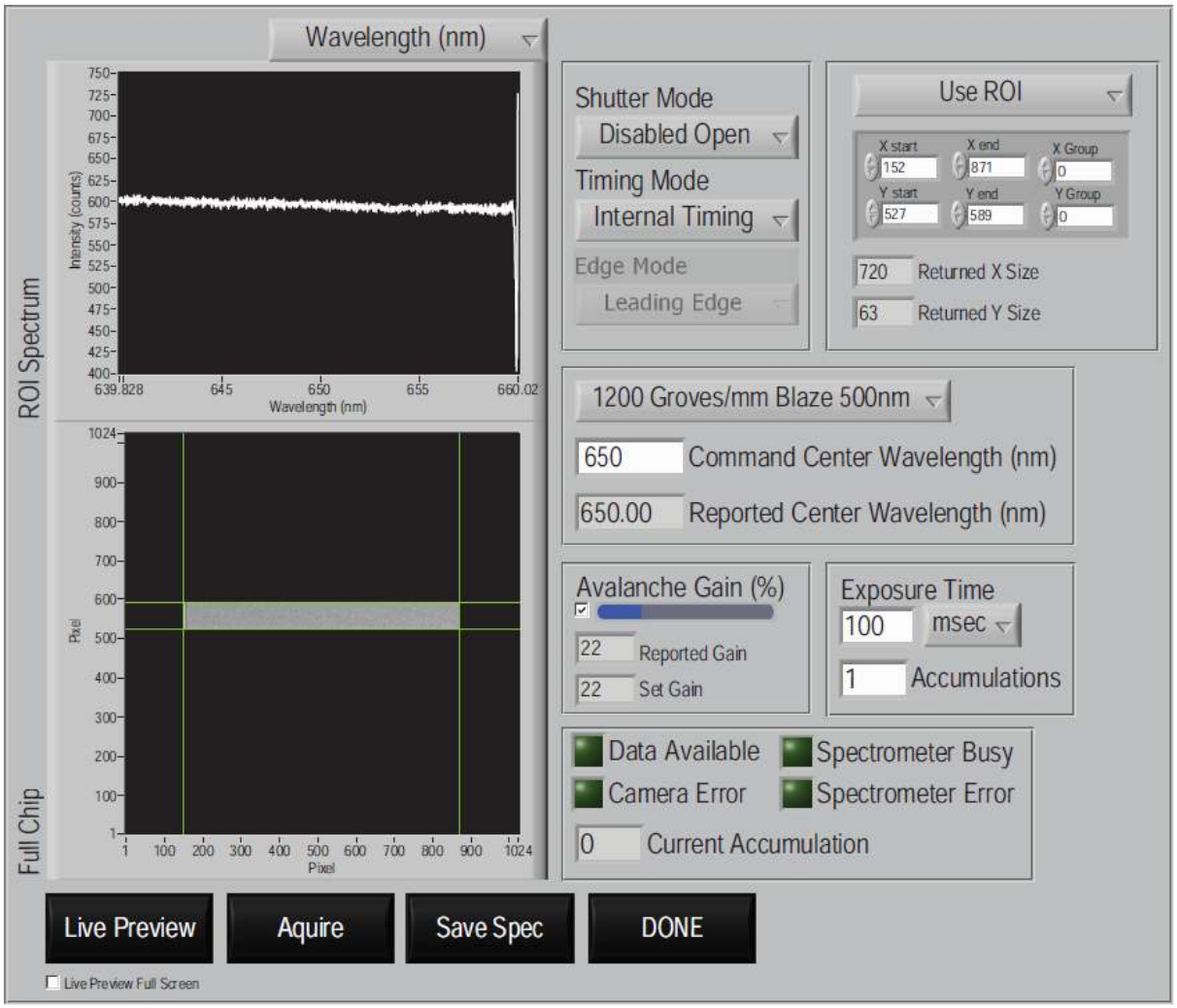

Figure 14. CCD camera and monochromator setup/control display.

C. Metrics / Standards

Calibration of the scan stage was verified by confocal reflectance imaging of a scanning electron microscope calibration standard (C1500-AB, SPI Supplies, West Chester, Pennsylvania) (Figure 15). This calibration sample is fabricated from pure silicon with a uniform lattice of orthogonal 1.9μm±5% wide grooves etched by electron beam lithography and spaced 10μm apart. Pure flat silicon is highly reflective and imaging was accomplished by collecting a small amount of reflected laser light from the sample. Interpolated images of the SPI standard are presented in Figure (3.11) and suggest the scan stage and all image acquisition components function correctly. As an additional test 20nm fluorescent beads (F8784, Invitrogen, Carlsbad, California) were imaged via wide-field excitation using a CCD camera and fluorescent confocal microscopy as presented in Figure 15. Good agreement between the confocal and wide-field images is clear from Figure (3.12) further demonstrating correct operation of the confocal imaging setup. Despite correct functioning confocal scanning hardware the potential affects of imaging with the highly sensitive APD while the SFS excitation beams are also incident on the sample must be considered.

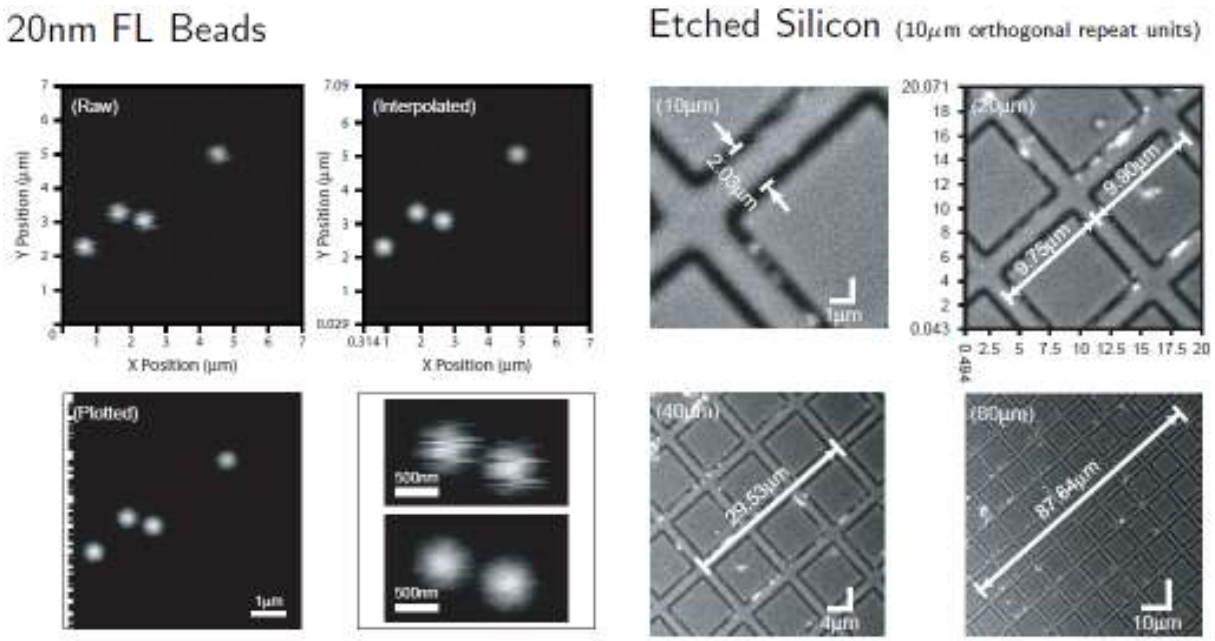

Figure 15. Scan stage fluorescence (left) and reflectance (right) calibration standard (left).

For assessment of the SF and FL capabilities of the instrument, a somewhat more complicated series of standards were created. These standards were composed of a series of etched void structures in a thin gold layer deposited on glass (Figure 16). The gold is known to generate a broad non-resonant SF background signal, and can be used to simultaneously generate a laser reflectance image in the confocal FL detection path (Figure 17). Alternatively a single layer of octadecane thiol (ODT) (bound to gold) was used to generate a well known SF signal.

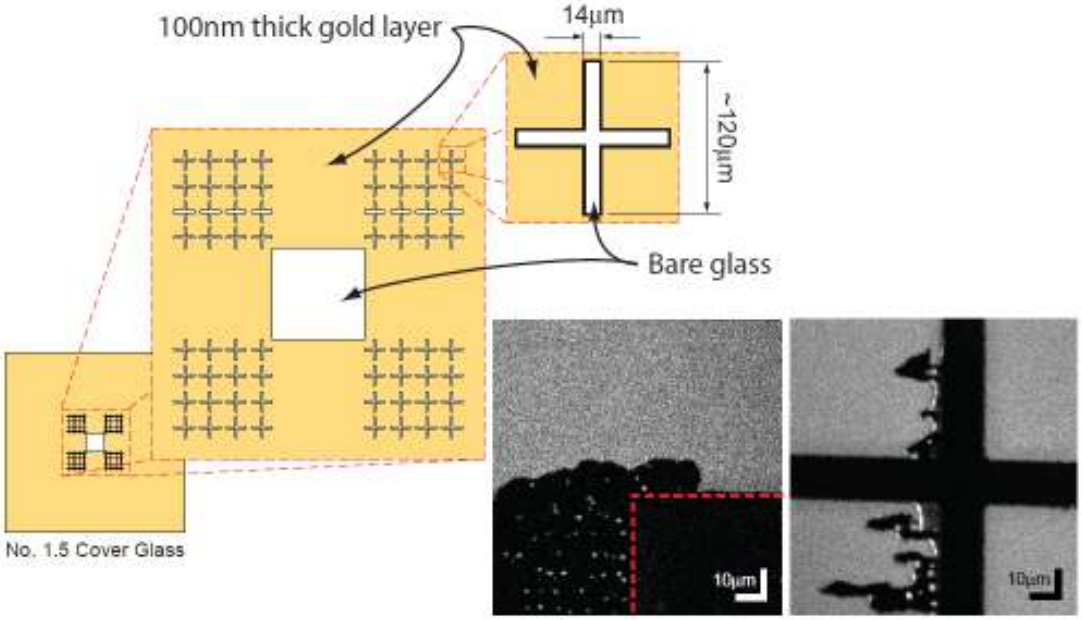

Figure 16. Gold patterned SF/FL standard. The image insets show the effect of laser ablation when the instrument is operated at elevated pump power.

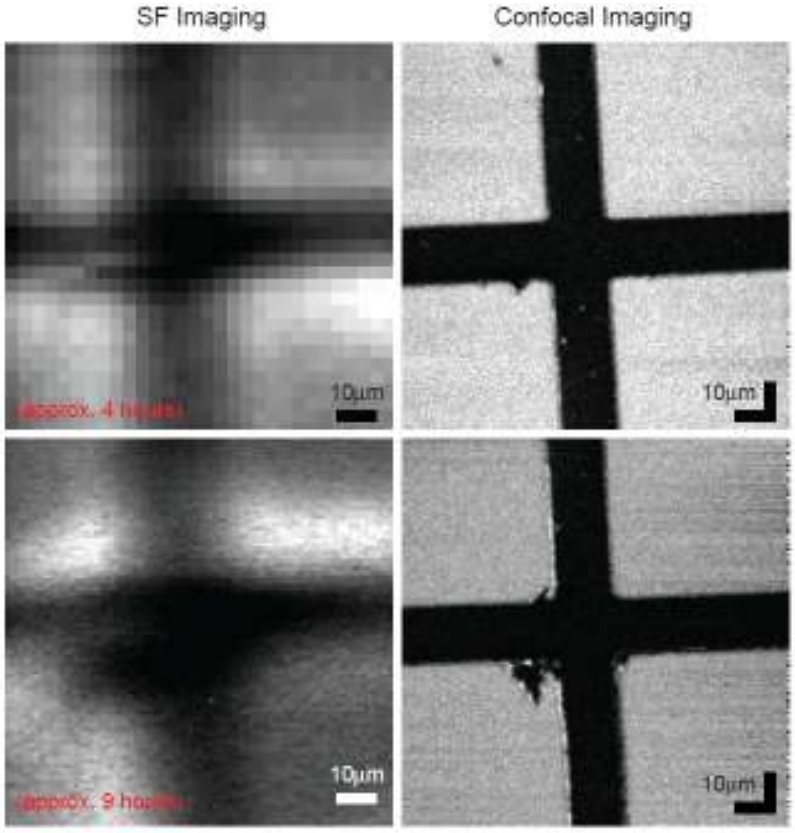

Figure 17. Simultaneous SF (ODT) and FL images acquired for the patterned gold standard (top). The same sample is reimaged at increased pixel resolution (bottom).

V. CAPABILITIES AND SAMPLE DATA

A. Spectral and Confocal Imaging Results

In addition to the patterned gold substrate described above, a second biologically interesting test sample was constructed consisting of a fluorescently labeled phase separated lipid monolayer deposited directly on the afore mentioned CaF_2 prism. Fabrication of this sample followed from an investigation of phase separation in lipid monolayers. 1,2-dilauroyl-*sn*-glycero-3-phosphocholine (DLPC), with a main phase transition temperature of -1°C, and 1,2-distearoyl(d70) *sn*glycero- 3-phosphocholine (perdeuterated DSPC, referred to as dDSPC herein), main phase transition temperature of 55°C, were mixed, doped with the fluorophore 1,2-dimyristoyl*sn*- glycero-3-phosphoethanolamine-N-(lissamine rhodamine B sulfonyl) (ammonium salt) (Rho-PE)(Avanti Polar Lipids, 810157), and deposited via the Langmuir-Blodgett technique. Wide field microscopy revealed apparent domain formation presumed to be that of solid phase (at room temperature) dDSPC, while the DLPC (liquid phase at room temperature) appeared uniformly distributed outside the domains (Lin *et al.*, 2006; Ratto & Longo, 2002) with the Rho-PE separating into the liquid phase DLPC (Crane & Tamm, 2004). Deposition conditions (subphase temperature, and deposition pressure), Rho-PE concentration, presence/concentration of cholesterol, and dDSPC to DLPC ratios were varied and their affects on domain size tracked. Ultimately a 1:1 DLPC to dDSPC mixture doped with 0.0005mol% Rho-PE and deposited at 35mN/m with a subphase temperature of 26°C was found to yield

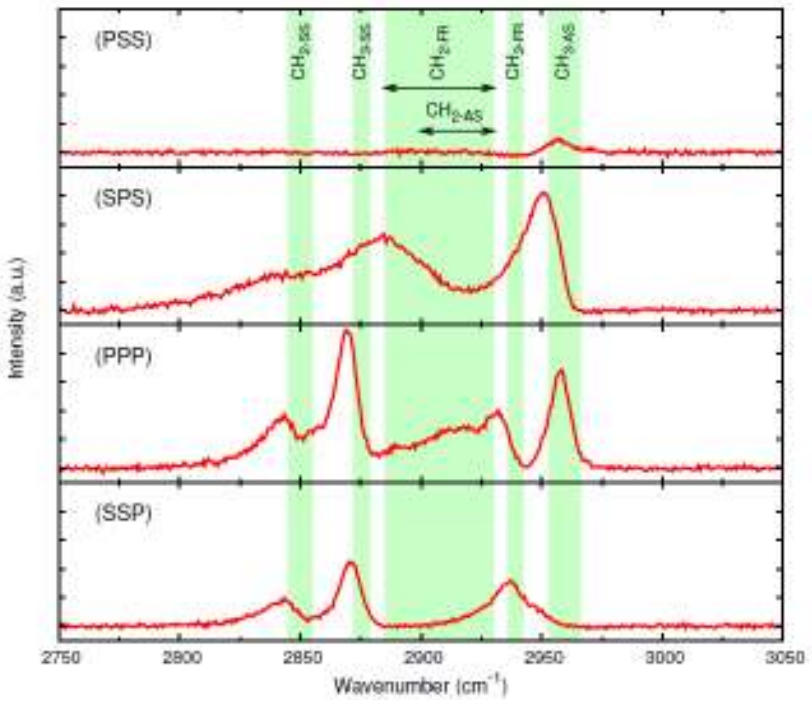

Figure 18. Background subtracted SFS-TIR spectra of a DLPC monolayer at the air-solid interface. All four spectra were acquired under identical conditions while the SF excitation polarizations were varied (1 min. integration time). The intensity on each y-axis is identical allowing comparison of the relative intensities of polarization combinations. The shaded boxes indicate the high and low limits for peak assignments found in literature where the vibrational modes are indicated at the top of the plot. The CH2−*FR* and CH2−*AS* modes overlap and the ranges of each have been indicated with arrows.

clusters of large phase separated solid phase dDSPC domains, while the Rho-PE remained mixed within the liquid phase DLPC. As perdeuterated material is inactive in the CH stretching region, the phase separated dDSPC will not generate SF signal. Because Rho-PE resides in the DLPC, which is active in the CH stretching region, this sample should yield matching SF and FL images with domains easily visualized by both. As such 1:1 DLPC to dDSPC, with 0.0005mol% Rho-PE monolayers, deposited by LB deposition with the above mentioned trough parameters were fabricated on the CaF_2 equilateral prism for instrumental validation and testing.

Example TIR spectra of DLPC, in the CH region, are presented in Figure 18. Spectra show excellent signal to noise despite a relatively short integration time (1 min.). The peaks evident in the spectra of Figure 18 are seen in the spectra of individual pixels, in the spectral images and should be considered representative. Although the peaks are close to the literature values they clearly fall on the edges of the respective ranges given by the high and low values as presented in Figure 18. Aside from the possibility that this is related to the spectral/temporal profile and delay of the SFS excitation pulses, two obvious factors can account for variation in the vibrational modes: the presence of Rho-PE and depositing the DLPC while in the fluid phase, as opposed to the highly ordered solid phase. A less ordered environment would clearly result in different interaction forces subsequently altering the vibrational modes of the methyl groups. In fact, the presence of methylene peaks in the spectra presented in Figure 18 is clear evidence of a less than ideally ordered monolayer.

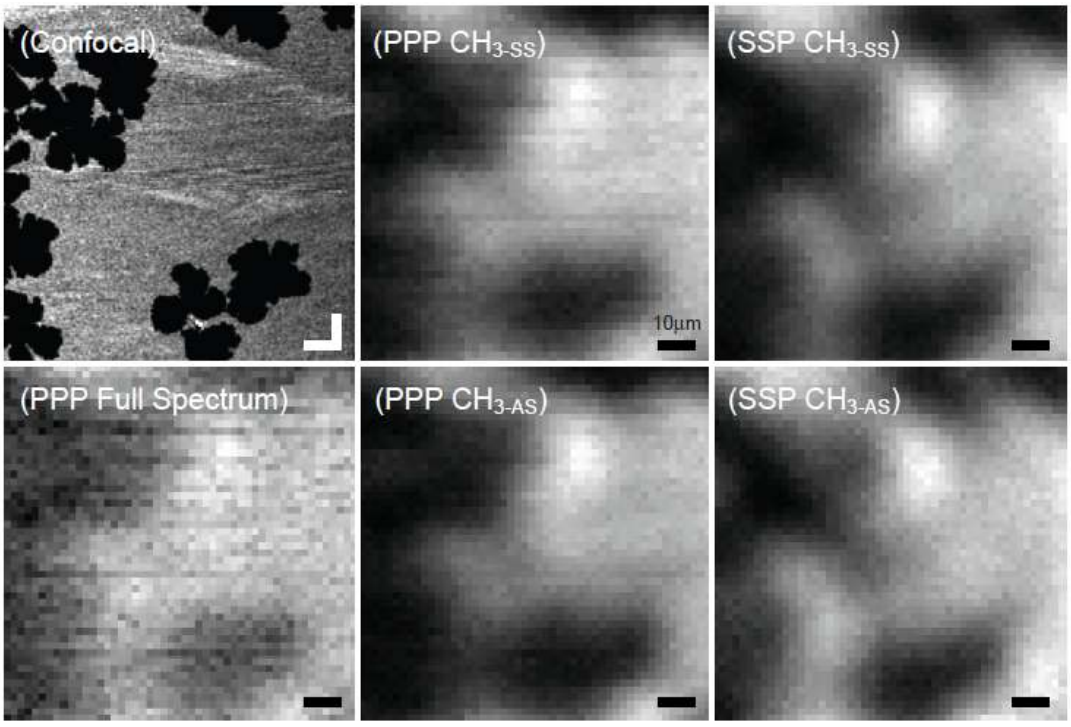

Figure 19. (A) Confocal image of DLPC/dDSPC monolayer on a CaF2 prism and the same area imaged using SF microscopy (B)-(F). Specifically (B) presents the results of integrating the entire spectrum at each pixel to assign a pixel value while (C) and (D) utilize the methyl symmetric and asymmetric stretch modes, using the PPP polarization combination, respectively. Images (E) and (F) likewise show the methyl symmetric and asymmetric stretches respectively with the SSP polarization combination employed. Scale bars are all 10μm.

Images from SF-TIR and confocal FL acquisitions are presented in Figure 19 and clearly demonstrate SF images that closely match the corresponding confocal FL images. In some cases the images are of slightly differing regions, however, features seen in the confocal images are clearly distinguishable in the accompanying SF images. Each pixel in the SF images can be derived from a full SF spectrum acquired at that location on the sample, or generated from specific spectral regions. Thus we may choose which spectral features should be used to set the pixel values. In all the SF images presented here each pixel value results from integration of either the CH3 symmetric or asymmetric stretch mode (with a width of 0.5nm centered around the peak's maximum value). Although the image is discernable for the entire SF spectrum (integrated) it is not particularly clear in contrast to images derived from the same data but with either the methyl symmetric stretch or asymmetric stretch integration used for the pixel value. Figure 19 also shows a detectable difference between images acquired using either the PPP or

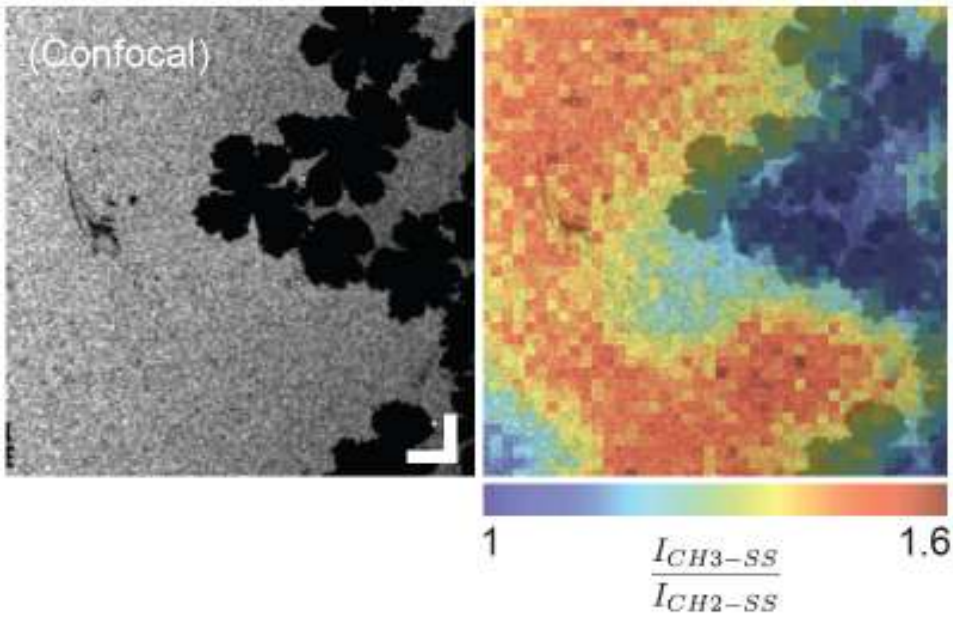

Figure 20. Confocal FL image of phase segregated Rho-PE (left). (Right) Hybrid image of SF determined lipid order (colorized) overlapped with FL data.

SSP polarization combinations. This suggests that not only is spatially resolved vibrational information present but further information, e.g. the spatial distribution of mean tilt angles, can be elucidated. All images are displayed on a linear scale ranging from the image's maximum (white) to minimum (black) value.

Possibly the best demonstration of the utility of the hybrid microscope is the simultaneous display of SF and FL information. This is accomplished, for example by comparing the intensity of CH_3 and CH_2 modes (a measure of relative order), and overlapping this information with the confocal (Rho-PE) data, as shown in Figure 20. Immediately, previously unforeseen spatial correlations, and interesting anti-correlations between phase separated and ordered regions are observed. The specific implications of this data are still being

considered (manuscript in progress). The data in Figure 20 are unique to this instrument and suggests successful completion of this MRI project. Future experiments will generate data of this form for other scientifically relevant sample types.

B. Instrument Resolution

The SFS-VIS has been observed to be well above the diffraction limit and subsequently its size could be measured direct or indirectly, e.g. photo bleaching a uniform dye film or by imaging with a CCD camera. However, the SFS imaging resolution is not a function of the SFS-VIS beam alone. Clearly the overlapping SFS-IR and -VIS beams define the spatial sensitivity of the system, the effective SFS excitation area. Were the SFS-VIS and SFS-IR beam sizes both known a reasonable estimate of the signal generating region could be made. This could, in turn, allow for an estimation of the SFS imaging resolution. Unfortunately direct measurement of the focused SFS-IR beam is not possible. Here we employ three methods for spectral imaging resolution estimation: an adapted knife edge method, simulation of an SF image with defined step edges, and finally direct visualization of the SFS-VIS beam. The results of this analysis are shown in Figures 21 and 22.

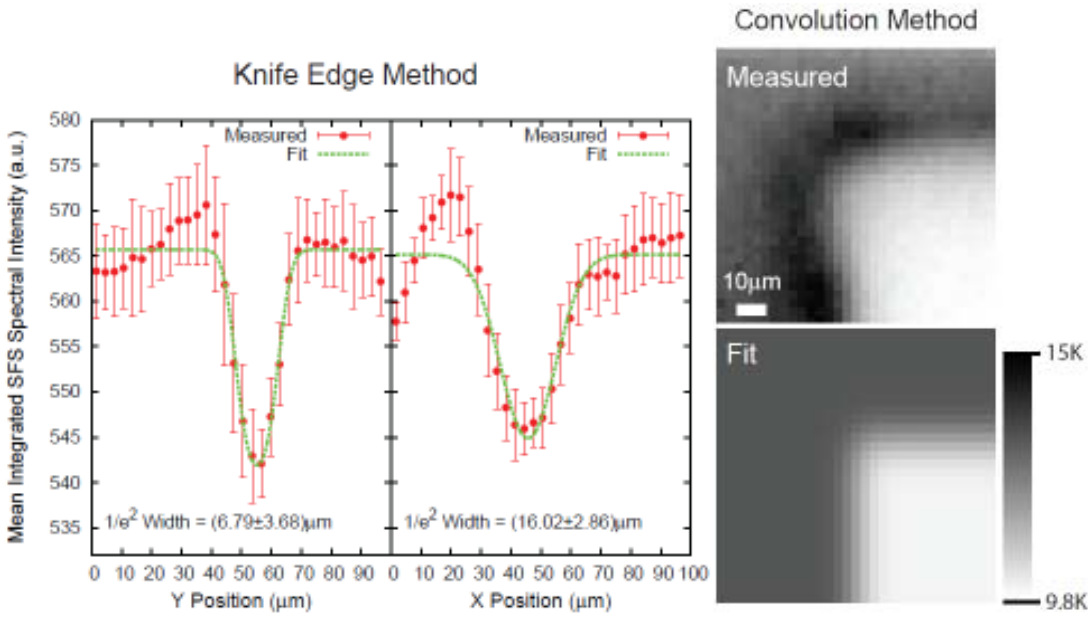

Figure 21. Line feature scan through SFS excitation beams fit with Equation (X) for the (A) Y and (B) X dimensions. Fitting yields 1/e2 radii of (16.02±2.86)μm and (6.79±3.68)μm in the X and Y dimensions respectively which is consistent with the observed elongated dimension of the SFS-VIS beam in the X dimension.

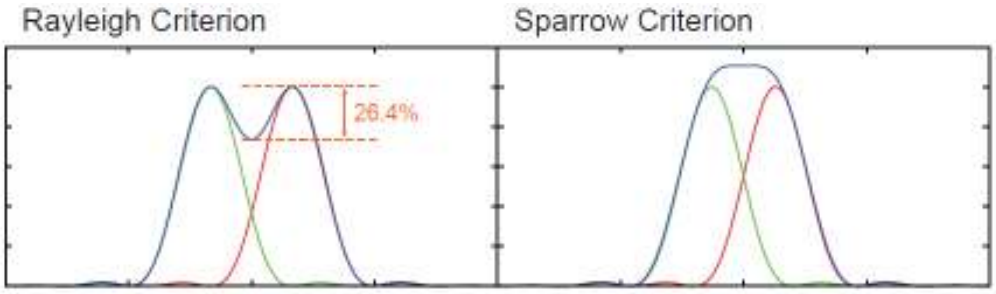

Method	Dimension	Diameter (μm)	Rayleigh (μm)	Sparrow (μm)
Convolved	X	12.77±1.11	17.88	14.06
	Y	12.55±1.12	17.57	13.854
Knife Edge	X	16.02±2.86	22.43	17.68
	Y	6.79±3.68	9.51	7.49
SFS-VIS Fit	X	22.37±5.05	31.32	24.69
	Y	16.62±7.40	23.27	18.348

Figure 22. Line feature scan through SFS excitation beams fit with Equation (X) for the (A) Y and (B) X dimensions. Fitting yields 1/e2 radii of (16.02±2.86)μm and (6.79±3.68)μm in the X and Y dimensions respectively which is consistent with the observed elongated dimension of the SFS-VIS beam in the X dimension.

VI. CONCLUSIONS AND FUTURE PLANS

Here we have detailed the construction and function of a hybrid SF/ FL spectral imaging sample scanning microscope as applied in both a reflection and TIR geometry. A number of test samples were investigated the results of which clearly illustrate the power of this new hybrid instrument. This one-of-a-kind instrument is now capable of generating unique data combining the capabilities of SF and FL and represents successful completion of this MRI project.

Although the proof of principle is now clear, a number of improvements would further benefit the system. On exiting the SSPS, clear spatial irregularities can be easily seen in SFS-VIS mode. Attempts were made at spatial filtering using high energy pin holes (5-50μm) but were found to have negligible affect (they either burned or were to large). As such implementation of a polarization preserving, low dispersion single mode, fiber optic could clean up the beam profile while simultaneously providing a simple method for delivering the beam to the hybrid microscope with greatly reduced risk of laser eye damage (the fiber would provide a closed beam path and allow the beam to be conveniently launched and sized on the microscope breadboard, additionally reducing table clutter).

While the Princeton Instruments EMCCD camera has proven sufficient for TIR- SFS collection, it lacks the extremely fast electronic shutter employed on the PI-Max camera. The PTG timing option on the PI-Max camera allows extremely low shutter and trigger delay times, on the order of hundreds of nanoseconds. Typically shutter times employed on the Neivandt SFS system are 250μs. The SSPS output is in the picosecond regime while the SFS-IR pulse width remains in the femtosecond. Clearly, even thought the PI-Max camera is shuttered on the scale of nanoseconds its exposure time is still three orders of magnitude larger than SF emission duration

per pulse. Unfortunately the ProEM camera employed for the hybrid microscope's spectral detection lacks the fast shuttering capabilities of the PI-Max camera. The ProEM camera runs in shutter mode, most often with exposure times above 1 second (certianly faster exposure speeds can be set but the ProEM camera cannot achive the 1kHz frame that would be required regardless of exposure time). In this case the ratio of shutter open time to actually signal generation time is extremely large. For an exposure time of 1 second with a 1kHz pulse repetition we assume signal is generated for 1 picosecond for each pulse, meaning SF light is collected by the camera for only 0.000001% of the exposure time. The remaining 99.999999% of the exposure provides no further signal but does allow collection of background noise. Switching to a fast electronically shuttered camera has the potential to greatly reduce the noise collected during spectral acquisition which, in turn, could allow for shorter acquisition times and subsequently much shorter spectral imaging times. The scanning apparatus employed here is limited to scanning a 100μm square. Although this is ideal for many samples, there are likely as many other systems for which a large scan area would be more applicable. In light of the instrument's current resolution a larger scanning area may prove a better match. Replacing the course, manually posi- tioned, XY stock Olympus scan stage with a stepper motor driven stage would allow for easy large area SF imaging. Additionally, the existing scan stage could be easily mounted on top of a large scanning stage for high resolution investigations of ROIs without the loss of FL imaging capabilities. This would allow conformational order over very large sample areas to be studied (something not currently found in the literature).

VII. BROADER IMPACTS / OUTREACH ACTIVITIES

To date 16 undergraduate students and 4 graduate students have been involved in this project. The graduate students involved have now completed advanced science degrees in Physics and Chemical Engineering. The 16 undergraduate students are pursuing bachelors degrees in Physics, Chemical Engineering, and Biological Engineering.

In conjunction with this cutting edge project educational and outreach programs were developed demonstrating to an audience of high school students and educators the capabilities of the proposed instrument as well as the importance of new instrument development to the broader research community. Through this program nearly 150 high school students have participated in a one day directed research experience, and 4 high school students and 2 science teachers participated in a two month NSF supported research program, and an additional 6 high school students have participate in related research based on an internal matching grant.

Over two summers (2008, 2009) a Master of Science and Teaching (MST) Student (Erik DeSilva) was hired in conjunction with this MRI development project to specifically develop 1) course curricula/teaching modules for a new Biological Engineering Instrumentation and Advanced Methods Course, 2) development of high school outreach activities and curricula including on-campus research experiences (BEAR Program http://www.umche.maine.edu/bear/). Funding for this position was provided by UMaine Sponsored Programs in response to the proposed MRI funded outreach and educational activities. In addition, this student has completed a high school classroom teaching module which he has implemented on a trial basis.

Also completed are the two halves of the online description of the technology development, including the underlying photophysics, associated with this project. This can be found online at: http://www.physics.umaine.edu/FPALM_SFS_NOV09/sfs.html.

REFERENCES

[i] Florsheimer, M.; Brillert, C.; Fuchs, H. "Chemical imaging of interfaces by sum frequency microscopy" *Langmuir* **1999**, *15*:5437-39.

[ii] Florsheimer, M.; Brillert, C.; Fuchs, H. "Chemical imaging of interfaces by sum-frequency generation" *Materials Science & Engineering C-Biomimetic and Supramolecular Systems* **1999**, *8-9*:335-41.

[iii] Kuhnke, K.; Hoffmann, D. M. P.; Wu, X. C.; Bittner, A. M.; Kern, K. "Chemical imaging of interfaces by sum-frequency generation microscopy: Application to patterned self-assembled monolayers" *Applied Physics Letters* **2003**, *83*:3830-32.

[iv] Cimatu, K.; Baldelli, S. "Sum Frequency Generation Imaging Microscopy of CO on Platinum" *Journal of the American Chemical Society.* **2006**, 128: 16016-16017.

[v] Cimatu, K.; Baldelli, S. "Sum Frequency Generation Microscopy fo Microcontact-Printed Mixed Self-Assembled Monolayers" *Journal of Physical Chemistry. B* **2006**, 110: 1807-1813.